Energy-aware Co-location of Scientific Workflow Tasks

Master's Thesis

Author
Niklas Fomin
464308
niklas.fomin@campus.tu-berlin.de

Advisor
Jonathan Bader

Examiners
Prof. Dr. habil. Odej Kao
Prof. Dr. Volker Markl

Technische Universität Berlin, 2025
Fakultät Elektrotechnik und Informatik
Fachgebiet Distributed and Operating Systems

Energy-aware Co-location of Scientific Workflow Tasks

Master's Thesis

Submitted by:
Niklas Fomin
464308
niklas.fomin@campus.tu-berlin.de

Technische Universität Berlin
Fakultät Elektrotechnik und Informatik
Fachgebiet Distributed and Operating Systems

2025

Hiermit versichere ich, dass ich die vorliegende Arbeit eigenständig ohne Hilfe Dritter und ausschließlich unter Verwendung der aufgeführten Quellen und Hilfsmittel angefertigt habe. Alle Stellen die den benutzten Quellen und Hilfsmitteln unverändert oder sinngemäß entnommen sind, habe ich als solche kenntlich gemacht.

Sofern generische KI-Tools verwendet wurden, habe ich Produktnamen, Hersteller, die jeweils verwendete Softwareversion und die jeweiligen Einsatzzwecke (z. B. sprachliche Überprüfung und Verbesserung der Texte, systematische Recherche) benannt. Ich verantworte die Auswahl, die Übernahme und sämtliche Ergebnisse des von mir verwendeten KI-generierten Outputs vollumfänglich selbst.

Die Satzung zur Sicherung guter wissenschaftlicher Praxis an der TU Berlin vom 8. März 2017* habe ich zur Kenntnis genommen.

Ich erkläre weiterhin, dass ich die Arbeit in gleicher oder ähnlicher Form noch keiner anderen Prüfungsbehörde vorgelegt habe.

(Unterschrift) Niklas Fomin, Berlin, 28. Oktober 2025

*https://www.static.tu.berlin/fileadmin/www/10000060/FSC/Promotion___Habilitation/Dokumente/Grundsaetze_gute_wissenschaftliche_Praxis_2017.pdf

KI

(https://www.chicagomanualofstyle.org/qanda/data/faq/topics/Documentation/faq0422.html) If you need a more formal citation—for example, for a student paper or for a research article—a numbered footnote or endnote might look like this:

1. Text generated by ChatGPT, OpenAI, March 7, 2023, https://chat.openai.com/chat.

If you've edited the AI-generated text, you should say so in the text or at the end of the note (e.g., "edited for style and content").

If the prompt hasnt been included in the text, it can be included in the note:

1. ChatGPT, response to "Explain how to make pizza dough from common household ingredients," OpenAI, March 7, 2023.

Abstract

FaaS is a cutting-edge new service model that has developed with the current advancement of cloud computing. It allows software developers to deploy their applications quickly and with needed flexibility and scalability, while keeping infrastructure maintenance requirements very low. These benefits are very desirable in edge computing, where ever-changing technologies and requirements need to be implemented rapidly and the fluctuation and heterogeneity of service consumers is a considerable factor. However, edge nodes can often provide only a fraction of the performance of cloud computing infrastructure, which makes running traditional FaaS platforms infeasible. In this thesis, we present a new approach to FaaS that is designed from the ground up with edge computing and IoT requirements in mind. To keep it as lightweight as possible, we use CoAP for communication and Docker to allow for isolation between tenants while re-using containers to achieve the best performance. We also present a proof-of-concept implementation of our design, which we have benchmarked using a custom benchmarking tool, and we compare our results with benchmarks of Lean OpenWhisk, another FaaS platform for the edge. We find that our platform can outperform Lean OpenWhisk in terms of latency and throughput in all tests but that Lean OpenWhisk has higher success rates for a low number of simultaneous clients.

Kurzfassung

FaaS ist ein innovatives neues Servicemodell, das sich mit dem aktuellen Vormarsch des Cloud Computing entwickelt hat. Softwareentwicklende können ihre Anwendungen schneller und mit der erforderlichen Flexibilität und Skalierbarkeit bereitstellen und gleichzeitig den Wartungsaufwand für die Infrastruktur sehr gering halten. Diese Vorteile sind im Edge-Computing sehr wünschenswert, da sich ständig ändernde Technologien und Anforderungen schnell umgesetzt werden müssen und die Fluktuation und Heterogenität der Service-Consumer ein wichtiger Faktor ist. Edge-Nodes können jedoch häufig nur einen Bruchteil der Leistung von Cloud-Computing-Infrastruktur bereitstellen, was die Ausführung herkömmlicher FaaS-Plattformen unmöglich macht. In dieser Arbeit stellen wir einen neuen Ansatz für FaaS eine Platform vor, die von Grund auf unter Berücksichtigung von Edge-Computing- und IoT-Anforderungen entwickelt wurde. Um den Overhead so gering wie möglich zu halten, nutzen wir CoAP als Messaging-Protokoll und Docker, um Applikationen voneinander zu isolieren, während Container wiederverwendet werden, um die bestmögliche Leistung zu erzielen. Wir präsentieren auch eine Proof-of-Concept-Implementierung unseres Designs, die wir mit einem eigenen Benchmarking-Tool getestet haben, und vergleichen unsere Ergebnisse mit Benchmarks von Lean OpenWhisk, einer weiteren FaaS-Plattform für die Edge. Wir stellen fest, dass unsere Plattform Lean OpenWhisk in Bezug auf Latenz und Durchsatz in allen Tests übertreffen kann, Lean OpenWhisk jedoch höhere Erfolgsraten bei einer geringen Anzahl gleichzeitiger Clients aufweist.

Contents

1 Introduction

1.1 Problem Motivation & Description

The carbon footprint of information and communication technologies (ICT) continues to increase, despite the urgent imperative to decarbonize society and remain within planetary boundaries [citation]. A key driver of this trend is the exponential growth in data collection, storage, and processing across scientific disciplines [citation]. Scientific Workflow Management Systems (SWMSs) have become essential tools for managing this complexity, enabling researchers to exploit computing clusters for large-scale data analysis in domains such as remote sensing, astronomy, and bioinformatics [citation]. However, workflows executed through SWMSs are often long-running, resource-intensive, and computationally demanding, which translates into high energy consumption and substantial greenhouse gas emissions [citation]. Techniques to mitigate these impacts include energy-efficient code generation for workflow tasks and energy-aware scheduling strategies [citation]. Nevertheless, practitioners face challenges in assessing which approaches are most applicable, effective, and feasible to implement without excessive effort [52].

Scientific workflows have become a central paradigm for automating computational workloads on parallel and distributed platforms. With the rapid growth in data volumes and processing requirements over the last two decades, workflow applications have grown in complexity, while computing infrastructures have advanced in processing capacity and workload management capabilities. A critical component of this evolution is energy management, where scheduling and resource provisioning strategies are designed to maximize throughput while reducing or constraining energy consumption [citation]. In recent years, energy management in scientific workflows has gained particular importance, not only because of rising energy costs and sustainability concerns but also due to the pivotal role workflows play in enabling major scientific breakthroughs [20].

High-performance computing (HPC) refers to the pursuit of maximizing computational capabilities through advanced technologies, methodologies, and applications, enabling the solution of complex scientific and societal problems [citation]. HPC systems consist of large numbers of interconnected compute and storage nodes, often numbering in the thousands, and rely on job schedulers to allocate resources, manage queues, and monitor execution. While these infrastructures provide the backbone for highly demanding applications, their intensive power draw—arising not only from computation but also from networking, cooling, and auxiliary equipment—makes them major consumers of electricity and significant contributors to climate change [citation]. The demand for HPC continues to rise across both public and private sectors, fueled by emerging computationally intensive domains such as artificial intelligence, Internet of Things, cryptocurrencies, and 5G networks [citation]. The transition from petascale to exascale performance has amplified sustainability concerns, as operational costs approach parity with capital investment and energy efficiency becomes a limiting factor [citation]. Recent exascale systems exemplify this trend: while achieving unprecedented performance, they consume tens of megawatts of power and highlight the urgency of energy-aware design. To increase efficiency, modern HPC architectures increasingly integrate heterogeneous hardware, combining multicore CPUs with specialized accelerators such as GPUs, enabling more operations per second but also driving higher power densities at the node and rack level. This creates additional challenges for energy management and cooling, compounded by scheduling constraints and the demand for near-continuous system availability. Addressing these issues is essential to

ensure that future HPC developments meet performance goals without exacerbating their environmental footprint [49].

As scientific workflows grow in scale and complexity, coarse models of resource usage are no longer sufficient for ensuring efficient and sustainable execution. Tasks within data-driven workflows often appear in multiple instances and may vary substantially depending on input data, parameters, or execution environments. This results in highly dynamic patterns of resource demand, energy consumption, and carbon emissions, which fluctuate during runtime rather than remaining constant. At the same time, the carbon intensity of the underlying infrastructure changes over time, reflecting variations in energy availability and network conditions across sites. To address these challenges, there is a need for fine-grained, time-dependent task models that capture detailed resource usage profiles, incorporate infrastructure energy characteristics, and adapt dynamically during execution. Such models would enable more accurate task-to-machine mappings, informed scheduling decisions across multiple sites, and strategies for co-locating complementary tasks to reduce interference, energy waste, and communication overhead. Developing these models requires continuous monitoring of tasks, predictive techniques to handle incomplete prior knowledge, and adaptive mechanisms that respond in real time to evolving infrastructure conditions. Ultimately, this approach provides the foundation for carbon-aware workflow execution, where tasks are scheduled and allocated in ways that minimize energy consumption and associated emissions while maintaining performance and scalability. Task mapping addresses the challenge of assigning tasks to machines in a way that not only satisfies resource requirements but also minimizes energy consumption and carbon emissions. Traditional approaches largely focused on matching resource demands with machine capabilities, but they overlooked the variability in energy efficiency and carbon intensity over time. By leveraging fine-grained task models and infrastructure profiles, mappings can be extended to consider spatio-temporal variations in energy supply and demand. A key component of this is task co-location: strategically placing tasks on the same machine, within the same cluster, or in proximity across sites. When executed with awareness of complementary resource usage patterns, co-location reduces interference, avoids idle resource blocking, and lowers communication overhead, thereby improving both performance and energy efficiency. Together, advanced task mapping and co-location strategies provide a pathway toward reducing the carbon footprint of computational workflows while maintaining scalability and reliability.

Reducing power consumption while maintaining acceptable levels of performance remains a central challenge in containerized High Performance Computing (HPC). Existing approaches to Dynamic Power Management (DPM) typically rely on profile-guided prediction techniques to balance energy efficiency and computational throughput. However, in multi-tenant containerized HPC environments, this balance becomes significantly more complex due to heterogeneous user demands and contention over shared resources. These factors increase the difficulty of accurately predicting and managing power-performance trade-offs. Furthermore, while containerization frameworks such as Docker are widely adopted, they were not originally designed with HPC workloads in mind, leading to limited research and insufficient software-level mechanisms for monitoring and controlling power consumption in such environments [32].

Task clustering is a technique aimed at improving workflow efficiency by aggregating fine-grained computational tasks into larger units, commonly referred to as jobs. This aggregation reduces the overhead associated with scheduling numerous small tasks individually, which in turn lowers energy consumption and shortens the overall makespan of the work-

flow. By combining coarse-grained and fine-grained tasks into clustered jobs, resource utilization becomes more balanced, and the performance of workflow execution can be significantly enhanced [47].

This paper focuses on effective energy and resource costs management for scientific workflows. Our work is driven by the observation that tasks of a given workflow can have substantially different resource requirements, and even the resource requirements of a particular task can vary over time. Mapping each workflow task to a different server can be energy inefficient, as servers with a very low load also consume more than 50% of the peak power [8]. Thus, server consolidation, i.e. allowing workflow tasks to be consolidated onto a smaller number of servers, can be a promising approach for reducing resource and energy costs.

We apply consolidation to tasks of a scientific workflow, with the goal of minimizing the total power consumption and resource costs, without a substantial degradation in performance. Particularly, the consolidation is performed on a single workflow with multiple tasks. Effective consolidation, however, poses several challenges. First, we must carefully decide which workloads can be combined together, as the workload resource usage, performance, and power consumption are not additive. Interference of combined workloads, particularly those hosted in virtualized machines, and the resulting power consumption and application performance need to be carefully understood. Second, due to the time-varying resource requirements, resources should be provisioned at runtime among consolidated workloads.

We have developed pSciMapper, a power-aware consolidation framework to perform consolidation to scientific workflow tasks in virtualized environments. We first study how the resource usage impacts the total power consumption, particularly taking virtualization into account. Then, we investigate the correlation between workloads with different resource usage profiles, and how power and performance are impacted by their interference. Our algorithm derives from the insights gained from these experiments. We first summarize the key temporal features of the CPU, memory, disk, and network activity associated with each workflow task. Based on this profile, consolidation is viewed as a hierarchical clustering problem, with a distance metric capturing the interference between the tasks. We also consider the possibility that the servers may be heterogeneous, and an optimization method is used to map each consolidated set (cluster) onto a server. As an enhancement to our static method, we also perform time varying resource provisioning at runtime [61].

1.2 Research Question & Core Contributions

The central questions this thesis seeks to address are:

RQ1 How can fine-grained, time-dependent models of workflow tasks be developed to capture fluctuating patterns of computational resource usage and energy consumption during execution?

RQ2 How can the co-location of workflow tasks be modeled so that their interference is minimized and the resulting shared usage of resources leads to lower overall energy consumption and carbon emissions while performance is maintained?

RQ3 How can co-location models and time-dependent task characterizations be integrated into resource management systems and workflow scheduling frameworks to enable adaptive, energy-aware execution at scale?

The resulting core contributions of this thesis are:

- An architectural mapping that defines which layers of workflow execution need to be monitored and systematically assigns suitable data exporters to them
- The implementation of a monitoring client, capable of serving the relevant monitoring layers for scientific workflow execution which collects fine-grained, time-dependent resource usage data for workflow tasks during execution that was used for data collection on running 10 nf-core pipelines.
- An analysis of co-location effects on the core and node-level that are later on used for implementing the proposed co-location approach.
- The design and implementation of a novel co-location approach that utilizes time series data to compute for any given set of tasks clusters where the resource usage patterns are complementary.
- The application of 2 multivariate, statistical learning methods on the time series data of the workflow tasks: Kernel Canonical Correlation Analysis (KCCA) and Random Forest Regressor (RFR).
- The development of an evaluation test-bed in the WRENCH simulation framework that integrates the proposed co-location approach and allows for the simulation of scientific workflow execution with and without co-location.
- The evaluation of the proposed co-location approach using 10 nf-core workflows, demonstrating its effectiveness in reducing energy consumption while maintaining performance.

1.3 Structure of the Thesis

The remainder of this thesis is structured as follows: Chapter 2 presents the fundamentals of this work, covering scientific workflow systems, the co-location problem, cluster resource management, machine learning and more. Chapter 3 introduces related work for monitoring scientific workflows, modeling the co-location of tasks and enabling energy-awareness through minimizing resource contention. In addition, the main state-of-the-art approaches for the co-location problem are presented. Furthermore, Chapter 4 depicts the approach to the problem in both a theoretical and practical manner and ultimately defines requirements for the realization of the approach. The corresponding implementation is elaborated in Chapter 5. Moreover, Chapter 6 evaluates the models compared to the state-of-the-art approaches using a simulation. Chapter 7 interprets the key findings and discusses some limitations of this work. Finally, Chapter 8 concludes this thesis and gives an outlook on the impact of this work for the future.

2 Background

This chapter provides the necessary background and concepts that are applied in **??** of this thesis. The sections will cover general concepts of High-Performance Computing and Scientific Workflows and will further elaborate on Monitoring, Co-location, and Machine Learning techniques applied in this work.

2.1 High Performance Computing

High-Performance Computing (HPC) encompasses a collection of interrelated disciplines that together aim to maximize computational capability at the limits of current technology, methodology, and application. At its core, HPC relies on specialized electronic digital machines, commonly referred to as supercomputers, to execute a wide variety of computational problems or workloads at the highest possible speed. The process of running such workloads on supercomputers is often called supercomputing and is synonymous with HPC. The fundamental purpose of HPC is to address questions that cannot be adequately solved through theory, empiricism, or conventional commercial computing systems. The scope of problems tackled by supercomputers extends beyond traditional scientific and engineering applications to include challenges in socioeconomics, the natural sciences, large-scale data management, and machine learning. An HPC application refers both to the problem being solved and to the body of code, or ordered instructions, that define its computational solution [51].

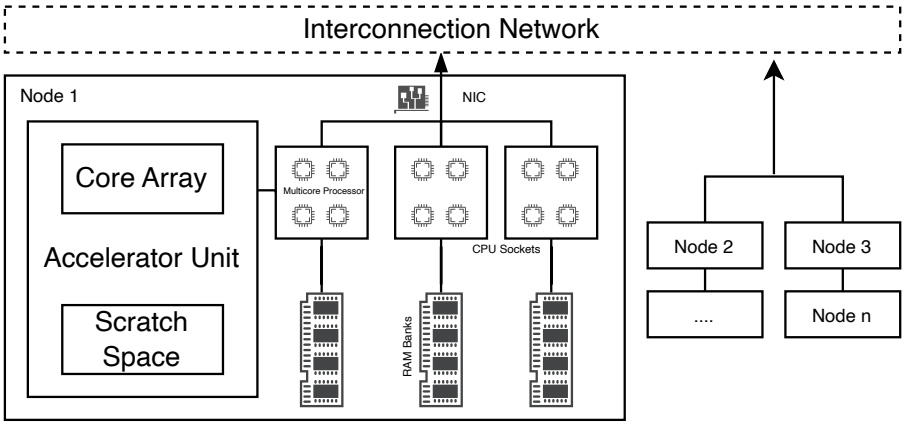

Figure 2.1: HPC Architecture
High-level Architecture of a HPC Data Center.

What distinguishes HPC systems from conventional computers is their organization, interconnectivity, and scale. Here, scale refers to the degree of both physical and logical parallelism: the replication of essential physical components such as processors and memory banks, and the partitioning of tasks into units that can be executed simultaneously. While parallelism exists in consumer devices like laptops with multicore processors, HPC systems exploit it on a vastly larger scale, structured across multiple hierarchical levels. Their supporting software is designed to orchestrate and manage operations at this level of complexity, ensuring efficient execution across thousands of interconnected components.

2.1.1 Modern HPC Hardware

High-performance computing (HPC) architecture defines how supercomputers are structured, how their components interact, and which instruction set architecture (ISA) they expose to the applications running on them. It is designed to use underlying hardware technologies efficiently to minimize time to solution, maximize computational throughput, and support large-scale, computation-intensive workloads. Increasingly, HPC systems are also used for data-intensive tasks such as big data analytics and graph processing. In both domains, the architecture is built to mitigate major performance bottlenecks such as latency, overhead, contention, and idle resources, while ensuring reliability and energy efficiency within the required performance and data constraints.

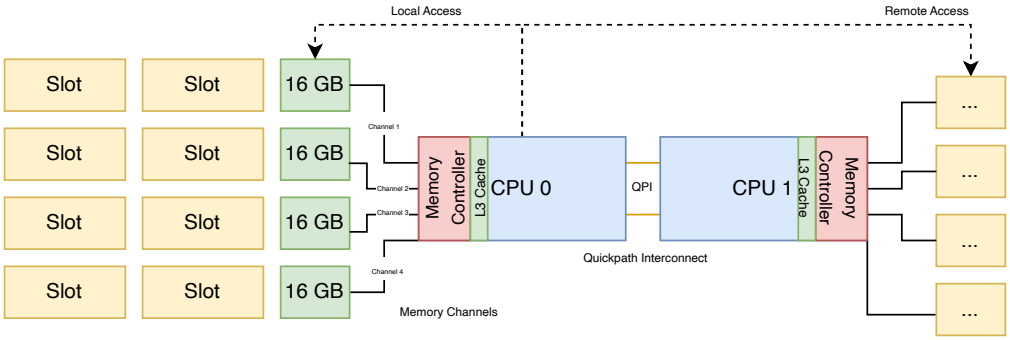

Figure 2.2: NUMA Core
NUMA Core Architecture showing Local and Remote Memory Access.

The performance of an HPC system depends largely on the speed and coordination of its components, with processor clock frequency playing a central role. A major challenge stems from the disparity between the rapid operation of processor cores and the comparatively slow access times of main memory (DRAM). To address this imbalance, modern architectures employ hierarchical memory systems that combine large DRAM capacities with faster SRAM cache layers. System performance is further influenced by communication efficiency, determined by bandwidth and latency, which vary across technologies and physical distances. Overall, HPC architectures aim to balance computation, memory, and communication performance while maintaining reasonable cost, power consumption, and ease of use to achieve high application throughput.

Power consumption is a critical factor in HPC, as processors, memory, interconnects, and I/O devices all require electricity, and the resulting heat must be removed to avoid failure. Air cooling suffices for smaller systems, but high-density, high-performance systems increasingly rely on liquid cooling to achieve higher packing density and performance. Modern processors further support power management through dynamic voltage and frequency scaling, variable core activation, and thermal monitoring. These mechanisms enable a balance between power consumption and performance, guided by software that can set or adjust configurations at runtime based on workload demands.

The multiprocessor class of parallel computer represents the dominant architecture in contemporary supercomputing. Broadly defined, it consists of multiple independent processors, each with its own instruction control, interconnected through a communication network and coordinated to execute a single workload. Three main configurations of multiprocessor systems exist: symmetric multiprocessors (SMPs), massively parallel processors (MPPs), and commodity clusters. The distinction lies in memory organization. SMPs use

a shared memory model accessible by all processors, MPPs assign private memory to each processor, and cluster-based designs combine both approaches by grouping processors into nodes that share memory locally while maintaining separation across nodes. Modern multicore systems often follow this hybrid structure, balancing performance, scalability, and complexity. Nonuniform memory access (NUMA) architectures extend shared-memory designs by allowing all processors to access the full memory space but with different access times depending on locality. NUMA leverages fast local memory channels alongside slower global interconnects, enabling greater scalability than SMPs.

2.1.2 Virtualization in HPC

With the growing demand for HPC, hardware resources have continued to expand in scale and complexity, with increasingly intricate interconnections between system components. A central challenge lies in maximizing both performance and resource utilization. Virtualization technologies offer a means to improve resource utilization in HPC environments, but often at the cost of performance overhead. Multi-user usage scenarios, combined with the stringent performance requirements of HPC workloads, place high demands on virtualization approaches. Furthermore, the highly customized nature of HPC systems complicates the integration of virtualization solutions. Virtualization enables the provisioning of resources to multiple users on the same physical machine with the goal of maximizing utilization. Depending on the abstraction layer, different virtualization technologies provide distinct benefits. Containers, which virtualize at the operating system level, offer lightweight isolation and have become widely adopted for deploying microservices.

Containers studies have shown that container performance often approaches native execution, particularly for CPU- and memory-intensive workloads, whereas VMs tend to suffer greater degradation for memory, disk, and network-intensive applications. In comparative analyses, Docker containers have demonstrated near-native efficiency for CPU and memory tasks but exhibit performance bottlenecks in certain networking and storage configurations [24].

In HPC the application-level virtualization operates above the kernel layer, sharing both the kernel and underlying hardware. This approach is most prominently represented by containers, with Docker introducing a transformative model of packaging and deployment. By encapsulating application dependencies into images and leveraging ecosystems such as Docker Hub, Docker enables rapid and portable application deployment through resource managers like Slurm. Container solutions support multiple container image formats, including compatibility with Docker images, and efficient integration with HPC resource managers. Its design ensures that containers incur minimal overhead, as virtualization occurs only at the application level with a shared kernel, making it particularly well-suited for HPC contexts where performance efficiency is critical.

2.2 Scientific Workflows

2.2.1 Scientific Workflow Management Systems

Scientific Workflow Management Systems (SWMSs) enable the composition of complex workflow applications by connecting individual data processing tasks. These tasks, often treated as black boxes, can represent arbitrary programs whose internal logic is abstracted away from the workflow system. The resulting workflows are typically modeled as directed acyclic graphs (DAGs), where channels define the dependencies between tasks: the output

of one task serves as the input for one or more downstream tasks. This abstraction allows users to design scalable, reproducible workflows while managing execution complexity across diverse computational environments [52].

Scientific Workflow Management Systems (SWMSs) provide a simplified interface for specifying input and output data, enabling domain scientists to integrate and reuse existing scripts and applications without rewriting code or engaging with complex big data APIs. This abstraction lowers the entry barrier for developing and executing large-scale workflows [5].

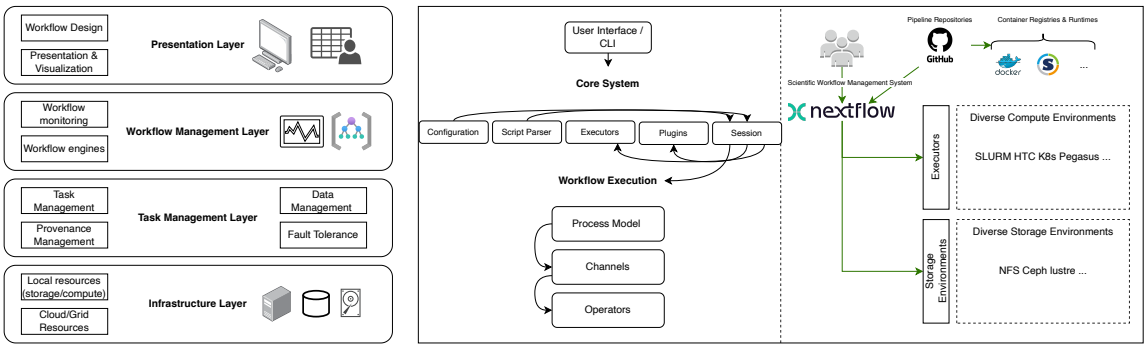

Figure 2.3: Scientific Workflow Management System
Structured Components of an exemplified Scientific Workflow Management System.

2.2.2 Examples of Scientific Workflows

Scientific workflows are compositions of sequential and concurrent data processing tasks, whose order is determined by data interdependencies. A task is the basic data processing component of a scientific workflow, consuming data from input files or previous tasks and producing data for follow- up tasks or output files. Scientific workflows exist at different levels of abstraction: abstract, concrete, and physical. An abstract workflow models data flow as a concatenation of conceptual processing steps. Assigning actual methods to abstract tasks results in a concrete workflow. To execute a concrete workflow, input data and processing tasks have to be assigned to physical compute resources. In the context of scientific workflows, this assignment is called scheduling and task mapping and results in a physical and executable workflow [15].

2.2.3 Scientific Workflow Tasks

Workflow applications are typically executed per input, or per set of related inputs, enabling coarse-grained data parallelism at the application level. Multiple tasks can run concurrently if independent inputs are processed by the same workflow, and parallelism also arises within a single input when workflow graphs fork, allowing downstream tasks to execute simultaneously. Conversely, many workflows begin with parallel execution of different tasks whose outputs are later joined, synchronizing multiple workflow paths. Due to their complexity and scale, workflows often consist of large numbers of tasks with multiple parallel paths and are executed on clusters—collections of interconnected compute nodes managed as a single system. SWMS's submit ready-to-run tasks to cluster resource managers such as Slurm or Kubernetes, which allocate resources according to user-defined requirements like CPU cores and memory. Task communication is typically implemented via persistent cluster storage systems like Ceph, HDFS, or NFS, where intermediate data is written and read between tasks [52].

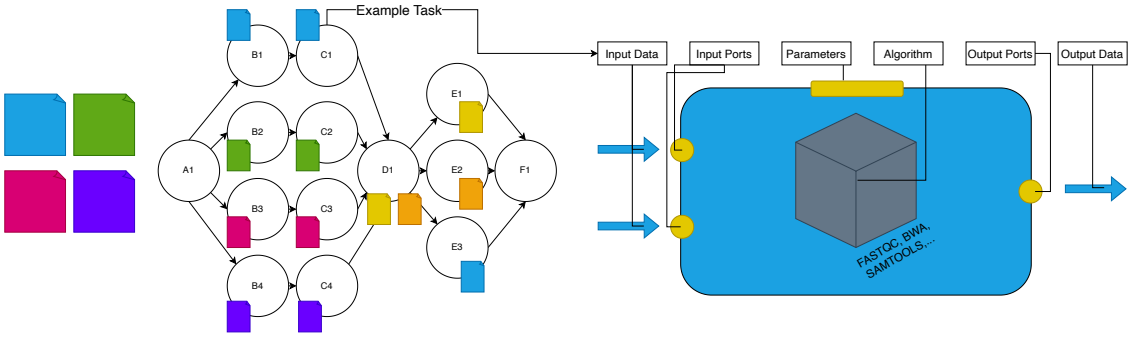

Figure 2.4: Workflow Task

A Scientific Workflow Task as part of a Workflow consuming input data and producing output data.

2.3 Monitoring of Scientific Workflows

Performance monitoring is a critical stage in application development, extending beyond functional correctness and validation of results. Even after thorough testing with diverse datasets and computational modes, hidden inefficiencies may remain that limit the applications ability to fully exploit the underlying hardware. Monitoring helps ensure that performance is not degraded by preventable factors, for example by checking whether computation times match processor capabilities or whether communication delays align with message sizes and network bandwidth. Instrumentation of code segments can provide such insights, though even basic measurements introduce latency and overhead that may distort results or even alter execution flow. Hardware-based approaches use modern CPUs to provide dedicated performance counters for events such as instruction retirement, cache misses, or branches. These counters operate transparently, incurring virtually no overhead, though they are limited to a predefined set of measurable events.

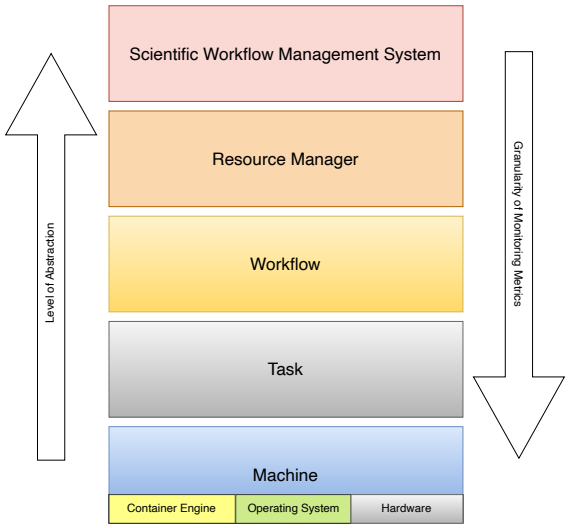

Figure 2.5: Monitoring Layers

Monitoring Layers in Scientific Workflows.

2.3.1 Distinct Monitoring Layers

Highl-level Monitoring While general HPC performance monitoring tools can provide detailed insights into system resource usage, linking these measurements to higher-level

abstractions such as workflow tasks remains challenging. In large-scale scientific workflows executed on distributed environments tasks may be scheduled on arbitrary nodes and may even share resources with other tasks. As a result, locally observed traces of CPU, memory, or I/O usage cannot be directly attributed to specific tasks. Moreover, metrics natively provided by workflow management systems are often coarse-grained, capturing only summary statistics for task lifetimes. To obtain fine-grained insights into task-level behavior, additional instrumentation and mapping strategies are required to connect low-level monitoring data with workflow abstractions. To deal with this lack of information, resource usage profiles from compute nodes must be correlated with metadata such as workflow logs or job orchestrator information [57].

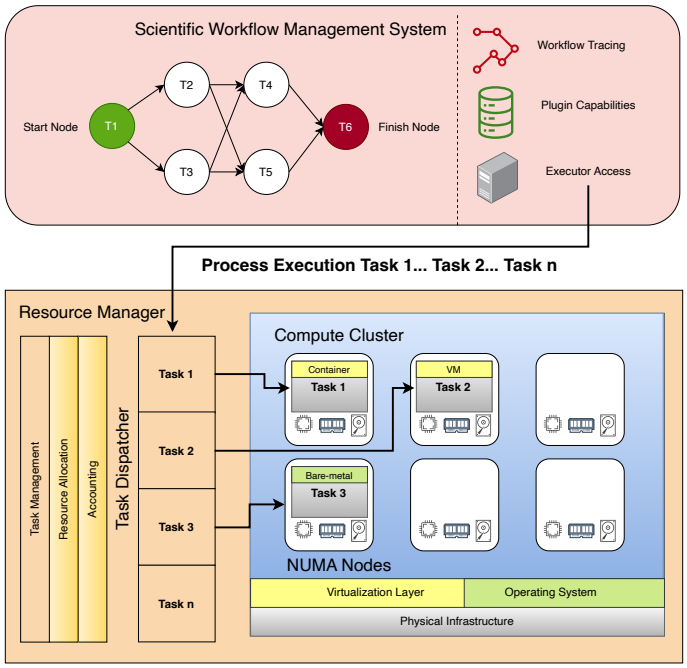

Figure 2.6: Monitoring Layers in Action.
Monitoring Layers during Workflow Execution.

To bridge this gap,proposed an architectural blueprint for workflow monitoring organized into four layers: the resource manager, the workflow, the machine, and the task layer. These layers represent logical distinctions within a scientific workflow execution environment, each focusing on a different monitoring subject and retrieving metrics from lower layers as needed. Unlike user-centric designs, this approach emphasizes system components rather than interaction flows. Higher layers provide increasingly abstract views, relying only on selected metrics from underlying layers while, in theory, being able to access all. For instance, at the resource manager level, systems such as Slurm, Kubernetes, or HTCondor only require aggregate metrics like task resource consumption or available machine resources, without depending on fine-grained traces such as syscalls. The workflow layer captures metrics tied to the workflow specification, while the machine layer delivers detailed reports of node-level resource usage. At the lowest level, the task layer focuses on fine-grained task execution metrics. Together, this hierarchy balances abstraction and granularity, ensuring that relevant monitoring information is exposed at the appropriate level to support both workflow execution and performance optimization [5].

Low-level Resource Monitoring Monitoring scientific workflows requires tools that can capture and relate information across different components of a computing system, since no single perspective provides sufficient detail for effective optimization. Low-level system monitors can reveal CPU, memory, or I/O usage but lack awareness of which workflow tasks generate that load, while workflow management systems expose task-level metrics that are often too coarse to identify inefficiencies. In the following, we briefly discuss tools and approaches for monitoring the low layers.

Central among low-level techniques is tracing, which captures fine-grained event-based records such as system calls, I/O operations, or network packets. Tracing provides detailed raw data, often with high volume, that can either be post-processed into summaries or analyzed on the fly using programmatic tracers such as those enabled by the Berkeley Packet Filter (BPF). BPF allows small programs to run directly in the kernel, making it possible to process events in real time and reduce the overhead of storing and analyzing massive trace logs. In contrast, sampling tools collect subsets of data at regular intervals to create coarse-grained performance profiles. While sampling introduces less overhead than tracing, it provides only partial insights and can miss important events. Together with fixed hardware or software counters, tracing and sampling form the backbone of observability—the practice of understanding system behavior through passive observation rather than active benchmarking. The BPF ecosystem provides several user-friendly front ends for tracing, most notably BCC (BPF Compiler Collection) and bpftrace. BCC was the first higher-level framework, offering C-based kernel programming support alongside Python, Lua, and C++ interfaces, and it introduced the libbcc and libbpf libraries that remain central to BPF instrumentation. It also provides a large collection of ready-to-use tools for performance analysis and troubleshooting [25].

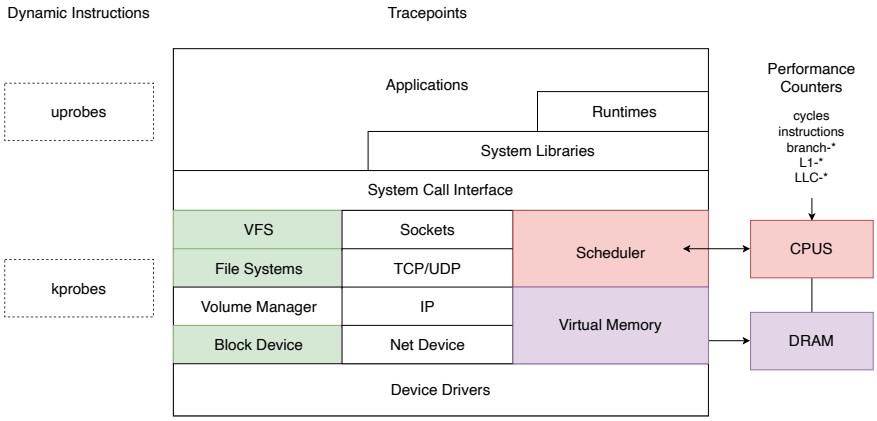

Figure 2.7: Low Level Monitoring Targets.
Low Level Monitoring Targets on the OS-Level using eBPF.

CPU, memory, and disk are central components for understanding system behavior. Monitoring the CPU usage fundamentally relies on understanding how time is distributed across the execution modes and how the scheduler allocates processor resources among competing tasks. Metrics such as user time, system time, and idle time provide the basis for identifying imbalances, while additional indicators like context switches, interrupt handling, and run queue lengths reveal how efficiently the scheduler manages concurrency. Since background kernel activities and hardware interrupts can consume significant CPU cycles outside of explicit user processes, distinguishing their contribution is essential for accurate

analysis. Additional steps include measuring time spent in interrupts, exploring hardware performance counters like instructions per cycle (IPC), and using specialized BPF tools for deeper insights into stalls, cache behavior, or kernel overhead. This structured approach helps progressively narrow down the root causes of performance issues. In close relation to CPU monitoring, effective memory performance analysis requires tracking how memory behavior influences compute efficiency. Since CPUs frequently stall waiting for data, metrics such as page faults, cache misses, and swap activity can directly translate into wasted cycles. A systematic strategy begins with checking whether the out-of-memory (OOM) killer has been invoked, as this signals critical memory pressure. From there, swap usage and I/O activity should be examined, since heavy swapping almost always leads to severe slowdowns. System-wide free memory and cache usage provide a high-level view of available resources, while per-process metrics help identify applications with excessive resident set sizes (RSS). Following CPU and memory, file system monitoring focusen on workload behavior at the logical I/O layer and its interaction with caches and the underlying devices. Key signals include operation mix and rates such as reads, writes, opens/closes and latency distributions for I/O, and the balance of synchronous versus asynchronous writes. Cache effectiveness is central: track page-cache hit ratios over time, read-ahead usefulness (sequential vs random access), volumes of dirty pages and write-back activity, and directory/inode cache hit/miss rates [cite].

From a performance monitoring perspective, containers introduce challenges that extend beyond those encountered in traditional multi-application systems. First, cgroups may impose software limits on CPU, memory, or disk usage that can constrain workloads before physical hardware limits are reached. Detecting such throttling requires monitoring metrics that are not visible through standard process- or system-wide tools. Second, containers can suffer from resource contention in multi-tenant environments, where noisy neighbors consume disproportionate shares of the available resources, leading to unpredictable performance degradation for co-located containers. A further complication lies in attribution. The Linux kernel itself does not assign a global container identifier. Instead, containers are represented as a combination of namespaces and cgroups, which complicates mapping low-level kernel events back to the higher-level abstraction of a specific container. While some workarounds exist—such as deriving identifiers from PID or network namespaces, or from cgroup paths—this mapping is non-trivial and runtime-specific. To address these issues, container monitoring must operate at multiple levels of abstraction. Metrics must capture both coarse-grained resource usage across cgroups and fine-grained kernel events such as scheduling latencies, memory allocation faults, and block I/O delays. At the same time, the collected data needs to be attributed correctly to the corresponding container environment in order to identify interference, diagnose bottlenecks, and evaluate orchestration policies. Monitoring hypervisors poses challenges similar to containers but with a different focus. Since each VM runs its own kernel, guest-level monitoring tools can operate normally, but they cannot always observe the virtualization overheads introduced by the hypervisor. Key concerns include the frequency and latency of hypercalls in paravirtualized environments, the impact of hypervisor callbacks on application scheduling, and the amount of stolen CPU time—periods when a guests vCPU is preempted by the hypervisor. From the host perspective, additional events such as VM exits provide insight into how often guests trigger traps to the hypervisor, for example on I/O instructions or privileged operations, and how long these exits last. Attribution is further complicated because exit reasons vary widely across workloads and hypervisor implementations. Effective analysis therefore requires combining guest-side monitoring of virtualized resources with host-side tracing of hypervisor interactions. Guest instrumentation can measure hypercall behav-

ior, detect high callback overheads, or quantify CPU steal time, while host tracing can expose exit patterns, QEMU-induced I/O delays, and hypervisor scheduling effects. As with containers, BPF-based tracing has become particularly valuable in this domain, since it can capture low-level kernel events with high resolution, linking them to hypervisor operations. With the shift toward hardware-assisted virtualization, fewer hypervisor-specific events remain visible to the guest, making host-level tracing and cross-layer correlation increasingly central to performance monitoring of virtualized environments.

2.3.2 Monitoring Energy Consumption

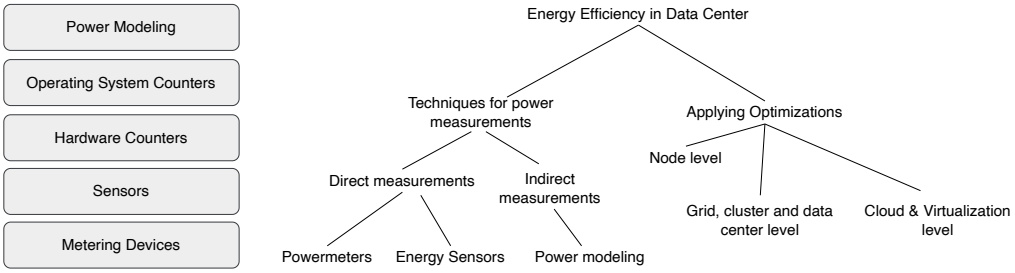

Figure 2.8: Power Measurements in Data Center.
Different Levels and Means of increasing energy efficiency in data centers.

Accurate and fine-grained energy monitoring is essential for improving the efficiency of HPC and data center systems. Traditional measurement methods, such as external power meters or chassis-level sensors, provide reliable but coarse readings at the node or rack level. These approaches are often expensive, intrusive, and insufficient for attributing power consumption to individual components or workloads. To achieve higher accuracy and temporal resolution, modern systems increasingly rely on hardware-assisted mechanisms and integrated interfaces that directly expose energy metrics from within the processor.

The most widely used of these interfaces is Intel's Running Average Power Limit (RAPL), introduced with the Sandy Bridge architecture. RAPL provides direct access to cumulative energy consumption for various hardware domains, including the CPU package, cores, integrated GPU, and DRAM. In newer architectures such as Skylake, an additional PSys domain represents the overall system-on-chip energy use. Each domain reports energy data through model-specific registers (MSRs) that can be read at millisecond-level resolution. These measurements can be accessed using the Linux MSR driver, the sysfs interface, performance monitoring tools like perf, or libraries such as PAPI. RAPL's low overhead and high sampling rate have made it a standard component of modern HPC monitoring frameworks, supporting tasks from energy profiling and performance analysis to power-aware scheduling. While originally an Intel-specific technology, RAPL functionality is also available on AMD Zen architectures, although with limited support for energy domains compared to Intel implementations.

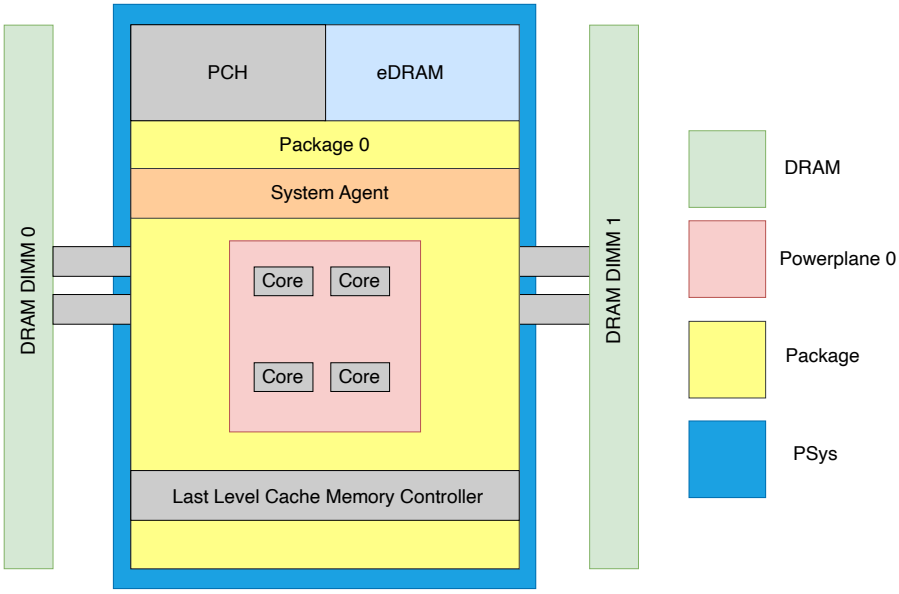

Figure 2.9: RAPL Domains
Overview of RAPL Energy Domains measured on a Processor.

As containerization becomes standard in HPC and cloud infrastructures, energy attribution must extend from node-level to container-level granularity. Workflows composed of numerous short-lived and heterogeneous tasks require monitoring that captures both process-level activity and resource-specific energy usage. Integrating RAPL data with container-level metrics bridges this gap, enabling per-task and per-workflow energy accounting. Tools such as DEEP-mon build on RAPL by combining kernel-level event tracing with container-level aggregation. They can attribute energy consumption to threads, processes, or containers in real time while maintaining low system overhead. Such tools extend traditional monitoring from static node metrics to dynamic, workload-aware measurements suitable for modern, containerized HPC environments. This integration of hardware-assisted measurement and software-level attribution forms the basis for energy-aware orchestration and supports the development of sustainable, performance-efficient scientific computing systems.

2.4 The Co-location Problem

The problem of co-location can be traced back to classical operating system scheduling, where the core challenge lies in allocating activities to functional units in both time and space. Traditionally, scheduling in operating systems refers to assigning processes or threads to processors, but this problem appears at multiple levels of granularity, from whole programs to fine-grained instruction streams executed within superscalar architectures. On multiprocessor and multicore systems, the scheduler must not only decide when to run a task but also where, since shared caches, memory bandwidth, and execution units create interdependencies between co-located workloads. Early work in operating systems introduced co-scheduling or gang scheduling, where groups of related tasks are executed simultaneously to reduce synchronization delays, exploit data locality, and minimize contention for shared resources. These concepts are directly relevant to modern scientific

workflows, where multiple interdependent tasks are often co-located on the same nodes or cores in high-performance computing environments. The performance and energy efficiency of workflows are therefore closely tied to scheduling decisions, as co-located tasks may either benefit from shared resource usage or suffer from interference, making scheduling a fundamental problem for efficient workflow execution. Building on the challenges of co-location in multi-core systems, the problem becomes even more pronounced when considering scientific workflows, which consist of heterogeneous tasks with highly variable and dynamic resource requirements. Assigning each task to a separate server leads to poor energy efficiency, as servers continue to draw a substantial fraction of their peak power even under low utilization. Server consolidation thus emerges as a promising strategy, where multiple workflow tasks are mapped onto fewer servers to reduce total power consumption and resource costs. In this context, the terms consolidation and co-location can be used interchangeably, as both refer to the placement of multiple tasks onto the same physical resources with the aim of improving efficiency. However, consolidation is far from trivial: the resource usage of colocated tasks is not additive, and interference effects can significantly impact both power consumption and application performance. Furthermore, the temporal variation in workflow task demands requires runtime-aware provisioning strategies to avoid resource contention and performance degradation [61]

2.4.1 Impacts of Co-location on Resource Contention and Interference

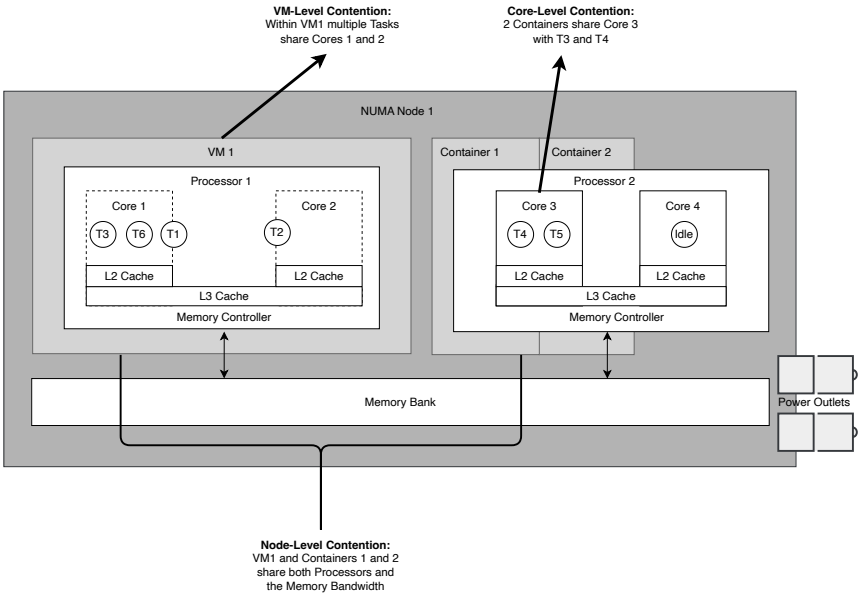

Figure 2.10: The Co-location Problem.
Different Levels of Co-location on a Compute Node.

The fundamental motivation for addressing co-location in HPC and cloud environments lies in the problem of resource contention. When processes execute on different cores of the same server, they inevitably share hardware resources. Modern multi-core architectures specifically processors share on-chip structures such as last-level caches, memory controllers, and interconnects, as well as off-chip memory bandwidth, creating significant opportunities for contention when multiple applications run concurrently. This contention can result in severe performance degradation, making it critical to understand and predict the impact of co-location on application efficiency.This sharing often leads to interference,

slowing down execution compared to scenarios where tasks have exclusive access to these resources. In extreme cases, memory traffic contention has been shown to cause super-linear slowdowns, where execution times more than double, making sequential execution more efficient than poorly chosen co-schedules. For large-scale systems hosting thousands of tasks, this contention complicates job scheduling, as schedulers must avoid placing workloads that compete heavily for the same resources. Without accurate estimates of resource usage or slowdown potential, scheduling decisions risk becoming guesswork, reducing overall efficiency. Importantly, poor scheduling is not limited to high-resource applications: even pairing computationally bound tasks that do not interfere can be suboptimal if it prevents beneficial co-scheduling with memory-bound applications. This highlights that effective co-location must avoid both high-contention pairings and missed opportunities for complementary workload placement [10] [53].

2.4.2 Shared Aspects and Distinctions from Scheduling and Task Mapping

Co-location differs fundamentally from scheduling and task mapping, even though all three aim to improve performance and energy efficiency in workflow execution. Scheduling determines when each task runs, while mapping decides where each task is placed. In contrast, co-location focuses on how tasks interact when they are executed simultaneously on shared resources. Scheduling and mapping operate primarily at the planning level—deciding task order and resource assignment to optimize overall throughput, energy use, or completion time. Co-location, however, concerns the execution-level effects that arise once multiple tasks occupy the same physical resources. It addresses the contention for shared hardware components such as caches, memory bandwidth, interconnects, and I/O subsystems. While scheduling seeks to allocate time and space efficiently, co-location must manage interference that emerges during concurrent execution. Poor co-location decisions can negate the benefits of an otherwise optimal schedule by causing resource contention, latency, or performance degradation. Therefore, co-location is not an extension of scheduling but a complementary consideration that governs how shared resource usage affects the actual efficiency and energy behavior of scheduled tasks.

2.5 Machine Learning Techniques applied in HPC

2.5.1 Intelligent Resource Management

When executing scientific workflows on large-scale computing infrastructures, researchers are required to define task-level resource limits, such as execution time or memory usage, to ensure that tasks complete successfully under the control of cluster resource managers. However, these estimates are often inaccurate, as resource demands can vary significantly across workflow tasks and between different input datasets, leading either to task failures when limits are underestimated or to inefficient overprovisioning when limits are set too conservatively. Overprovisioning, while preventing failures, reduces cluster parallelism and throughput, as excess resources are reserved but left unused, while incorrect runtime estimates can distort scheduling decisions and degrade overall system efficiency. To address this, recent research has explored workflow task performance prediction as a means to automate the estimation of runtime, memory, and other resource needs. Machine learning plays a central role in these efforts, with approaches ranging from offline models trained on historical execution data, to online models that adapt dynamically during workflow execution, to profiling-based methods applied before execution. Performance prediction models can integrate into both workflow management systems and resource managers,

enabling more informed scheduling, efficient resource utilization, and improved energy- and cost-aware computing [**bader2025predictingperformancescientificworkflows**] [58].

2.5.2 Utilized Machine Learning Models in this Thesis

Ordinary Least Squares and Extensions

Kernel Ridge Regression

Kernel Ridge Regression (KRR) builds on ordinary least squares (OLS) regression. OLS learns a linear relationship between input variables and a target variable by minimizing the squared difference between predictions and actual values. Ridge regression extends OLS by adding a penalty to the model coefficients, which controls overfitting and improves stability when features are correlated or data are noisy. KRR further extends ridge regression by applying the kernel trick. Instead of fitting a linear model directly in the input space, KRR implicitly maps the data into a high-dimensional feature space defined by a kernel function, such as a Gaussian or polynomial kernel. A linear model is then learned in this new space, which corresponds to a nonlinear function in the original space when a nonlinear kernel is used. Overall, Kernel Ridge Regression combines the simplicity and stability of ridge regression with the flexibility of kernel-based learning to model nonlinear relationships effectively.

Kernel Canonical Correlation Analysis

Kernel Canonical Correlation Analysis (KCCA) is a statistical technique designed to identify and maximize correlations between two sets of variables. Unlike Principal Component Analysis, which focuses on variance within a single dataset, CCA aims to find linear projections of two datasets such that their correlation is maximized. The result is a set of canonical variables that capture the strongest relationships between the two domains. KCCA extends this idea by applying kernel methods, allowing the detection of nonlinear relationships. In KCCA, the data are implicitly mapped into high-dimensional feature spaces through kernel functions, and correlations are then maximized in that transformed space. This enables KCCA to capture more complex dependencies than linear CCA, making it particularly powerful in settings where relationships between datasets are not strictly linear [4] [61].

Random Forest Regression

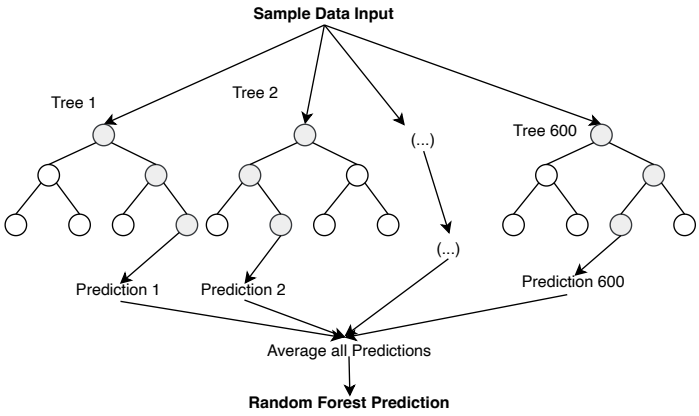

Figure 2.11: Random Forest Procedure
The iterative process of building a Random Forest for prediction.

A Random Forest Regressor is an ensemble learning method that builds multiple decision tree regressors on random subsets of the training data and combines their predictions through averaging. This approach reduces variance compared to a single decision tree, improving predictive accuracy and robustness against overfitting. Each tree is constructed using the best possible splits of the features, while the randomness introduced through bootstrap sampling and feature selection ensures diversity among the trees. An additional advantage is the native handling of missing values. During training, the algorithm learns how to direct samples with missing entries at each split, and during prediction, such samples are consistently routed based on the learned strategy. This makes Random Forest a flexible and powerful method for regression tasks with heterogeneous and potentially incomplete data [12].

Agglomerative Clustering

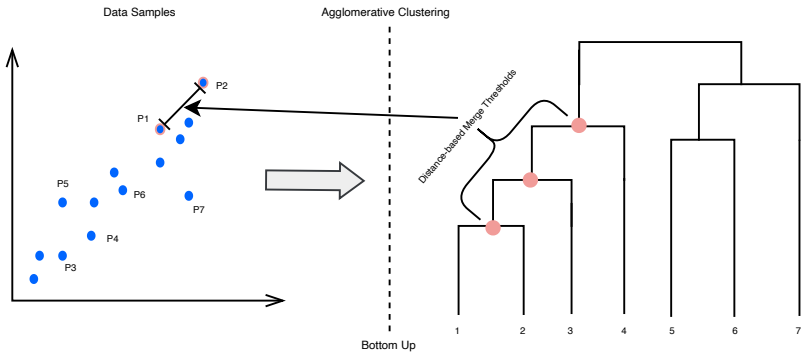

Figure 2.12: Agglomerative Clustering Procedure
Agglomerative Clustering applied on a distribution using a distance criterion.

Agglomerative clustering, also called hierarchical clustering is a family of algorithms that group data into nested clusters, represented as a tree-like structure called a dendrogram. In this hierarchy, each data point starts as its own cluster, and clusters are successively merged until all points form a single cluster. The commonly used agglomerative approach follows this bottom-up process, with the merging strategy determined by a chosen linkage criterion. Ward linkage minimizes the total variance within clusters, producing compact

and homogeneous groups, while complete linkage minimizes the maximum distance between points in different clusters, emphasizing tight cluster boundaries. Average linkage instead considers the mean distance across all points between clusters, and single linkage focuses on the minimum distance, often resulting in elongated or chain-like clusters. Although flexible, agglomerative clustering can be computationally expensive without additional constraints, as it evaluates all possible merges at each step.

2.6 Research-oriented Simulation of Distributed Computing

Scientific workflows have become essential in modern research across many scientific domains, supported by SWMSs that automate resource selection, data management, and task scheduling to optimize performance metrics such as latency, throughput, reliability, or energy consumption. Despite significant engineering progress in WMS design, many fundamental challenges remain unresolved, as theoretical approaches often rely on assumptions that fail to hold in production infrastructures. As a result, most improvements in WMS algorithms and architectures are evaluated experimentally on specific platforms, workflows, and implementations, which makes systematic evaluation and fair comparisons difficult. Addressing this limitation, WRENCH was introduced as a simulation framework that provides accurate, scalable, and expressive experimentation capabilities. Built on SimGrid, WRENCH abstracts away the complexity of simulating distributed infrastructures while preserving realistic models of computation, communication, storage, and failures. It provides a Developer API for implementing simulated WMSs and a User API for creating simulators that run workflows on simulated platforms with minimal code. Through these abstractions, WRENCH allows researchers to test scheduling, resource allocation, and fault-tolerance strategies at scale without the prohibitive cost of real-world deployments. Importantly, WRENCH supports a wide range of distributed computing scenarios, including cloud, cluster, and HPC environments, enabling reproducible and comparative studies of WMS design choices. By lowering the barrier to simulating complex workflows and providing visualization and debugging tools, WRENCH facilitates the systematic exploration of workflow scheduling, performance prediction, and energy-aware computing strategies in controlled yet realistic settings [16].

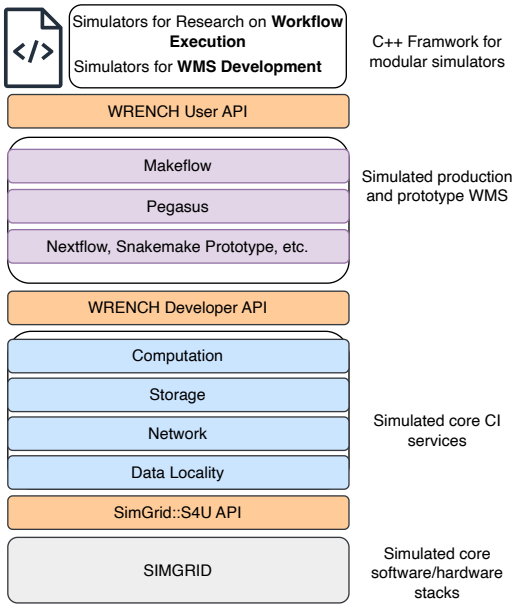

Figure 2.13: WRENCH
The WRENCH framework's layered architecture.

3 Related Work

The following section introduces related research that has informed and inspired the development of this thesis. It reviews selected works addressing key themes such as workflow monitoring, performance modeling, and scheduling in distributed environments. Much prior research has focused on co-scheduling in high-performance computing (HPC) at the operating system level, on contention management between batch workloads and long-running latency-critical services in cloud data centers, or on multi-objective optimization and metaheuristic approaches for job placement. In contrast, this thesis takes a novel perspective by combining machine learningbased scheduling with online consolidation techniques, explicitly targeting scientific workflows in HPC cluster environments. By embedding this adaptive scheduling logic within a simulation framework that captures resource contention and task-level dynamics, the work extends beyond existing literature and, to the best of our knowledge, represents the first integrated exploration of learning-driven, contention-aware scheduling for workflow execution in simulated HPC systems.

Bader et al. present a conceptual framework for advanced monitoring in scientific workflow environments, emphasizing the heterogeneity of metrics and abstraction layers involved in large-scale workflow execution. Their work identifies four distinct monitoring layers—spanning from infrastructure-level telemetry to workflow-level behavior—and positions these as an architectural blueprint for integrating and correlating performance observations across distributed systems. The authors analyze several state-of-the-art workflow management systems to assess their monitoring capabilities and to highlight existing fragmentation in metric collection and interpretation. Their approach is primarily descriptive and infrastructural, focusing on how to organize and harmonize monitoring responsibilities across system components. In contrast, the work presented in this thesis goes beyond the architectural structuring of monitoring layers and instead operationalizes monitoring data for performance modeling and scheduling decisions. While Bader et al. focus on multi-layer metric aggregation, the present work uses collected measurements—such as runtime and power consumption under co-location—to infer quantitative models of interference and task affinity. Thus, where their contribution establishes the foundation for integrated observability in workflow systems, this thesis builds upon that idea by applying the monitored data directly to predictive, learning-driven scheduling mechanisms that adapt resource allocation based on empirically derived contention profiles [5].

Witzke et al. address the persistent challenge of connecting low-level monitoring data with high-level workflow semantics in distributed scientific computing environments. Their work focuses on tracing I/O behavior across heterogeneous compute nodes, where workflow tasks may execute concurrently and share resources. By integrating system-level telemetry with metadata extracted from workflow logs and container orchestration frameworks such as Kubernetes, the authors propose a methodology to attribute observed resource consumption—particularly I/O activity—to specific workflow tasks. This enables a task-level analysis of performance bottlenecks and inefficiencies, offering valuable insights for optimization. In contrast to their work, which centers on establishing a traceability chain between metrics and logical workflow components, the approach presented in this thesis operates at a higher abstraction level by using modeled and predicted resource interactions to inform scheduling decisions dynamically. Rather than correlating observed traces post-execution, it leverages learned contention patterns and predictive models to influence online task placement, thus turning monitoring insights into proactive scheduling intelligence [57].

Characterizing scientific workflow applications has been a central topic in understanding performance variability and optimization opportunities in large-scale computing environments. Early foundational work by Juve et al. systematically profiled diverse scientific workflows from domains such as astronomy, bioinformatics, and seismic modeling, revealing that despite differences in scientific goals, workflows often exhibit recurring structural and computational patterns. Their study demonstrated that a few dominant job types typically account for most of the total runtime and I/O activity, and that inefficiencies often arise from repeated data access or imbalanced task configurations. This characterization work established the importance of profiling-based insights as a prerequisite for improving workflow scheduling and system utilization.

Subsequent research extended this line of inquiry toward predictive and analytical modeling. Bader et al. conducted a broad survey of workflow task runtime prediction methods, categorizing models by their statistical or machine learning approach, training mode (offline, online, or pre-execution), and level of infrastructure awareness. Their synthesis demonstrated that accurate task-level performance prediction requires both application features and system state information, including heterogeneity and GPU support. In the context of this thesis, such predictive modeling is regarded as a necessary step toward understanding not just isolated task behavior but also inter-task interference when workflows are executed under shared resource conditions. A related direction emerged from Zhu et al., who developed power- and performance-aware workflow consolidation models based on kernel canonical correlation analysis. Their work introduced temporal signatures to represent CPU, memory, and I/O behavior as time-series features and correlated them with task runtime and power consumption. While their focus remained on offline analysis and consolidation, this approach inspired the feature representation adopted in this thesis, where resource usage patterns are used to model contention and energy impact during online workflow scheduling. Complementing these modeling efforts, Brondolin et al. introduced DEEP-Mon, a monitoring framework capable of attributing fine-grained power consumption to containerized workloads with negligible system overhead. This kind of container-level observability provides the instrumentation backbone necessary for empirically characterizing workflow behavior, as it enables associating power and performance traces with specific workflow tasks and execution contexts. Collectively, these works advanced the field from static profiling toward analytical and predictive characterization of workflow behavior. However, they generally focused on offline measurement, individual task modeling, or coarse-grained consolidation in data center contexts.

Recent research on task co-location has increasingly focused on balancing performance isolation with resource efficiency, particularly in heterogeneous or multi-tenant computing environments. While the motivation—to improve utilization through concurrent execution—is common across contexts, the techniques differ widely depending on whether the target system is a cloud, containerized service infrastructure, or HPC cluster.

Task co-location has become a central strategy for improving resource utilization and energy efficiency in large-scale distributed systems. Early work by Zhu et al. introduced pSciMapper, a consolidation framework designed for scientific workflows in virtualized environments. Their approach treated consolidation as a hierarchical clustering problem, using kernel canonical correlation analysis to model interference between CPU, memory, disk, and network resource profiles. By correlating resource requirements with task runtime and power consumption, pSciMapper achieved significant power savings with minimal slowdown. However, it operated primarily in an offline mode—optimizing workflow place-

ment decisions before execution—and focused on static virtualized environments rather than dynamic HPC workflows.

More recent research has expanded co-location techniques toward data- and container-level optimization. WOW (Workflow-Aware Data Movement and Task Scheduling) by Lehmann et al. proposed a coupled scheduling mechanism that simultaneously steers data movement and task placement to minimize I/O latency and network congestion during workflow execution. Implemented in Nextflow and deployed on Kubernetes, WOW demonstrated how co-location of data and tasks can drastically improve makespan for dynamic scientific workflows. This approach, however, primarily addresses data movement and distributed file system bottlenecks, rather than the interplay of compute, memory, and I/O contention among co-located workflow tasks.

Complementary to WOW, CoLoc by Renner et al. explored distributed data and container co-location in analytic frameworks such as Spark and Flink. By pre-aligning file placement and container scheduling on Hadoop YARN and HDFS, CoLoc improved data locality and reduced network overhead, resulting in execution time reductions of up to 35%. This work demonstrated the benefits of cross-layer scheduling coordination but focused on recurring, data-intensive jobs rather than the complex, dependency-driven task graphs typical of scientific workflows.

In cloud and service-oriented systems, studies such as OLPart (Chen et al., 2023) and the Interference-Aware Container Orchestration framework (Li et al., 2023) address the challenge of resource partitioning under performance interference. OLPart employs online learning via contextual multi-armed bandits to dynamically partition CPU and memory resources between latency-critical and best-effort jobs, using performance counters to infer sensitivity to contention. Its strength lies in operating without prior workload knowledge, adapting to runtime behavior. Similarly, Li et al. propose a machine learningdriven orchestration approach that introduces scheduling latency as a more accurate interference metric for mixed workloads. Their system predicts host-level interference and adjusts resource allocation in real time to preserve QoS while maximizing utilization. Both works demonstrate how adaptive learning mechanisms can manage contention in containerized or service-oriented environments but are inherently focused on online services rather than scientific workflows with inter-task dependencies.

In the HPC domain, co-location has traditionally been explored through hardware-level modeling and scheduling heuristics. Zacarias et al. present an intelligent resource manager that predicts performance degradation between co-located HPC workloads using performance monitoring counters (PMCs) as model features. The scheduler then selects application mixes that minimize degradation while improving node utilization. This approach achieves measurable improvements over conventional batch scheduling, but it remains focused on pairwise job co-location at the job-manager level and lacks integration with workflow-level task orchestration. Complementary to this, Álvarez et al. introduce nOS-V, a system-wide scheduler enabling fine-grained co-execution of HPC applications at the task level. By dynamically managing shared node resources and bypassing traditional oversubscription mechanisms, nOS-V demonstrates notable gains in throughput and resource efficiency, though it does not incorporate predictive or learning-based adaptation.

A broad body of research has addressed the challenge of performance interference in multi-tenant and consolidated environments, where multiple tasks, processes, or virtual machines share physical resources. Much of this work stems from efforts to optimize system throughput, energy efficiency, and fairness in cloud and HPC contexts, yet the focus typically lies

at the level of system services or job managers rather than workflow-specific task scheduling.

Early work by Dwyer et al. pioneered the use of machine learning for online interference estimation on multi-core processors. Their model predicts performance degradation in real time without instrumenting workloads, helping operators in data centers and HPC clusters make informed consolidation decisions. This approach was notable for applying learning-based methods to shared-resource contention but focused primarily on thread- and process-level interference rather than workflow-level orchestration. Complementary to this, Breitbart et al. analyzed co-scheduling of memory-bound and compute-bound applications in supercomputing environments. Their AutoPin+ tool automatically determines suitable combinations of applications to maximize throughput and energy efficiency, demonstrating up to 28% runtime reduction. However, their strategy remains reactive and application-type specific, without predictive or adaptive capabilities. Further refinement came from the work of Alves and Drummond, who developed a multivariate model for predicting cross-application interference in virtualized HPC environments. By considering simultaneous access patterns to shared caches, DRAM, and network interfaces, they achieved high accuracy in predicting interference effects across workloads. This work, along with their later Interference-aware Virtual Machine Placement Problem (IVMPP) formulation, demonstrated that combining interference modeling with optimization can effectively reduce degradation while minimizing physical machine usage. Nonetheless, these methods were still anchored in offline modeling and VM placement optimization rather than dynamic or online scheduling. In data center research, adaptive resource management has evolved toward online learning and multi-objective optimization. The Orchid framework (Chen et al.) and OLPart system introduced contextual multi-armed bandit algorithms for real-time resource partitioning among co-located jobs. These approaches enable systems to autonomously explore and learn optimal resource splits between latency-critical and best-effort workloads, achieving improved throughput and fairness without prior workload knowledge. Similar efforts, such as ScalCCon by Li et al., addressed scalability challenges in correlation-aware VM consolidation through hierarchical clustering, improving both consolidation speed and performance predictability for large-scale infrastructures. Finally, Sampaio and Barbosa proposed an interference- and power-aware scheduling mechanism incorporating a slowdown estimator that predicts task completion under noisy runtime conditions. Their simulations based on Google Cloud traces demonstrate effective SLA compliance with energy cost reductions, bridging the gap between consolidation efficiency and QoS guarantees.

Related Work: Energy Awareness

Energy measurement at fine granularity has been a recurring challenge across HPC and cloud environments. Raffin and Trystram dissect software-based CPU energy metering with a critical analysis of RAPL mechanisms and an exploration of eBPF as a low-overhead path for accurate, resilient measurements. Their Rust implementation emphasizes pitfalls in timing and counter handling, providing a blueprint for building correct energy profilers on modern x86 platforms. Complementing measurement, Arjona Aroca et al. conduct a component-level characterization of server energy, showing super-linear CPU power behavior and offering validated models that keep estimation error below 5% for real analytics workloads, while also identifying efficient operating points for NICs and disks. Warade et al. bring these concerns to containers, empirically breaking down the energy footprint of common Dockerized workloads to motivate energy-aware container development and deployment practices.

A parallel line of work focuses on forecasting and control. Algarni et al. evaluate classical time-series models—AR, ARIMA, and ETS—for predicting per-container power, demonstrating that method choice should be tuned to workload/container characteristics, with ETS frequently achieving the lowest MAPE. At the orchestration level, Kuity and Peddoju propose pHPCe, a containerized HPC framework that couples an online LSTM with rolling updates to predict power/performance and a contention-aware power-cap selection mechanism, yielding double-digit power savings at low overhead. In cloud consolidation, Abdessamia et al. apply Binary Gravitational Search for VM placement in heterogeneous data centers, reporting substantial energy savings over first/Best/Worst-fit and particle-swarm baselines. Kumar et al. similarly address green consolidation with task mapping and sleep-state strategies, arguing for policies that explicitly consider both active and idle energy draw to reduce total consumption in multi-tenant clouds.

Energy-aware scheduling for scientific workflows has been studied from both modeling and algorithmic angles. Silva et al. analyze two production I/O-intensive workflows on power-instrumented platforms and show that power is not linearly tied to CPU load; I/O—and even waiting for I/O—materially impacts energy. They introduce an I/O-aware power model that, when integrated into simulation, improves accuracy by orders of magnitude relative to traditional CPU-only models. Building on the importance of accurate models for policy quality, Coleman et al. evaluate popular energy-aware workflow schedulers under this improved model and find that CPU-linearity assumptions can underestimate power by up to 360% on I/O-heavy workloads; a simple I/O-balancing scheduler guided by the accurate model produces more attractive energymakespan tradeoffs. From an optimization perspective, Durillo, Nae, and Prodan extend HEFT into MOHEFT, a Pareto-based multi-objective scheduler that captures empirical energy behavior on heterogeneous systems, achieving up to 34.5% energy reductions with marginal makespan impact. Mohammadzadeh et al. pursue metaheuristics, hybridizing Ant Lion Optimizer with Sineosine and chaos-enhanced exploration in WorkflowSim to jointly minimize makespan, cost, and energy for scientific workflows. Choudhary et al. propose a framework that combines task clustering, partial critical path sub-deadlines, and DVFS on compute nodes to reduce transmission and execution energy across several benchmark workflows. Saadi et al. revisit the interplay between clustering and scheduling choices, showing that vertical clustering paired with MaxMin scheduling tends to save energy by lowering makespan, though sensitivity to workflow structure remains.

Energy awareness often intersects with interference management and QoS. Blagodurov and Fedorova advocate contention-aware HPC scheduling, arguing for cluster schedulers that reason about shared resource bottlenecks (e.g., caches, memory controllers) to avoid pathological slowdowns that also waste energy. Sampaio and Barbosa explicitly tie consolidation, slowdown, and power via a slowdown estimator feeding an interference- and power-aware scheduler; simulations based on cloud traces suggest SLA compliance with 12% cost reductions. Finally, several lines of work underscore that accurate performance/energy prediction is a precondition for effective energy-aware orchestration: from measurement robustness (Raffin and Trystram) and component characterization (Arjona Aroca et al.), to container-level prediction (Algarni et al., Warade et al.), to model-informed workflow scheduling (Silva et al., Coleman et al., Durillo et al.). Together, these studies advance the state of practice in measuring, modeling, and optimizing energy across the stack—from microarchitectural counters and container runtimes up to workflow-level schedulers and consolidation controllers.

4 Approach

The following chapter presents the methodological approach of this thesis. While the subsequent chapter discusses the concrete implementation aspects, this section establishes the theoretical foundation that builds upon the concepts introduced in the background. The structure of this chapter follows the sequence of steps illustrated in Figure **??**, beginning with an outline of the central objective of the thesis. This is followed by a set of assumptions that define the scope, applicability, and limitations of the proposed approach. The remainder of the chapter then describes each step in detail, explaining how the individual components contribute to the overall objective of enabling energy-aware and contention-conscious co-location of scientific workflow tasks.

4.1 Central Objective

The central objective of this work is to model the co-location of scientific workflow tasks with a focus on achieving energy awareness and determining how this knowledge can be applied during workflow execution to improve resource utilization and overall energy efficiency. To accomplish this, we introduce two key concepts: (i) *ShaReComp* and (ii) *ShaRiff*. Both address the idea of shared resource usage but from different perspectives. *ShaReComp* defines the modeling approach for resource sharing during computation. It focuses on understanding and representing co-location with respect to resource usage, contention, and energy behavior. In contrast, *ShaRiff* introduces an algorithmic framework that applies the *ShaReComp* model during workflow execution to enable informed and feasible resource sharing. Together, these concepts provide both the theoretical foundation and practical mechanism for energy-aware co-location in scientific workflows. *ShaReComp* is inspired by the work presented in [61], which introduced a mathematical formulation of the co-location problem. However, the implementation of *ShaReComp* differs significantly in its scope and application. By combining *ShaReComp* with *ShaRiff*, this work aims to investigate how co-location can be directly integrated into the dynamic scheduling and task mapping process, emphasizing that co-location and scheduling are inherently interdependent and should be addressed jointly. To achieve this, workflow tasks are characterized prior to execution, enabling contention-aware co-location decisions at runtime. In this setting, co-location is implemented at the virtual container level, focusing on virtual machines deployed on physical hosts. Additionally, this work extends the scope of co-location from merely determining which tasks should share resources to understanding how the performance behavior of co-located tasks can be modeled and predicted, thereby providing actionable insights for resource managers in future workflow executions.

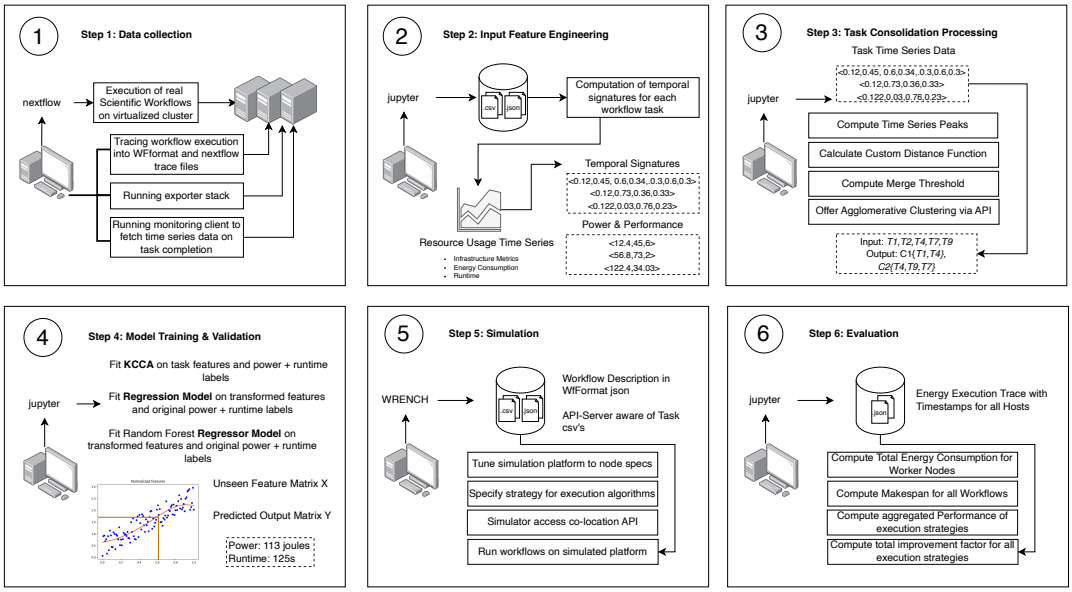

Figure 4.14: Overview
Das ist eine Beschreibung der Abbildung.

The proposed research problem, introduced in Section **??**, is decomposed into six main steps, as illustrated in Figure **??**. Step 1, described in Section**??**, involves a data collection phase that captures detailed execution metrics from scientific workflow runs. In Step 2, this collected data undergoes structural processing and formatting to extract relevant performance characteristics, as outlined in Section **??**. The raw data treatment of Step2 is performed immediately after data collection, while Steps 3 and 4 require more specialized data preparation tailored to their respective analytical goals. Details for these stages are provided in Sections**??** and **??**. Step 3 focuses on consolidating time-series data by identifying tasks with complementary resource usage patterns through clustering, as discussed in Section **??**. Step 4 reorganizes the data collected in Step 1 into a format suitable for learning the relationship between task behavior, runtime, and energy consumption, as described in Section **??**. Finally, Steps 5 and 6, presented in Section**??**, demonstrate how the theoretical concepts developed in Step 3 can be applied during workflow execution and how their potential benefits in terms of performance and energy efficiency can be evaluated through simulation.

4.1.1 Assumptions

To outline the scope, boundaries, and methodological constraints of this work, the following guiding assumptions were defined:

1. **Monitoring Configuration Limits**: Workflow tasks are described by 80 monitoring features. This work does not investigate the influence of monitoring data dimensionality on clustering and predictive performance.

2. **Monitoring Data Coverage**: Short-lived tasks under one second are only partially captured or occasionally missed due to high system load and sampling intervals exceeding one second during workflow execution.

3. **Offline Data Analysis**: The data preprocessing and predictive model fitting are performed offline after workflow execution. The co-location clustering algorithm is

evaluated offline but also transformed into a suitable format for integration into the simulation environment.

4. **Simulation Environment and Platform Equivalence**: The simulated platform is assumed to approximate the physical execution environment. It is expected that the overall behavior observed in simulation aligns with real-world execution trends.
5. **Simulation Capabilities and Contention Modelling**: The WRENCH framework currently supports simulation of memory contention by limiting per-Host memory consumption, where exceeding the limit results in extended task execution times. Similarly, CPU contention is modeled through proportional increases in task runtime. Other low-level contention effects like cache interference, interconnect bottlenecks, or I/O contention are not modeled in this iteration. The energy model provided by SimGrid is assumed to realistically approximate energy consumption variations when tasks with differing resource usage profiles are co-located on the same virtual machine. The impact on energy efficiency is attributed to CPU utilization behavior and derived from the platform description where different load levels map to consumed energy amount.

4.2 Online Task Monitoring

The online task monitoring approach builds on a hierarchical architecture designed to capture a broad range of metrics relevant to the execution of scientific workflows. Its design is inspired by [5] and follows a four-layered structure comprising the Resource Manager, Workflow, Machine, and Task layers. Each layer represents a distinct level of abstraction within the workflow execution environment, providing insights into specific aspects of system performance and resource utilization.

Table **??** provides an overview of the tools and data collection options considered to achieve these monitoring objectives, outlining how different metrics could be gathered and integrated across the hierarchical layers to form a comprehensive view of workflow behavior.

To enable access to detailed performance metrics in time-series format, Prometheus was selected as the central time-series database. As shown in Table **??**, the monitoring setup therefore focused on tools that are interoperable with Prometheus as data exporters and that operate effectively within the layered monitoring framework. During the evaluation of several potential exporters, some were excluded due to limited compatibility, excessive overhead, or incomplete metric coverage—particularly for short-lived or multi-process workflow tasks. After comparative testing, the combination of *cAdvisor* and a custom fork of the DEEP-mon system [14] produced the most stable and comprehensive results across varying workloads and resource types. These two tools were therefore selected as the foundation of the final monitoring setup.

The following table presents the final selection of data sources that were retained for the monitoring setup, along with the specific metrics enabled for each source.

cAdvisor is an open-source daemon for monitoring resource usage and performance of containers. It continuously discovers containers via Linux cgroups under the path /sys/fs/cgroup. Once started, cAdvisor subscribes to create/delete events in the cgroup filesystem, converts them to internal add/remove events, and configures per-container handlers. Metrics originate from machine-level facts parsed from /proc and /sys directories and most

Monitoring Features	Data Sources						
	cAdvisor	ebpf-energy-exporter	docker-activity	scaphandre	slurm-exporter	process-exporter	cgroups-exporter
Resource Manager							
Infrastructure status	x						
File system status	x						
Running workflows	x						
Workflow							
Status	x	x					
Workflow specification		x					
Graphical representation		x					
Workflow ID	x	x					
Execution report		x					
Previous executions		x					
Machine							
Status			x	x			
Machine type			x	x			
Hardware specification			x	x			
Available resources			x	x			
Used resources			x	x			
Task							
Task status				x			
Requested resources				x			
Consumed resources				x			
Resource consumption for code parts				x			
Task ID				x			
Application logs				x			
Task duration				x			
Low-level task metrics				x			
Fault diagnosis				x			

Table 4.1: Technologies and their capabilities evaluated against a 4-layered Monitoring Framework for Scientific Workflows.

Software Tool	**Used Metrics**
nextflow	trace file summary
cAdvisor	container_memory_working_set_bytes container_memory_usage_bytes container_memory_rss container_fs_reads_bytes_total container_fs_writes_bytes_total container_fs_io_current
Deep-Mon	container_memory_working_set_bytes container_memory_usage_bytes container_memory_rss container_fs_reads_bytes_total container_fs_writes_bytes_total container_fs_io_current container_mem_rss container_mem_pss container_mem_uss container_kb_r container_kb_w container_num_reads container_disk_avg_lat container_num_writes container_cycles container_cpu_usage container_cache_misses container_cache_refs container_weighted_cycles container_power container_instruction_retired

Table 4.2: Metrics for workflow monitoring components for task-level profiling.

prominently container and process usage collected at cgroup boundaries. In practice, cAdvisor provides low-overhead, per-container telemetry.

DEEP-Mon is a per-thread power attribution method to translate coarse-grained hardware power measurements into fine-grained, thread-level energy estimates by exploiting hardware performance counters. The Intel RAPL interface provides power readings per processor package or core, but it cannot distinguish how much of that energy was consumed by each thread. DEEP-Mon bridges this gap by observing how actively each thread uses the processor during each sampling interval. It does so by monitoring the number of unhalted core cycles—a counter that measures how long a core spends executing instructions rather than idling. Since power consumption correlates almost linearly with unhalted core cycles, the fraction of total cycles attributed to each thread provides a reasonable proxy for its share of energy usage. DEEP-mon first computes the weighted cycles for each thread—combining its active cycles when alone with its proportionally reduced cycles when co-running. These weighted cycles determine how much of the total core-level RAPL energy should be assigned to that thread. The final per-thread power estimate is then derived by distributing the total measured power of each socket proportionally to the weighted cycle counts of all threads running on that socket. This approach allows DEEP-mon to infer realistic thread-level power usage even in systems with simultaneous multithreading and time-shared workloads, without modifying the scheduler or requiring any application-specific instrumentation. The DEEP-mon tool was modified in this work to export container-level metrics directly to Prometheus.

Based on the identification of relevant metrics and the selection of appropriate monitoring technologies, we designed an architectural model and an accompanying algorithm to define how the individual components interact. The resulting architecture integrates the selected exporter stack into a coherent monitoring workflow, ensuring that metric collection, event handling, and data aggregation are performed in a structured and automated manner. Figure **??** provides an overview of the system components required for this setup, illustrating how they interact to realize the monitoring logic proposed in this work. The technical implementation details are discussed later in Section **??**.

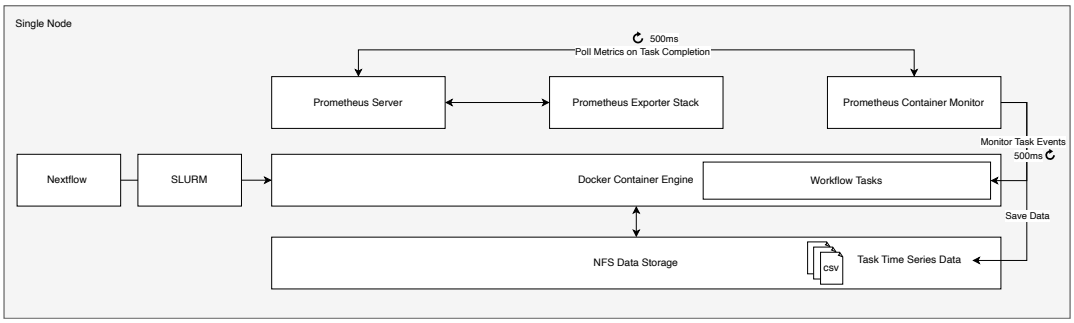

Figure 4.15: Monitoring Client
Schematic Overview of the Components of the Monitoring Client.

Figures **??** and **??** together describe the behavior of the monitoring client. The system operates in an event-driven fashion, where an event listener continuously observes container lifecycle events—such as start and termination—emitted by the runtime environment. When a relevant event occurs, the data query interface dynamically constructs PromQL queries based on the configuration and metadata of the corresponding container. These queries are executed against the Prometheus database to retrieve fine-grained time-series

metrics. The raw data is then processed by the aggregation module, which aligns and consolidates the collected metrics into unified container-level records, ready for subsequent analysis and task-level correlation.

?? and ?? show the behavior of the monitoring client. The event listener continuously observes container lifecycle events—such as start and termination—emitted by the runtime environment. Once an event is detected, the data query interface dynamically formulates PromQL queries based on the configuration and metadata of the affected container. These queries are sent to Prometheus to retrieve fine-grained time-series data. The retrieved raw metrics are then passed to the aggregation module, which aligns and consolidates them into a unified record per container.

Algorithm 1: Event-Driven Monitoring and Metric Aggregation Framework

Input: Configuration C defining monitoring targets
Output: Aggregated container-level time-series metrics for each Nextflow process

```
initialize_monitoring(C)
init_event_listener()
while true do
    event ← wait_for_container_event()
    meta ← extract_metadata(event)
    if event.type = START then
        register_process(meta.id, meta.workflow_label)
    if event.type = TERMINATE then
        metrics ← {}
        foreach target ∈ C.targets do
            query ← build_promql(target, meta.id, meta.time_window)
            metrics[target] ← execute_prometheus_query(query)
        data ← aggregate(metrics, meta.workflow_label)
        store(data)
```

The algorithm outlined in Algorithm ?? is designed to minimize monitoring overhead while ensuring that only relevant data is collected during workflow task execution. When a container start event is detected, the monitoring client extracts essential metadata—such as the container ID, the associated workflow label, and the start timestamp—and registers this information in an internal mapping to maintain a link between container identifiers and workflow tasks. When a termination event occurs, the client initiates a targeted data collection phase, querying only the relevant metrics for the specific container and execution period.

This event-driven approach ensures efficient monitoring by restricting data retrieval to the active lifecycle of workflow tasks. Furthermore, the monitoring client supports dynamic configuration of the metrics listed in Table ??, allowing users to define which metrics are collected and analyzed. This flexibility enables fine-grained, task-specific monitoring while maintaining low overhead and adaptability to different experimental requirements.

4.3 Modelling the Co-location of Task Behavior based on Time-Series

This section corresponds to Steps2,3, and4 in Figure ?? and explains how the collected monitoring data is transformed into structured representations of task behavior. The focus lies on preparing and processing the raw time-series metrics to generate meaningful

feature sets that can be used for two main purposes: identifying complementary tasks for co-location through clustering and building predictive models that capture the relationship between task behavior, runtime, and energy consumption.

General Preprocessing of Raw Time-Series Data

The collected monitoring data is obtained as raw time-series files in CSV format and must therefore undergo several preprocessing steps before further analysis. The goal of this stage is to transform heterogeneous monitoring outputs into a consistent and structured representation that links system-level metrics to individual workflow tasks. The general preprocessing workflow includes the following steps:

1. Parsing of raw time-series CSV files.
2. Alignment of timestamps across different sources.
3. Merging of per-task data into unified records.
4. Matching Entities between execution layer and workflow layer

During workflow execution, data is produced at multiple abstraction levels—from the resource manager down to container metrics. To transform this heterogeneous data into a unified, task-level format, a structured preprocessing pipeline was developed. First, all monitoring outputs are recursively traversed and scoped according to the desired data sources and metric types. The resulting directory tree is then filtered to retain only relevant metrics, such as task metadata and power measurements. Each dataset is subsequently split into per-task CSV files based on container identifiers. As an anchor for this process, the started and died container tracking files are used, which record general container lifecycle information such as container names, identifiers, and timestamps. To establish a consistent mapping between workflow tasks and their corresponding container traces, entity matching is performed. Here, container lifecycle records—capturing task identifiers, container names, and working directories—serve as the linking mechanism between workflow-level entities and container-level monitoring data. The working directories are attached to every container trace, enabling a reliable cross-reference with workflow metadata extracted from Nextflow trace files. This ensures that each monitored container is correctly associated with the corresponding workflow task, providing a coherent, task-centric dataset for subsequent analysis.

4.3.1 Task Clustering for Contention-Aware Consolidation

Following the preprocessing and structuring of raw time-series data, we now address step 3 of the overall approach outlined in **??**. This step focuses ShaReComp's mechanics - task clustering as a means of identifying tasks that can be co-located without causing severe resource contention. The goal is to refine the processed monitoring data into representations that capture each task's characteristic resource usage patterns and to use these representations for forming complementary task groups. This clustering step forms the conceptual foundation for contention-aware consolidation

Preprocessing Raw Time-Series Data for Task-Clustering

To prepare the data for contention-aware task clustering, the processed time-series must be transformed into a compact yet expressive representation of each task's resource usage behavior. This ensures that the clustering algorithm can meaningfully capture similarities and differences between tasks across multiple resource domains. We therefore apply the following two main preprocessing steps prior to executing the clustering algorithm.

1. **Peak-pattern construction**. For every task and monitored workload type, we first derive a peak time series: the raw per-second resource signal is resampled into three-second buckets and the maximum per bucket is retained. When two peak series must be compared, we truncate both to the shorter length so that correlation is computed on aligned vectors without padding artifacts.
2. **Computing Workload-type affinity**. Different resource domains interfere to different degrees such as CPU vs CPU peaks are typically more contentious than CPU vs file I/O. We encode this by computing an affinity score between workload types which is described in **??**. High affinity means higher potential interference when peaks align; low affinity reflects benign coexistence.

While the first step focuses on constructing consistent temporal representations of task behavior, the second step introduces a quantitative measure of how different workload types interact when co-located. To provide a clearer understanding of this relationship and its role in the clustering process, we examine the computation of workload-type affinity in more detail.

Measuring Resource Interference of Co-located Benchmarks

The measurement of resource contention follows a two-stage protocol that first establishes isolated baselines for each workload class and then repeats the same workloads under controlled co-location. In the baseline stage, CPU-bound, memory-bound, and file-I/O-bound benchmark containers are executed one at a time on pinned logical CPUs. Each run records a start and finish timestamp at microsecond resolution. In parallel, Deep-Mon is used to record the power time series for each container. After a run finishes, the power streams of the containers are retained, aligned to the containers lifetime, and summarized to a representative mean value. After isolated benchmark execution we replay the same benchmarks in pairs to expose interference effects by CPU pinning. The experiment binds pairs of benchmarks to siblings on the same physical core to amplify shared-core effects. Each co-located container is measured in exactly the same way as in isolation, producing a matched set of durations and power summaries.

In order to derive a workload affinity from the contention experiments we define contention effects to occur when co-located workloads exceed their duration and power consumption compared to their isolated measurements.

Isolated and Co-located Metrics.

For each workload $i \in \{1, 2\}$, let

$$t_i^{(iso)},\ t_i^{(coloc)} \quad \text{denote the isolated and co-located runtimes,}$$

$$P_i^{(iso)},\ P_i^{(coloc)} \quad \text{denote the average isolated and co-located power consumption.}$$

Per-workload Slowdown Factors.

The per-workload slowdowns are defined as

$$S_i^{(t)} = \frac{t_i^{(coloc)}}{t_i^{(iso)}}, \qquad S_i^{(P)} = 1 + \log\left(\max\left(\frac{P_i^{(coloc)}}{P_i^{(iso)}}, 1\right)\right),$$

ensuring that both runtime and power slowdowns are non-negative and at least one in value.

The mean slowdowns across the workload pair are

$$\bar{S}^{(t)} = \frac{S_1^{(t)} + S_2^{(t)}}{2}, \qquad \bar{S}^{(P)} = \frac{S_1^{(P)} + S_2^{(P)}}{2}.$$

A weighted average combines both effects:

$$\bar{S} = \alpha\, \bar{S}^{(t)} + (1 - \alpha)\, \bar{S}^{(P)}, \quad \text{with } \alpha \in [0, 1],$$

where higher α emphasizes runtime effects, and lower α gives more weight to power efficiency.

The final combined slowdown factor is

$$\bar{S}_{\text{final}} = \max(1, \bar{S}),$$

guaranteeing that co-location never yields an apparent speedup (values ≥ 1 indicate slowdown).

Affinity Score.

The affinity score A quantifies the degree of interference between two co-located workloads.

First, compute pairwise affinity ratios:

$$A^{(t)} = \frac{t_1^{(coloc)} + t_2^{(coloc)}}{t_1^{(iso)} + t_2^{(iso)}}, \qquad A^{(P)} = 1 + \log\left(\max\left(\frac{P_1^{(coloc)} + P_2^{(coloc)}}{P_1^{(iso)} + P_2^{(iso)}}, 1\right)\right).$$

A weighted average combines both effects:

$$A_{\text{raw}} = \alpha\, A^{(t)} + (1 - \alpha)\, A^{(P)}, \qquad A_{\text{raw}} \geq 1.$$

The normalized affinity score is then:

$$A = \frac{1 - \frac{1}{A_{\text{raw}}}}{\beta}, \qquad A \in [0, 1],$$

where $\beta > 0$ controls scaling sensitivity. Values of $A \approx 0$ indicate minimal interference, while $A \to 1$ signifies strong co-location interference.

Algorithmic Approach to Task Consolidation

Building on the previously derived peak time-series representations and the computed workload-type affinity scores, we now turn to the algorithmic formulation of the clustering, or consolidation, process. Consolidation is formulated as a clustering problem with an important modification: rather than grouping tasks that are similar, the goal is to cluster tasks with complementary resource usage patterns to minimize contention during co-location. Building on the previously established notion of affinity—which quantifies how strongly workloads interfere when sharing resources—the clustering process now incorporates this measure directly into its distance metric. The distance between tasks increases when two tasks exert pressure on the same resources simultaneously, indicating potential contention, and decreases when their resource usage peaks complement one another.

Algorithm **??** showcases the ShaReComp task consolidation procedure developed in this work, integrating both the peak-pattern representations and affinity scores into a unified clustering process. The method first computes pairwise similarities between all task signatures, where each signature encodes the temporal evolution of multiple resource metrics. These similarities are weighted by the experimentally derived affinity values to reflect the degree of potential interference between workloads. The resulting similarity matrix thus provides a contention-aware view of task compatibility. A percentile-based threshold is then applied to adaptively determine the stopping condition for cluster formation, ensuring that only task pairs with sufficiently low contention potential are merged. Finally, agglomerative clustering is executed using average linkage criterion to form consolidated task groups that exhibit complementary resource utilization.

Algorithm 2: ShaReComp - Task Consolidation Algorithm

Input: task signatures sig, affinity weights w, percentile τ, linkage
Output: clusters $\mathcal{C}$
$S \leftarrow$ `compute_similarity` (sig, w) ; `// resource-aware similarity`
$\theta \leftarrow$ `percentile_threshold` (S, τ) ; `// percentile-based stopping rule`
$\mathcal{C} \leftarrow$ `agglomerative_merge` (S, θ, linkage) ; `// agglomerative clustering`
return $\mathcal{C}$

We examine each stage of Algorithm **??** in turn.

Anti-similarity distance. For any pair of tasks i,j, we iterate over their workload types and use two factors: (i) the affinity between the two types; (ii) the correlation between their corresponding peak series computed twice, once per type, to capture both sides of the pairing. We then aggregate these terms so that highly correlated peaks in high-affinity domains increase the distance, whereas low or negative correlations in low-affinity pairs decrease it. The result is a symmetric task distance matrix whose off-diagonal entries quantify how bad it would be to co-locate the two tasks, and whose diagonals are zero by definition.

Inter-Task Distance and Resource Correlation Model

To quantify the similarity and potential contention between two workloads i and j, we define a composite distance measure that integrates both resource affinity and correlation of peak usage. Each workload utilizes a set of resources $R = \{\text{CPU}, \text{Memory}, \text{Disk}\}$, yielding

in total ten pairwise combinations of resource types across two tasks. The distance term combines the precomputed affinity score with the correlation of peak resource intensities.

$$D_{i,j} = \sum_{R_1,R_2} \Big((\text{aff-score}(R_1^i, R_2^j)) \cdot \text{Corr}(\text{peak } R_1^i, \text{peak } R_1^j) \cdot \text{Corr}(\text{peak } R_2^i, \text{peak } R_2^j) \Big) \quad (1)$$

where:

$$R_1^i, R_2^j \text{ denote resource types of workloads } i \text{ and } j, \quad (1)$$

$$\text{Corr}(\text{peak } R_1^i, \text{peak } R_1^j) \text{ is the Pearson correlation between the peak usages of resource } R_1, \quad (2)$$

$$\text{aff-score}(R_1^i, R_2^j) \in [0, 1] \text{ measures the degree of interference between } R_1^i \text{ and } R_2^j. \quad (3)$$

Interpretation

The intuition behind this distance metric is to *promote dissimilar task pairings* for co-location. If two workloads exhibit highly correlated peak usage on the same resources, their corresponding correlation terms will be large, thus increasing $D_{i,j}$ and discouraging their co-location. Conversely, tasks with uncorrelated or complementary resource peaks yield smaller distance values and are therefore more suitable to merge.

The affinity score modulates this behavior: smaller values of aff-score indicate lower interference between resource pairs, which can offset strong peak correlations.

Finally, clustering proceeds by iteratively merging task clusters whose inter-cluster distance satisfies:

$$D_{i,j} < \text{merge\_threshold}.$$

This ensures that only compatible workloads, in terms of both resource affinity and temporal peak correlation, are grouped together.

Computing the merge threshold. Because the distance matrix is data-dependent, we estimate a merge threshold directly from its empirical distribution. In our appraoch we select the 20th percentile on the raw distances as an automatic cut-level: any pair below this threshold is safe enough to consider for co-location, while pairs above it are kept apart.

Agglomerative clustering with precomputed distances. We run average-linkage agglomerative clustering on the precomputed distance matrix with the chosen distance threshold and no preset cluster count. This yields variable-sized clusters whose members are mutually non-contentious under our metric. Because we use a threshold rather than a fixed k, the method adapts to each workload mix, producing more or fewer groups as warranted by the observed interference structure.

4.3.2 Predicting the Runtime and Energy Consumption of Task Clusters

Following the reasoning of [61], we investigate whether the formed task clusters exhibit shared structures in terms of correlations between their time-series behavior and their corresponding energy and performance metrics. To this end, we adopt their proposed approach for preprocessing time-series data into temporal signatures on a per-task basis.

Preprocessing Raw Time-Series Data for Predictive Modelling

Unlike the preprocessing described in Section **??**, the following procedure prepares the data specifically for step 4 of the overall approach shown in Figure**??**, focusing on transforming raw time-series inputs into a form suitable for predictive modeling.

1. Temporal signature construction.

   Sampling and smoothing.

   Equal-length normalization.

   Container-wise collation.

2. Model Input Construction.

   Normalization and Scaling.

   Extraction of Input Features and Output Labels.

Temporal Signature and Model Input Construction.

We denote by $\mathcal{T} = \{T_1, T_2, \ldots, T_N\}$ the set of temporal signatures extracted from the monitored resource-usage profiles of N workflow tasks. Each task i is characterized by time-varying utilization traces for the monitored resource dimensions

$$R = \{\text{CPU}, \text{Memory}, \text{Disk}\}.$$

For each resource $r \in R$ and task i, the temporal signature $T_i^{(r)}$ is defined as a coarse-grained summary of the normalized resource usage signal $x_i^{(r)}(t)$:

$$T_i^{(r)} = \langle p_{1,i}^{(r)},\ p_{2,i}^{(r)},\ \ldots,\ p_{10,i}^{(r)} \rangle, \tag{1}$$

where each component $p_{k,i}^{(r)}$ represents the mean usage value within segment k of the time-normalized execution window ($k = 1, \ldots, 10$). This yields a ten-dimensional vector describing the temporal pattern of resource consumption.

The feature vector for task i is obtained by concatenating the resource-specific signatures:

$$x_i = \left[T_i^{(\text{CPU})},\ T_i^{(\text{Memory})},\ T_i^{(\text{Disk})},\ \right] \in \mathbb{R}^{d_x},$$

where $d_x = 3 \times 10 = 30$ in this example configuration.

$$X = [x_1^\top, x_2^\top, \ldots, x_N^\top]^\top \in \mathbb{R}^{N \times d_x}$$

denotes the complete input matrix used for model training.

Similarly, for each task i, the execution-level targets (time and mean power consumption) are given by

$$y_i = [\, t_i,\ P_i \,] \in \mathbb{R}^2, \quad Y = [y_1^\top, y_2^\top, \ldots, y_N^\top]^\top \in \mathbb{R}^{N \times 2}.$$

Example.

Consider $N = 3$ workflow tasks with simplified CPU and memory usage signatures (each consisting of 3 representative pattern points for brevity):

Task	$p_1^{(\text{CPU})}$	$p_2^{(\text{CPU})}$	$p_3^{(\text{CPU})}$	$p_1^{(\text{Mem})}$	$p_2^{(\text{Mem})}$	$p_3^{(\text{Mem})}$
1	0.40	0.75	0.90	0.35	0.55	0.60
2	0.20	0.50	0.70	0.25	0.40	0.50
3	0.30	0.65	0.85	0.30	0.45	0.55

Concatenating these signatures yields the input matrix

$$X = \begin{bmatrix} 0.40 & 0.75 & 0.90 & 0.35 & 0.55 & 0.60 \\ 0.20 & 0.50 & 0.70 & 0.25 & 0.40 & 0.50 \\ 0.30 & 0.65 & 0.85 & 0.30 & 0.45 & 0.55 \end{bmatrix}, \quad Y = \begin{bmatrix} 12.4 & 65 \\ 14.1 & 72 \\ 10.8 & 58 \end{bmatrix}.$$

Here, each row of X encodes the temporal resource-usage pattern of a task, while Y provides the corresponding runtime and mean power consumption used for model learning or correlation analysis.

This preprocessing yields: (i) a standardized and fixed-length feature matrix X that preserves per-metric usage distributions and (ii) a label matrix Y capturing runtime and energy

Building upon Algorithm **??** in Section **??**, we extend the ShaReComp concept by linking task clustering with predictive modeling. This step introduces a follow-up procedure that uses the clustered task groups and their extracted temporal features from Section **??** to model and predict the expected runtime and energy behavior of consolidated task clusters.

Algorithm 3: ShaReComp — Prediction of Energy and Performance Behavior of Consolidated Task Clusters

Input: task clusters $\mathcal{C}$, per-task signatures sig, trained model $\mathcal{M}$ (KCCA or Random Forest)

Output: predicted runtime energy pairs $\hat{Y} = \{(\hat{t}_k, \hat{E}_k)\}$

foreach *cluster* $C_k \in \mathcal{C}$ **do**

  $F_k \leftarrow$ `sum_cluster_features` $(\{\, \text{sig}[t_i] \mid t_i \in C_k \,\})$; `// sum task signatures to form cluster feature`

$X \leftarrow$ `build_feature_matrix` $(\{F_k\})$; `// construct consolidated feature matrix`

foreach *cluster feature* $X_k \in X$ **do**

  $(\hat{t}_k, \hat{E}_k) \leftarrow$ `predict_runtime_and_energy` $(X_k, \mathcal{M})$

return $\hat{Y} = \{(\hat{t}_k, \hat{E}_k)\}_{k=1}^{|\mathcal{C}|}$

The statistical models used in **??** are described in the following.

Kernel Canonical Correlation Analysis

KCCA wants to identify relationships between task-specific features and their corresponding performance and energy characteristics. To achieve this, the dataset is divided into two parts: approximately 70% of the tasks are used for training the models, while the remaining 30% are reserved for testing and validation.

KCCA itself does not perform prediction but rather uncovers shared structures between task feature data performance outcomes. Through the data preprocessing described in the previous step, we prepare the feature matrices so that a regression model can generalize from the learned shared space to unseen inputs—for instance, the aggregated features of a new task cluster. We use KCCA to project both input and target data into a common latent space that captures nonlinear relationships between task resource usage and performance behavior. During training, we then fit a Kernel Ridge Regression model on the latent-space representations of the input features and the original, unnormalized target values Y (runtime and energy). This approach leverages KCCA's ability to transform unseen data into the same latent space, allowing KRR to predict concrete runtime and energy values for previously unseen X inputs. KRR is chosen because, as outlined in Chapter 1, it extends ordinary least squares regression by capturing nonlinear dependencies through kernel-based feature mappings.

Kernel Canonical Correlation Analysis (KCCA).

To capture nonlinear dependencies between the resource signatures and performance power outcomes, we apply Gaussian kernels to both input and output feature spaces.

KCCA seeks directions A and B in the reproducing kernel spaces of K_x and K_y that maximize the correlation between K_xA and K_yB. This is expressed as the generalized eigenvalue problem:

$$\begin{bmatrix} 0 & K_yK_x \\ K_xK_y & 0 \end{bmatrix} \begin{bmatrix} A \\ B \end{bmatrix} = \lambda \begin{bmatrix} K_x^2 & 0 \\ 0 & K_y^2 \end{bmatrix} \begin{bmatrix} A \\ B \end{bmatrix}. \tag{2}$$

Solving (2) yields paired canonical directions (A, B) that define latent projections

$$X' = K_xA, \qquad Y' = K_yB,$$

maximally correlated across the two feature spaces. These projections represent a shared latent space relating resource utilization dynamics to task performance and energy.

Illustrative Example.

Consider three workflow tasks $i = 1, 2, 3$ with aggregated temporal signatures over CPU and memory:

$x_1 = [0.40, 0.75, 0.90, 0.35, 0.55, 0.60], \quad x_2 = [0.20, 0.50, 0.70, 0.25, 0.40, 0.50], \quad x_3 = [0.30, 0.65, 0.85, 0.$

Their corresponding runtime power outcomes are:

$$y_1 = [12.4, 65], \quad y_2 = [14.1, 72], \quad y_3 = [10.8, 58].$$

KCCA maps both the temporal patterns x_i and the performance power pairs y_i into high-dimensional kernel spaces and finds projections that maximize their mutual correlation. In this example, the first canonical mode reveals that tasks with higher sustained CPU activity (x_1, x_3) correspond to lower execution time and reduced power consumption, while the less efficient task (x_2) shows a distinct temporal signature characterized by fluctuating utilization and higher runtime.

Random Forest Regression
To complement the KCCA model, we trained two non-parametric regressors based on Random Forests—one to predict mean task power and one to predict task runtime from the same preprocessed feature matrix. We reuse the exact same data as we did for the KCCA model as Random Forests perform well on both multivarita input and output data. The power model is trained on mean per-task energy-rate labels, while the runtime model uses task durations as targets. As a sanity check, we established simple baselines by predicting the training-set mean once for power and once for runtime on the test split. These baselines quantify the minimum improvement any learned model must exceed.

To illustrate this concept, we consider the following example.

Example on Predicting the Performance of Task Cluster with ShaReComp.

Assume two clusters:

$$C_1 = \{t_1, t_2\}, \quad C_2 = \{t_3\},$$

and each task has a CPU Memory signature with three pattern points:

$$t_1 = [0.4, 0.7, 0.9, 0.5, 0.6, 0.7], \quad t_2 = [0.3, 0.5, 0.8, 0.4, 0.5, 0.6], \quad t_3 = [0.2, 0.4, 0.6, 0.3, 0.4, 0.5].$$

Applying **??** Cluster features are summed:

$$F_1 = t_1 + t_2 = [0.7, 1.2, 1.7, 0.9, 1.1, 1.3], \quad F_2 = t_3.$$

Model predictions from both Kernel Ridge Regression or the Random Forest Regressor yield

$$\hat{Y} = \begin{bmatrix} 10.8 & 62.5 \\ 14.2 & 75.1 \end{bmatrix},$$

representing predicted runtime (seconds) and energy (joules) per cluster.

4.4 Simulation of Task Co-location during Workflow Execution

We now advance to steps 5 and 6 of the overall approach shown in Figure **??**, where the previously developed concepts are embedded into a workflow execution environment. In this stage, the focus shifts from modeling and clustering individual tasks to simulating their co-location during execution, eventually allowing us to evaluate how these strategies affect overall performance and energy efficiency.

Outline of Simulation Components

We build upon generic design pillars that structure the simulation environment.

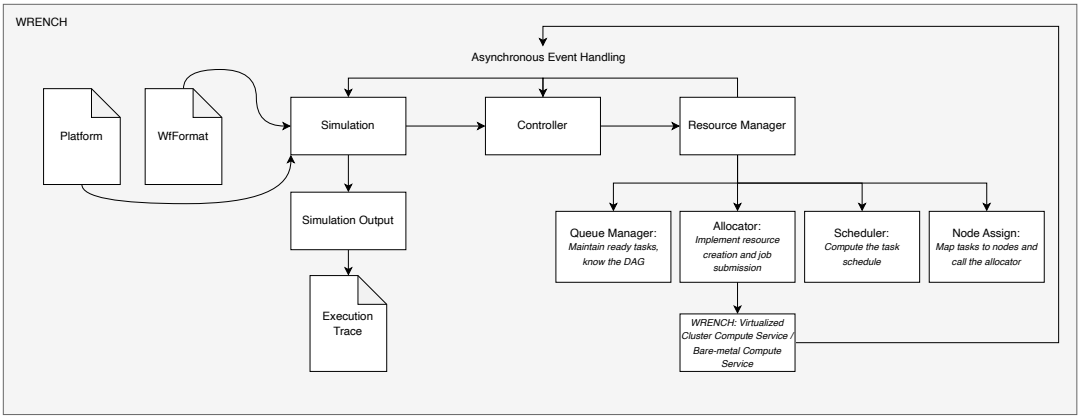

Figure 4.16: Wrench design
Simulator Design for studying Energy-aware Co-location of Scientific Workflow Tasks.

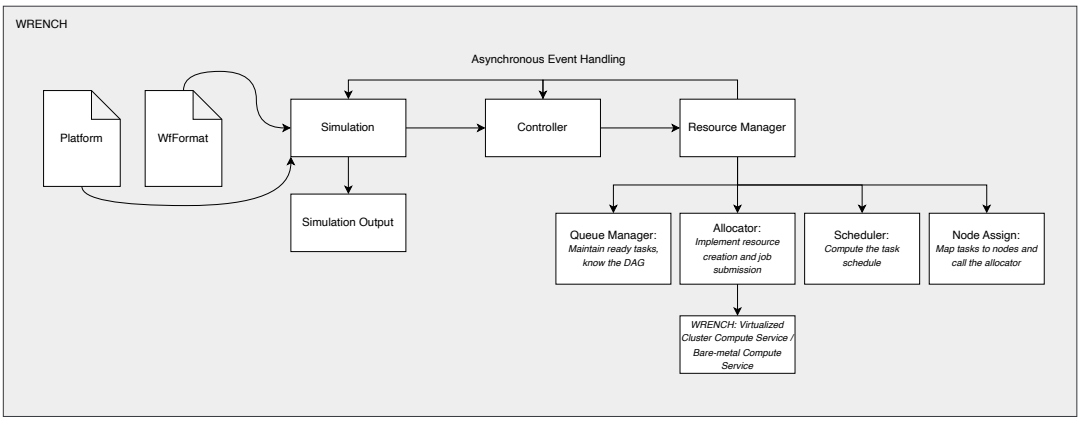

Figure 4.17: Wrench design
Simulator Design for studying Energy-aware Co-location of Scientific Workflow Tasks.

The design of distributed HPC systems typically revolves around three fundamental mechanisms: resource allocation, queue management and dispatching, and job placement. As illustrated in Figure **??**, these principles are adapted and integrated into our simulator through a dedicated controller component that interacts with a central resource manager. This resource manager orchestrates task scheduling, DAG-aware queue handling, task-to-node assignment, and the eventual allocation and execution of tasks on compute resources. Because the objective of this work is to analyze the effects of task co-location, the simulator's processing engine is designed with extensible interfaces that support alternative scheduling, mapping, and allocation strategies—from traditional First-In-First-Out (FIFO) execution to heuristic or energy-aware methods that emphasize beneficial co-location patterns.

4.4.1 Embedding Task Co-location into Scheduling Heuristics

Our algorithmic design for the resource manager, allocator, and scheduler components shown in Figure **??** follows heuristic principles. Instead of formulating co-location within the scheduling process as an explicit optimization problem, we embed it through a set of simple, interpretable decision rules. Heuristic algorithms are particularly suited for this purpose, as they enable deterministic, rule-based navigation of the scheduling space with-

out requiring exhaustive or stochastic search, thus ensuring transparency and efficiency in evaluating co-location strategies. We divide the task-to-node mapping process into two distinct stages, as illustrated in Figure **??**. The simulation begins by launching the controller component, which invokes the resource manager. Through its queue management mechanism, the resource manager identifies all ready-to-run tasks that have no remaining dependencies. In the depicted example, tasks 1, 2, 4, 8, 11, 12, and 15 are selected for scheduling. For this process, we adopt list-scheduling algorithms, one of the most established heuristic approaches in workflow scheduling. These algorithms assign each task a priority or ranking based on topological and performance characteristics such as critical path length, estimated execution time, or communication cost. Tasks are then scheduled iteratively, with the highest-priority unscheduled task being mapped to an available resource until all ready tasks have been assigned.

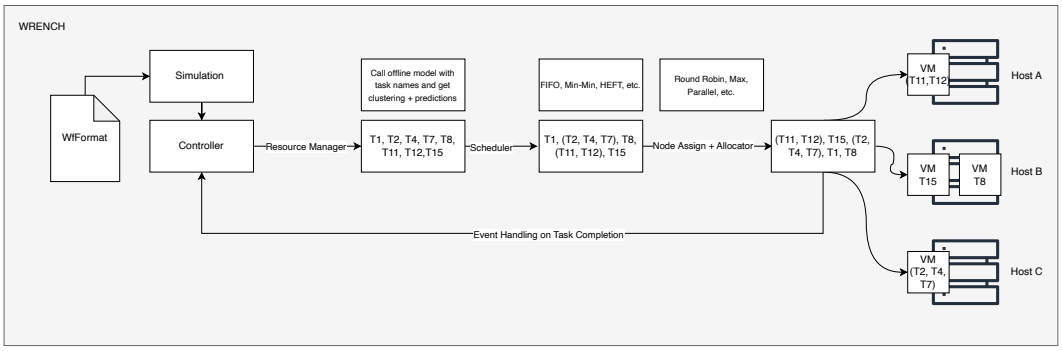

Figure 4.18: Coloc Problem
Das ist eine Beschreibung der Abbildung.

Since our goal is to map not individual tasks but clusters of tasks, we embed the retrieval of co-location information derived from ShaReComp directly into this stage of the scheduling process. In the illustrated example, the co-location hints result in consolidated groups such as T1, (T2, T4, T7), T8, (T11, T12), and T15. After clustering, the next step is to determine which compute host can best accommodate each task group. To this end, we define an interface for node assignment strategies that can either prioritize hosts with the most idle compute cores or distribute task clusters evenly across all available nodes to ensure balanced utilization. Finally, the allocation component creates virtual machines for each task cluster and launches them on their designated hosts, completing the mapping and allocation workflow. Through this exemplified design, we establish a foundation that not only enables the embedding and study of the co-location problem within an execution environment but also allows for systematic comparison through modular component interfaces. The following section formally introduces the simulation environment and the system model that represents our algorithmic formulation of the co-location problem.

Simulation System Model

Workflow Properties

Let the workflow be represented as a directed acyclic graph (DAG)

$$G = (T, E)$$

where

- $T = \{t_1, t_2, \ldots, t_n\}$ denotes the set of **tasks**, and
- $E \subseteq T \times T$ denotes **data or control dependencies** between tasks.

A directed edge $(t_i, t_j) \in E$ indicates that task t_j can start only after t_i has completed.

Task Properties

Each task $t_i \in T$ is associated with the following attributes:

$$\begin{aligned} \text{req\_cores}(t_i) &\in \mathbb{N}_{\geq 1} \quad \text{number of CPU cores required,} \\ \text{req\_mem}(t_i) &\in \mathbb{R}_{>0} \quad \text{memory requirement in bytes.} \end{aligned}$$

Infrastructure Model

Let $\mathcal{H} = \{h_1, h_2, \ldots, h_m\}$ denote the set of available **hosts**, where each host h_j is characterized by

$$C_j \in \mathbb{N}_{>0} \text{ (total number of cores)}, \qquad c(h_j) \in \mathbb{N}_{\geq 0} \text{ (current number of idle cores).}$$

A **virtual machine (VM)** is represented as

$$v = (C_v, M_v, h_j),$$

where C_v is the number of virtual cores, M_v the assigned memory, and h_j the physical host on which it is instantiated.

The set of currently **ready tasks** (those whose dependencies are satisfied) is denoted by

$$\mathcal{Q} = \{t_1, t_2, \ldots, t_k\}.$$

Resource Assignment

A mapping of tasks to hosts and VMs is represented as

$$M = (h, \mathcal{T}_h, \text{colocMap}_h, \Phi_h),$$

where

- $h \in \mathcal{H}$ is the assigned host,
- $\mathcal{T}_h \subseteq T$ is the set of tasks mapped to h,
- colocMap_h describes task clusters on h, and
- Φ_h represents associated file or data locations.

The set of mappings for an allocation interval is written as

$$\mathcal{M} = \{M_1, M_2, \ldots, M_p\}.$$

Task Co-location

A **co-location mapping**, produced by a scheduler is defined as

$$\text{colocMap} = \{(C_i, \mathcal{C}_i) \mid \mathcal{C}_i \subseteq T\},$$

where $\mathcal{C}_i$ is a **cluster of tasks** to be executed together within a single virtual machine, ideally selected based on their resource affinity or complementary utilization patterns.

Oversubscription

An **oversubscription factor** $\alpha \in [0, 1]$ allows up to

$$N_{\max}(h_j) = \lceil C_j(1 + \alpha) \rceil$$

tasks to be scheduled concurrently on a VM on host h_j.

Execution Dynamics

At runtime:

- **Node Assigners** determine host placement.
- **Schedulers** generate task queues and co-location groupings.
- **Allocators** instantiate and start VMs according to host-task mappings.
- The **Job Manager** executes tasks, monitors VM lifecycles, and updates resource states.

We now present the unified algorithm that governs the overall behavior of our simulation framework. This algorithm formalizes how workflow tasks are scheduled, assigned, and executed under different resource management strategies, including optional co-location support through ShaReComp.

Algorithm 4: ShaReComp Simulation - WRENCH Framework

Input: workflow $G = (T, E)$, hosts $\mathcal{H} = \{h_1, \ldots, h_m\}$, scheduling policy π, oversubscription factor α, optional co-location API $\mathcal{S}$

Output: workflow executed with policy-driven scheduling, node assignment, and adaptive resource management

Initialize system state: host capacities, ready queue $\mathcal{Q}$, and monitoring layer
while *workflow G not completed* **do**
  Update $\mathcal{Q}$ with all newly ready tasks
  Perform **task scheduling**: prioritize tasks in $\mathcal{Q}$ according to policy π
  Perform **node assignment**: select suitable host(s) $h \in \mathcal{H}$ using π
  Perform **resource allocation**: determine allowed capacity $n_{\max} = f(c(h), \alpha)$ and reserve resources
  if *policy π supports co-location* **then**
    Optionally query $\mathcal{S}$ to group tasks by affinity and launch them on shared VMs
  else
    Launch one task per VM on assigned host
  Monitor execution and task completions
  Release resources and enqueue successors of completed tasks
return *workflow complete*

To evaluate the effectiveness of the ShaReComp approach, we define several scheduling and node assignment algorithms that differ in their treatment of resource sharing and task placement. All of these algorithms build upon the unified simulation blueprint presented in **??** and serve as comparative baselines. The first category of baselines executes each task in its own virtual machine, thereby avoiding any form of co-location. The second category

enables task co-location by grouping multiple tasks within shared virtual machines and applying different host prioritization and allocation strategies. A third category extends this idea through controlled oversubscription, where more tasks are assigned to a virtual machine than the available reserved resources allow, deliberately inducing resource contention to test system robustness. Detailed algorithmic definitions are provided in the appendix, while **??** discusses their comparative behavior in depth. The ShaRiff algorithms build directly on top of these baselines, extending them with co-location awareness derived from ShaReComp. In doing so, they replace random or static task grouping with data-driven consolidation decisions that account for resource affinity and contention characteristics.

Algorithmic Examples of Task Mapping with guided Co-location

This section concludes our approach by introducing the main contribution of this thesis: the integration of the ShaReComp methodology into the workflow execution process. To this end, we design four scheduling algorithms collectively referred to as ShaRiff (Share Resources if Feasible). Each ShaRiff variant implements a distinct strategy for mapping consolidated task clusters onto available compute hosts, while the co-location decisions themselves are consistently guided by the ShaReComp approach introduced in Section **??**. An overview of the four ShaRiff variants and their respective strategies is provided in Table **??**.

Algorithm	**Type**
ShaRiff 1	Biggest Host first, parallel Host-backfilling and mapping of Task Clusters
ShaRiff 2	Biggest Host first, parallel Host-backfilling and mapping of Task Clusters with controlled VM Oversubscription
ShaRiff 3	Round-Robin Assignment of Task Clusters, No parallelism
ShaRiff MinMin	Biggest Host first, parallel Host-backfilling and mapping of ordered Task Clusters

Table 4.3: Overview of the ShaRiff scheduling variants that make use of ShaReComp.

In the following, we provide a detailed description of the behavior of each ShaRiff algorithm, followed by its formal algorithmic representation.

Algorithm 5: ShaRiff 1 — Biggest Host first, parallel Host-backfilling and mapping of Task Clusters

Input: workflow $G = (T, E)$, hosts $\mathcal{H} = \{h_1, \ldots, h_m\}$, idle cores $c(h_j)$, ShaReComp co-location API $\mathcal{S}$

Output: all tasks $t_i \in T$ executed with contention-aware co-location for improved efficiency and utilization

Initialize idle cores $c(h_j) \leftarrow C_j$ for all $h_j \in \mathcal{H}$; Initialize ready queue $\mathcal{Q}$ with all source tasks of G (FIFO order)

while *not all tasks* $t_i \in T$ *completed* **do**

  if $\mathcal{Q}$ *is empty* **then**

    Wait until any task t_r completes; Release its cores: $c(h(t_r)) \leftarrow c(h(t_r)) + \text{req\_cores}(t_r)$; For each successor t_s of t_r, enqueue t_s into $\mathcal{Q}$ if all predecessors are completed; **continue**

  Build available-host list $L = \{\, h \in \mathcal{H} \mid c(h) > 0 \,\}$, sorted by $c(h)$ descending; Initialize empty host task mapping list $\mathcal{M}$;

  foreach *host* $h \in L$ *and while* $\mathcal{Q}$ *not empty* **do**

    Select up to $c(h)$ ready tasks from $\mathcal{Q}$ into $\mathcal{T}_h$; Compute file-location map $\Phi(\mathcal{T}_h)$; Query ShaReComp API: colocMap $\leftarrow \mathcal{S}(\mathcal{T}_h)$; `// returns co-location groups`

    Add mapping $(h, \mathcal{T}_h, \Phi(\mathcal{T}_h), \text{colocMap})$ to $\mathcal{M}$;

  foreach *mapping* $(h, \mathcal{T}_h, \Phi, \mathit{colocMap}) \in \mathcal{M}$ **do**

    foreach *group* $\mathcal{C}_k \in \mathit{colocMap}$ **do**

      $C_{\text{req}} \leftarrow \text{sum}(\text{req\_cores}(\mathcal{C}_k))$; $M_{\text{req}} \leftarrow \text{sum}(\text{req\_mem}(\mathcal{C}_k))$; Allocate $v_h = (C_{\text{req}}, M_{\text{req}}, h)$; Launch all $t \in \mathcal{C}_k$ on v_h; $c(h) \leftarrow \max(0, c(h) - C_{\text{req}})$; Remove $\mathcal{C}_k$ from $\mathcal{Q}$;

  Wait until any task t_r completes; Release its cores: $c(h(t_r)) \leftarrow c(h(t_r)) + \text{req\_cores}(t_r)$; **if** *no active tasks remain on its VM* **then**

    Destroy VM

  For each successor t_s of t_r: if all predecessors are completed, enqueue t_s into $\mathcal{Q}$;

return *workflow complete*

This variant implements ShaRiff 1, which augments a FIFO pipeline with the external co-location adviser ShaReComp and a cluster-aware allocator. Tasks are dequeued in strict arrival order. Before placement, the scheduler invokes ShaReComp with the current set of ready tasks and receives clusters of jobs that are computed to co-locate well. The node-assignment stage then ranks hosts by descending idle-core capacity and fills the largest host first. It forms a batch of up to that hosts idle cores and attaches the ShaRiff cluster map to the batch. If tasks remain, it proceeds to the next host in the ranked list. A small queue path ensures dispatch even when only a few tasks are available. The allocator realizes the advisers plan one VM per recommended cluster on the chosen host. For each multi-task cluster, it provisions a VM whose vCPU count and memory equal the sum of the clustered tasks declared requirements, starts the VM, and submits the tasks to that same virtual compute service. Singleton clusters are grouped into a shared VM on

the host to avoid VM fragmentation. Conceptually, ShaRiff preserves FIFO ordering and capacity-ranked host filling, but replaces random batching with adviser-driven clustering.

Algorithm 6: ShaRiff 2 — Biggest Host first, parallel Host-backfilling and mapping of Task Clusters with controlled VM Oversubscription

Input: workflow $G = (T, E)$, hosts $\mathcal{H} = \{h_1, \ldots, h_m\}$, idle cores $c(h_j)$, oversubscription factor α, ShaReComp co-location API $\mathcal{S}$

Output: workflow executed with affinity-based co-location, maximal host parallelism, and safe oversubscription

Initialize idle cores $c(h_j) \leftarrow C_j$ for all $h_j \in \mathcal{H}$ Initialize ready queue $\mathcal{Q}$ with all source tasks of G (FIFO order)

while *not all tasks* $t_i \in T$ *completed* **do**

  if $\mathcal{Q}$ *is empty* **then**

    Wait until any task t_r completes Release its cores: $c(h(t_r)) \leftarrow c(h(t_r)) + \text{req\_cores}(t_r)$ For each successor t_s of t_r, enqueue t_s into $\mathcal{Q}$ if all predecessors are completed

    continue

  Build available-host list $L = \{\, h \in \mathcal{H} \mid c(h) > 0 \,\}$, sorted by $c(h)$ descending Initialize empty host task mapping list $\mathcal{M}$

  foreach *host* $h \in L$ *and while* $\mathcal{Q}$ *not empty* **do**

    Compute oversubscription limit $n_{\max} = \lceil c(h) \times (1 + \alpha) \rceil$ Select up to $n_{\max}$ ready tasks from $\mathcal{Q}$ into $\mathcal{T}_h$ Compute file-location map $\Phi(\mathcal{T}_h)$ Query ShaReComp API: colocMap $\leftarrow \mathcal{S}(\mathcal{T}_h)$; `// returns co-location groups`

    Add mapping $(h, \mathcal{T}_h, \Phi(\mathcal{T}_h), \text{colocMap})$ to $\mathcal{M}$

  foreach *mapping* $(h, \mathcal{T}_h, \Phi, \mathit{colocMap}) \in \mathcal{M}$ **do**

    foreach *group* $\mathcal{C}_k \in \mathit{colocMap}$ **do**

      $C_{\text{req}} \leftarrow \text{sum}(\text{req\_cores}(\mathcal{C}_k))$ $M_{\text{req}} \leftarrow \text{sum}(\text{req\_mem}(\mathcal{C}_k))$ **if** $C_{req} > c(h)$ **then**

        Allocate $v_h = (c(h), M_{\text{req}}, h)$; ; `// oversubscription active`

      else

        Allocate $v_h = (C_{\text{req}}, M_{\text{req}}, h)$

      Launch all $t \in \mathcal{C}_k$ on v_h $c(h) \leftarrow \max(0, c(h) - C_{\text{req}})$ Remove $\mathcal{C}_k$ from $\mathcal{Q}$

  Wait until any task t_r completes Release its cores: $c(h(t_r)) \leftarrow c(h(t_r)) + \text{req\_cores}(t_r)$ **if** *no active tasks remain on its VM* **then**

    Destroy VM

  For each successor t_s of t_r: if all predecessors are completed, enqueue t_s into $\mathcal{Q}$

return *workflow complete*

This variant extends ShaRiff 1 by controlled oversubscription during placement and VM sizing. Tasks are dequeued in arrival order. Before dispatch, the scheduler queries ShaReComp with the current ready set and receives clusters of tasks pcomputed to co-locate well. Hosts are ranked by descending idle-core capacity; the assigner then fills the largest host first with a batch whose size may exceed the hosts free cores by a fixed factor of in our example 25%. If tasks remain, it proceeds to the next host and repeats. The allocator implements the advisers plan one VM per cluster on the chosen host, but with oversubscription semantics. For multi-task clusters, it provisions a VM whose vCPU and memory equal the sum of the clusters requests—even if that exceeds the hosts currently free cores. For single task clusters collected on the same host, it provisions a shared VM and caps

vCPUs at the hosts free cores when necessary. Because ShaReComp groups complementary tasks, oversubscription holds the potential to translate into higher throughput and energy efficiency. However, when clustered tasks are less complementary, contention can surface, making this variant an explicit trade-off between utilization and interference.

Algorithm 7: ShaRiff 3 — Round-Robin Assignment of Task Clusters, No parallelism

Input: workflow $G = (T, E)$, hosts $\mathcal{H} = \{h_1, \ldots, h_m\}$, idle cores $c(h_j)$, ShaReComp co-location API $\mathcal{S}$

Output: tasks executed using round-robin host selection with affinity-based VM co-location

Initialize idle cores $c(h_j) \leftarrow C_j$ for all $h_j \in \mathcal{H}$ Initialize ready queue $\mathcal{Q}$ with all source tasks of G (FIFO order) Initialize round-robin index $r \leftarrow 0$

while *not all tasks* $t_i \in T$ *completed* **do**

  if $\mathcal{Q}$ *is empty* **then**

    Wait until any task t_r completes Release its cores: $c(h(t_r)) \leftarrow c(h(t_r)) + \text{req\_cores}(t_r)$ For each successor t_s of t_r, enqueue t_s into $\mathcal{Q}$ if all predecessors are completed

    continue

  Select next host $h = \mathcal{H}[r \bmod |\mathcal{H}|]$ Update round-robin index: $r \leftarrow (r + 1) \bmod |\mathcal{H}|$ Retrieve available cores $C = c(h)$ Select up to C ready tasks from $\mathcal{Q}$ into $\mathcal{T}_h$ Query ShaReComp API: colocMap $\leftarrow \mathcal{S}(\mathcal{T}_h)$;

  `// returns co-location groups`

  foreach *group* $\mathcal{C}_k \in$ *colocMap* **do**

    $C_{\text{req}} \leftarrow \text{sum}(\text{req\_cores}(\mathcal{C}_k))$ $M_{\text{req}} \leftarrow \text{sum}(\text{req\_mem}(\mathcal{C}_k))$ Allocate $v_h = (C_{\text{req}}, M_{\text{req}}, h)$ Launch all $t \in \mathcal{C}_k$ on v_h $c(h) \leftarrow \max(0, c(h) - C_{\text{req}})$ Remove $\mathcal{C}_k$ from $\mathcal{Q}$

  Wait until any task t_r completes Release its cores: $c(h(t_r)) \leftarrow c(h(t_r)) + \text{req\_cores}(t_r)$ **if** *no active tasks remain on its VM* **then** Destroy VM

  For each successor t_s of t_r: if all predecessors are completed, enqueue t_s into $\mathcal{Q}$

return *workflow complete*

ShaRiff 3 combines round-robin first-fit placement with ShaReComp-guided intra-VM co-location. The scheduler releases tasks strictly in arrival order. The node-assignment component scans hosts in round-robin fashion and picks the first host reporting at least one idle core. It then pulls up to that hosts idle-core capacity worth of ready tasks and queries ShaReComp for a co-location plan over this batch. The allocator realizes ShaReComps plan one VM per suggested cluster on the chosen host. For each multi-task cluster, it sizes the VM by summing vCPU and memory requirements of the clusters tasks, starts the VM, and submits all cluster tasks to the same virtual compute service. Conceptually, the policy is first-fit host, adviser-driven packing. Unlike the other variants, this strategy does not oversubscribe cores. It fills only the currently free capacity of the first eligible host and relies on ShaReComp's clustering to raise utilization and efficiency through informed co-location.

This scheduler variant extends the ShaRiff framework with a MinMin ordering layer, a classical heuristic from list scheduling. Instead of operating on individual tasks, it applies the MinMin principle to task clusters generated by ShaReComp's co-location analysis. At

each scheduling interval, the scheduler requests a new clustering of ready tasks, queries the prediction service using the models introduced in **??** with **??** for estimated runtimes, and orders clusters in ascending order of predicted execution time. The ShaRiff node assignment and VM allocator then manage placement and resource provisioning. In essence, this forms a MinMin scheduler over co-located clusters, combining ShaRiff's affinity-based co-location with prediction-guided execution ordering to minimize queueing delays and improve overall workflow completion time.

5 Implementation

This chapter details the technical implementation of the concepts introduced in the previous section. While the Approach chapter established the conceptual and algorithmic foundations of the proposed scheduling framework, the following sections focus on how these ideas were realized in practice. The implementation emphasizes architectural modularity, clear component interfaces, and the integration of machine learning-based decision layers within a simulation-driven environment. Each subsystem—from the monitoring client and statistical modeling backend to the simulation environment—was designed to remain functionally independent while communicating through well-defined data and control flows. This decoupled design not only facilitates reproducibility and maintainability but also enables future extensions, such as the replacement of predictive models or the addition of new scheduling policies, without major structural changes. The remainder of this chapter outlines the overall system architecture, mentions the chosen technologies and design principles, and describes the concrete implementation of the monitoring client, the statistical learning components, and the simulator setup.

5.1 System Architecture

5.2 Technology and Design Choices

Table 5.4: Monitoring features and associated technical components.

Component Category	Software Used	Comments / Functionality
Workflow Execution		
Operating System	Ubuntu 22.04.5 LTS	Base system environment for all components.
Kernel	Linux 5.15.0-143-generic	Provides low-level system resource management.
Workflow Management Engine	Nextflow 25.06.0	Controls workflow DAG execution and task dependency resolution.
Virtualization Layer	Docker Engine 28.3.1 (Community)	Provides isolated VM environments for task execution.
Resource Manager	Slurm 24.05.2	Allocates CPU and memory resources dynamically across hosts.
Monitoring System		
Time-Series Database	Prometheus Server 3.3.1	Central metric collector and time-series database.
Monitoring Client	Go 1.24.1	Collects per-node and per-container resource metrics.
Workload Experiments		
Benchmark Execution	stress-ng 0.13.12	Generates controlled CPU, memory, and I/O workloads.
Monitoring	Deep-Mon (custom fork) with Python 3.10.12 & BCC 0.35.0	Captures resource traces during workload execution.
Data Analysis		
Feature Engineering	Jupyter Kernel 6.29.5, Python 3.10.12, Poetry 2.1.2	Derives and normalizes temporal task signatures.
Clustering	scikit-learn 1.5.2	Groups similar task behaviors into consolidated classes.
KCCA	CCA-Zoo 2.5.0	Learns correlations between performance and energy domains.
Random Forest Regressor	scikit-learn 1.5.2	Predicts runtime and power consumption from task signatures.
Kernel Ridge Regression	scikit-learn 1.5.2	Baseline model for non-linear regression comparison.
Simulation Framework		
Workflow Tracing	Nextflow Tracer (custom fork)	Records execution-level metadata for simulation replay.
Simulation Engine	WRENCH 2.7 & C++17	Evaluates scheduling strategies under controlled conditions.
Clustering API	FastAPI 0.1.0, Python 3.10.12	Provides task grouping via ShaReComp integration.
Prediction API	FastAPI 0.1.0, Python 3.10.12	Interfaces learned models for runtime and energy estimation.

5.3 Decoupled Design for further Research

The extensibility of the overall system is achieved through a decoupled design that separates monitoring, modeling, and simulation components while maintaining clear communication interfaces between them. Each part of the system can evolve independently without impacting others, enabling modular experimentation with new data sources, predictive models, or scheduling strategies. This modularity supports reproducibility and future extensibility, as new data collection layers or simulation backends can be added by extending interfaces rather than rewriting existing code.

5.3.1 Configurable Monitoring Client

The monitoring client exemplifies this philosophy by relying on a flexible configuration-driven architecture. Using a YAML-based configuration file, it dynamically defines which metrics to collect from heterogeneous data sources such as Prometheus exporters, cAdvisor, eBPF probes, or SNMP-based sensors. The configuration specifies not only the metric names and queries but also the identifiers and units, allowing seamless adaptation to different environments or workflow engines. This separation of logic and configuration enables the same client to operate across diverse infrastructures without recompilation. The clients implementation, built on the Prometheus API, abstracts away the complexity of time-range queries and concurrent metric fetching through lightweight threading and synchronization mechanisms. As a result, developers can extend the monitoring framework simply by adding new data sources or metrics to the configuration file, without altering the underlying collection logic.

```
1
2  server_configurations
3    config_path
4    prometheus
5      target_server
6        controller
7        workers
8        address
9        timeout 5s
10 monitoring_targets
11   cpu
12     enabled true
13     data_sources
14       - source cAdvisor
15         labels [id, image, job,name]
16         identifier name
17         metrics
18           - name container_cpu_user_seconds_total
19             query container_cpu_user_seconds_total
20             unit seconds
21       - source ebpf-mon
22         labels [container_id, name]
23         identifier name
24         metrics
25           - name container_weighted_cycles
26             query container_weighted_cycles
27             unit counter
28   memory
29     enabled true
30     data_sources
31       - source
32         labels
```

```
        identifier
        metrics
```

Listing 1: Example YAML Configuration File

5.3.2 Enabling Access to Co-location Hints in the Simulator

The statistical modeling component, implemented as a standalone FastAPI service, follows a similar modular design. It exposes a clean, language-agnostic HTTP API that separates the inference logic from data ingestion and model management. The service maintains state for clustering and prediction requests, delegating core computational tasks to dedicated helper functions. This decoupling makes it straightforward to replace or add new predictive models, such as neural architectures or alternative regression approaches, without modifying the API contract. The clustering and prediction endpoints can interact with any external workflow manager or simulator via standardized JSON payloads, ensuring flexibility in integrating new pipelines or retraining procedures. This independence between model serving and data processing pipelines also simplifies scalability, allowing the modeling service to be containerized and deployed independently for distributed or cloud-based setups.

Table 5.5: Overview of REST API Endpoints Exposed by the ShaReComp Service.

#	**Endpoint**	**Method**	**Description / Response Schema**
1	`/clusterize_jobs`	POST	Clusters nf-core jobs based on historical data. *Request:* `ClusterizeJobsRequest` (list of job names). *Response:* `ClusterizeJobsResponse` (cluster mapping with run ID).
2	`/predict`	POST	Predicts runtime and power consumption for consolidated job clusters. *Request:* `PredictRequest` (cluster IDs, model types). *Response:* `PredictionResponse` (predicted values for each model).
Component Schemas			
–	`ClusterizeJobsRequest`	Object	**Fields:** `job_names` (array of strings). Required.
–	`ClusterizeJobsResponse`	Object	**Fields:** `run_id` (string), `clusters` (map of arrays). Required.
–	`PredictRequest`	Object	**Fields:** `cluster_ids` (array), `prediction_models` (array of `PredictionModel`). Required.
–	`PredictionModel`	Object	**Fields:** `model_type` (array of strings). Required.
–	`PredictionResponse`	Object	**Fields:** `run_id` (string), `predictions` (nested map of numeric values). Required.

5.3.3 Used Simulator Components

The simulator setup further demonstrates the benefits of this decoupled design. The resource management layer of the simulator exposes generic interfaces for allocators, schedulers, and node assigners, allowing any of them to be replaced or combined dynamically at runtime. This separation allows the same simulator to execute both baseline and experimental resource allocation strategies without modifying the controller logic. Through this design, the simulator can execute diverse workflow types by merely switching configuration parameters or class bindings. Moreover, the integration of energy and performance tracing

through independent services ensures that extending the simulator with new measurement capabilities does not interfere with the scheduling or execution logic.

```cpp
int main(int argc, char **argv)
{
    auto simulation = wrench::Simulation::createSimulation();

    simulation->init(&argc, argv);

    auto workflow = wrench::WfCommonsWorkflowParser::createWorkflowFromJSON(workflow_file, "100Gf", true);

    simulation->instantiatePlatform(platform_file);

    std::set<std::shared_ptr<wrench::StorageService>> storage_services;
    auto storage_service = simulation->add(wrench::SimpleStorageService::createSimpleStorageService(
        "WMSHost", {"/scratch/"}, {{wrench::SimpleStorageServiceProperty::BUFFER_SIZE, "50MB"}}, {}));

    std::vector<std::string> hostnames = {"VirtualizedClusterHost1", "VirtualizedClusterHost2", "VirtualizedClusterHost3"};

    std::cerr << "Instantiating an EnergyMeterService on WMSHost that monitors VirtualizedClusterHost1 every 10 seconds ..." << std::endl;
    auto energy_meter_service = simulation->add(new wrench::EnergyMeterService("WMSHost", hostnames, 10));

    simulation->getOutput().enableEnergyTimestamps(true);

    auto virtualized_cluster_service = simulation->add(new wrench::VirtualizedClusterComputeService(
        "VirtualizedClusterProviderHost", virtualized_cluster_hosts, "", {}, {}));
    auto wms = simulation->add(
        new wrench::Controller(workflow, virtualized_cluster_service, storage_service, "WMSHost"));

    auto file_registry_service = new wrench::FileRegistryService("WMSHost");
    simulation->add(file_registry_service);

    simulation->launch();

    auto energy_trace = simulation->getOutput().getTrace<wrench::SimulationTimestampEnergyConsumption>();

    simulation->getOutput().dumpHostEnergyConsumptionJSON("../results/{strategy}_{workflow}rnaseq_host_energy_consumption.json", true);

    return 0;
}
```

Listing 2: WRENCH C++ Simulation File

6 Evaluation

6.1 Evaluation Setup

6.1.1 Infrastructure

The experiments were conducted on a single-node system equipped with an AMD EPYC 8224P 24-core, 48-thread processor and 188 GB of RAM. The processor supported simultaneous multithreading and frequency boosting up to 2.55 GHz, with 64 MB of shared L3 cache and a single NUMA domain ensuring uniform memory access across all cores. Storage was provided by a 3.5 TB NVMe SSD, and the system ran a 64-bit Linux environment configured for stable and reproducible execution. To collect accurate power usage data, the node was connected to a 12-way switched and outlet-metered PDU (Expert Power Control 8045 by GUDE), which provided per-outlet power measurements via a REST API.

6.1.2 Workflows

Table 6.6: Overview of evaluated nf-core workflows and their inputoutput characteristics.

Workflow	Number of Tasks	Input Files	Output Files	Data Profile
`atacseq`	72	24	185	Bulk chromatin accessibility sequencing (ATAC-seq)
`chipseq`	68	22	172	Bulk chromatin immunoprecipitation sequencing (ChIP-seq)
`rnaseq`	54	18	160	Bulk RNA-seq expression quantification
`scnanoseq`	83	25	210	Single-cell nanopore RNA-seq
`smrnaseq`	59	20	142	Small RNA sequencing (miRNA/siRNA profiling)
`pixelator`	44	16	125	Spatial transcriptomics pixel-based expression mapping
`methylseq`	65	21	170	Whole-genome or targeted DNA methylation sequencing
`viralrecon`	51	19	150	Viral genome assembly and variant analysis
`oncoanalyser`	97	28	260	Comprehensive somatic cancer genome analysis

6.1.3 Monitoring Configuration

Table 6.7: Adaptable Monitoring Configuration Overview.

Monitoring Target	Enabled	Supported Data Sources	Collected Metric Types / Adaptability Notes
Task Metadata		slurm-job-exporter	Collects job metadata (state, runtime, working directory). Can adapt to other job schedulers.
CPU		cAdvisor, ebpf-mon, docker-activity	Captures CPU time and cycles from both container and kernel levels. Supports switching sources for varying granularity.
Memory		cAdvisor, docker-activity	Tracks memory utilization at container or process level. Configurable for byte- or percentage-based metrics.
Disk		cAdvisor	Monitors block I/O and filesystem throughput. Supports extension with storage exporters.
Network		cAdvisor (optional)	Disabled by default due to noise. Can be enabled for network-intensive workflows.
Energy		docker-activity, ebpf-mon, ipmi-exporter, snmp-exporter	Multi-layer energy monitoring from container to node level. Adaptable to hardware sensors and external power meters.
Prometheus Configuration			
The Prometheus backend collects all metrics via configurable scrape intervals and targets. Controller and worker nodes can be flexibly defined, enabling distributed monitoring setups.			

6.1.4 Implemented Models for Task Clustering and Prediction

As described in Chapter 5, the statistical models—including the clustering and prediction components—are provided through a FastAPI implementation, allowing external simulation engines to interact with them programmatically. At the same time, the core functionality of the coloc-app FastAPI service is based on a Jupyter Notebook that contains all implementations of the clustering and predictive models discussed in Chapter 5. Both the notebook and the coloc-app were executed on the host system described in Section

6.1.5 Simulation Setup

Simulated Platform Configuration The infrastructure described in Section **??** was replicated within the SimGrid simulation environment using its platform description tool, as shown in the following XML configuration. The hosts core performance was calibrated by executing stress-ng benchmarks to determine realistic CPU speeds, while network throughput was measured using sysbench. To determine power states (P-states), the GUDE power meter was used to record power consumption in both idle and active conditions under varying load profiles generated with stress-ng. This procedure ensured that the simulated environment accurately reflected the performance and energy characteristics of the physical test system.

```
1 <?xml version='1.0'?>
```

```
<!DOCTYPE platform SYSTEM "https://simgrid.org/simgrid.dtd">
<platform version="4.1">
    <zone id="AS0" routing="Full">
        <host id="VirtualizedClusterHost1" speed="32Gf,28Gf,20Gf,12Gf,8Gf" pstate="0" core="24">
            <prop id="ram" value="188GiB" />
            <!-- The power consumption in watt for each pstate (idle:all_cores) -->
            <prop id="wattage_per_state" value="116:133:220, 114:129:202, 111:125:186, 108:121:170,106:118:156"/>
            <prop id="wattage_off" value="10" />
        </host>
        <host id="VirtualizedClusterHost2" speed="32Gf,28Gf,20Gf,12Gf,8Gf" pstate="0" core="24">
            <prop id="ram" value="188GiB" />
            <!-- The power consumption in watt for each pstate (idle:all_cores) -->
            <prop id="wattage_per_state" value="116:133:220, 114:129:202, 111:125:186, 108:121:170,106:118:156"/>

            <prop id="wattage_off" value="10" />
        </host>
        <host id="VirtualizedClusterHost3" speed="32Gf,28Gf,20Gf,12Gf,8Gf" pstate="0" core="24">
            <prop id="ram" value="188GiB" />
            <!-- The power consumption in watt for each pstate (idle:all_cores) -->
            <prop id="wattage_per_state" value="116:133:220, 114:129:202, 111:125:186, 108:121:170,106:118:156"/>
            <prop id="wattage_off" value="10" />
        </host>
</platform>
```

Listing 3: Example XML Configuration File

Baseline Scheduling Algorithms To evaluate the effectiveness of the proposed approach, we compare it against a series of progressively refined baseline algorithms that address the co-location problem with increasing complexity. These baselines range from simple scheduling heuristics to more advanced strategies that gradually incorporate awareness of co-location effects. The following table summarizes all baselines considered in this study. It is important to note that while some of them already involve concurrent execution of tasks, this represents uncontrolled co-location rather than informed or optimized placement. For clarity and conciseness, detailed algorithmic designs of these baselines are provided in the appendix, while this section focuses on describing their conceptual behavior.

Table 6.8: Overview of Baseline Scheduling Algorithms.

Algorithm	**Type**	**Description**
Baseline 1	FIFO + Round-Robin	Executes tasks in FIFO order and assigns them to hosts in a round-robin fashion without co-location or backfilling.
Baseline 2	FIFO + Backfilling	Assigns tasks in FIFO order to the first available host, allowing idle hosts to be backfilled opportunistically.
Baseline 3	FIFO + VM Co-location	Groups multiple ready tasks on the same host within a single VM if sufficient resources are available.
Baseline 3.1	Max-Core VM Co-location	Prefers the host with the largest number of idle cores for task co-location to maximize utilization.
Baseline 3.2	Max-Parallel VM Co-location	Distributes ready tasks across all available hosts in parallel, promoting high concurrency across nodes.
Baseline 4	VM Co-location + Over-Subscription	Extends co-location by allowing controlled CPU over-subscription on selected hosts using an oversubscription factor α.
Baseline 4.1	Max-Parallel Co-location + Over-Subscription	Combines parallel host utilization with co-location and controlled CPU over-subscription for improved throughput.

The baseline scheduling algorithm implements a simple, sequential execution model designed to simulate isolated task processing within a virtualized cluster. The scheduling process is divided into three abstract components that operate in a fixed order: task scheduling, node assignment, and resource allocation. The scheduler applies a first-in, first-out (FIFO) policy, maintaining a queue of workflow tasks sorted by their readiness. Tasks are retrieved from this queue strictly in order of arrival, preserving dependency

constraints and ensuring a fully deterministic execution sequence without reordering or prioritization. Once a task is selected for execution, the node assignment component distributes it across available compute hosts using a round-robin policy. This mechanism cycles through hosts in sequence, ensuring an even and systematic distribution of tasks across the cluster. No host is assigned more than one active task at a time, enforcing exclusive execution and preventing contention for shared resources. The next variant keeps the same FIFO scheduler and VM-based allocator as Baseline 1, but replaces exclusive node assignment with a greedy backfilling policy. Tasks are still dequeued strictly in arrival order by the FIFO scheduler. For each ready task, the node assignment component queries the cluster for the current number of idle cores per host and performs a first-fit scan: it selects the first host that reports at least one idle core, without requiring the host to be completely idle. The allocator then provisions a VM on the chosen host, binds the tasks inputs/outputs, submits the job to that VM, and on completion shuts the VM down and destroys it. Conceptually, this turns the placement step into gap filling rather than strict exclusivity. Multiple tasks can be co-located on the same host up to its core capacity, increasing instantaneous parallelism and utilization. Baseline 3 does not differ in the scheduling behavior but replaces the standard allocator and node assignment with components that allow for co-location. When the node assignment component queries the cluster for idle-core availability, it again selects the first host with available cores. However, instead of launching one VM per task, all ready tasks that fit within the hosts idle-core capacity are grouped into a single batch. These tasks are then co-located inside one shared VM instance that is dimensioned according to the aggregate resource requirements of the batch—its vCPU count and memory size are computed as the sum of the respective task demands. Conceptually, this baseline captures the behavior of intra-VM co-location, where multiple independent tasks share the same virtual machine instead of being distributed across separate ones. Baseline 3 is extended by 2 variants where the first one extends thenode assignment component to query the cluster for idle-core availability and selects the host with the maximum amount of available cores. However, instead of launching one VM per task, all ready tasks that fit within the hosts idle-core capacity are grouped into a single batch. These tasks are then co-located inside one shared VM instance that is dimensioned according to the aggregate resource requirements of the batch—its vCPU count and memory size are computed as the sum of the respective task demands. The second extension replaces the placement policy with a selection step for the host with maximum idle cores. At each dispatch, the node-assignment component queries the cluster for the current idle cores per host map and picks the host with the largest number of free cores. It then forms a batch by taking as many ready tasks from the FIFO head as the chosen host can accommodate. Compared to first-fit co-location, it tends to reduce residual fragmentation by packing work onto the most spacious node, while still honoring FIFO ordering and leaving task runtime/I/O handling unchanged. The 4th baseline retains the same FIFO scheduler but introduces a node assignment and allocation policy focused on maximizing parallel host utilization. Upon each scheduling cycle, the node assignment component queries the cluster for the current number of idle cores per host, filters out fully occupied nodes, and ranks the remaining hosts in descending order of available cores. It then assigns tasks in batches, filling the host with the highest idle capacity first and grouping as many ready tasks as the hosts idle-core count allows. Once the first host is filled, the process continues with the next host until all tasks in the ready queue are mapped. The allocator provisions one VM per host batch, sizing it to match the aggregate requirements of all tasks assigned to that host. The resulting VMs vCPU and memory configuration reflect the total core and memory demands of the

batch. Each task in the batch is submitted as an independent job to the same virtual compute service, and the VM remains active until all its co-located tasks have finished, at which point it is shut down and destroyed. The last baseline extends the previous one by allowing controlled CPU over-subscription during co-location. At each scheduling cycle, the node assignment component queries per-host idle cores, sorts hosts in descending idle capacity, and fills the largest host first. Unlike the non-oversubscribed version, the per-host batch may exceed the currently idle cores by a fixed factor the batch limit is set to. The procedure continues down the ranked host list, forming one batch per host in the same cycle. The allocator provisions one VM per host batch, but caps the VMs vCPU count to the hosts actual idle cores at allocation time not the sum of task core demands, while sizing memory to the aggregate of the batched tasks. All tasks in the batch are then submitted to that single VM and execute concurrently on a vCPU pool intentionally smaller than their combined declared cores. The VM remains active until all co-located tasks complete, then it is shut down and destroyed. Crucially, the degree of contention—and thus realized speedup or slowdown—depends on the complementarity of the co-located task profiles. When CPU-, memory-, and I/O-intensive phases overlap unfavorably oversubscription amplifies interference and queueing on scarce vCPUs. When profiles are complementary, the same oversubscription admits more useful overlap with less contention, improving per-host throughput. Conceptually, this variant implements parallel, capacity-ranked co-location with controlled oversubscription.

6.2 Experiment Results

The section on experimental results is organized as follows. We begin with a brief discussion of the monitoring results obtained using the configuration described earlier. Next, we revisit the approach introduced in Chapter 4 by examining the workload experiments and the resulting measurements that form the basis for subsequent evaluation steps. We then present the outcomes of the statistical methods applied in this work, starting with an in-depth analysis of the task consolidation approach introduced in Chapter 4. Building on these results, we continue with an interpretation of the outcomes from training two predictive models on the clustering data. Finally, we integrate all components into a unified simulation framework. Using this setup, we execute all workflows introduced at the beginning of Chapter 6 with the algorithms detailed in Chapter 4 and the appendix. Several aspects of the simulation results are discussed before Chapter 7 concludes with an overall evaluation and interpretation of the findings.

6.2.1 Measuring Interference during Benchmark Executions

Table 6.9: Summary of Synthetic Benchmarks Used in Evaluation

Benchmark Label	Image / Version	
CPU	`stress-ng-cpu:latest`	`stress-ng -cpu 1 -`
Memory (VM)	`stress-ng-mem-vm:latest`	`stress-ng -v`
File I/O	`fio:latest`	`fio -name seqread -rw read -bs 1M -size 18G -`

For measuring resource contention, as described in Chapter 4, we use the stress-ng tool with the commands listed in **??**. The benchmark code is executed inside Docker containers, and the Docker API is used to capture the execution time of each benchmark. Since the benchmark instructions are fixed and not time-dependent, this provides consistent and

comparable measurements. To record the containers' energy consumption, we again use the ebpf-based Deep-Mon tool.

?? shows the results of running each benchmark sequentially on different CPU cores of the node. This reveals how long a container pinned to a single core takes to complete the specified benchmark. Next, we execute all possible pairs of workloads, running each pair sequentially on the same pinned CPU core. For each pair, we plot the runtime of both benchmarks in grouped bars, where the grey area represents the runtime of the benchmark when executed in isolation. The same procedure is repeated for collecting and visualizing the corresponding energy consumption data.

We observe in **??** that the runtime increases for every co-located pair of workloads. While memory-intensive benchmarks show only a slight increase, file I/O workloads tend to take roughly one quarter longer than their isolated runs. The most pronounced effect appears when compute-heavy workloads are co-located, where the execution time nearly doubles. This confirms that CPU-bound applications experience the strongest interference when sharing the same physical core.

The power measurements for the co-located workloads, however, show much higher variance and inconsistency across repeated runs. For example, in the CpuCpu case, the isolated power draw averages around 3.43W, whereas the co-located readings drop to approximately 0.008 joules. Similarly, for FileIOFileIO, the measured power decreases from 0.054W in isolation to about 0.009W when co-located. These values are clearly unrealistic and indicate that the RAPL-based measurements on AMD hardware are unreliable in this setup.

This discrepancy stems from the fact that AMD's RAPL interface does not expose per-core or per-container energy readings in a consistent manner. When two containers share a single CPU core, RAPL counters may fail to attribute power consumption correctly between them, resulting in near-zero or erratic readings. In contrast, for the CpuMem combination, the measured power values 27.93 joules and 15.58 joules are much higher and closer to expected magnitudes. This pairing likely produced a more stable measurement because the CPU and memory subsystems were stressed differently, allowing RAPL to record distinct and more accurate energy counters.

Overall, while the runtime data clearly demonstrate the expected contention effects, the power data highlight a measurement limitation. We therefore do not include the plotted power measurements for the co-located benchmark executions but account for the impact of contention in the following evaluation.

Figure 6.19: Bar Plot iso

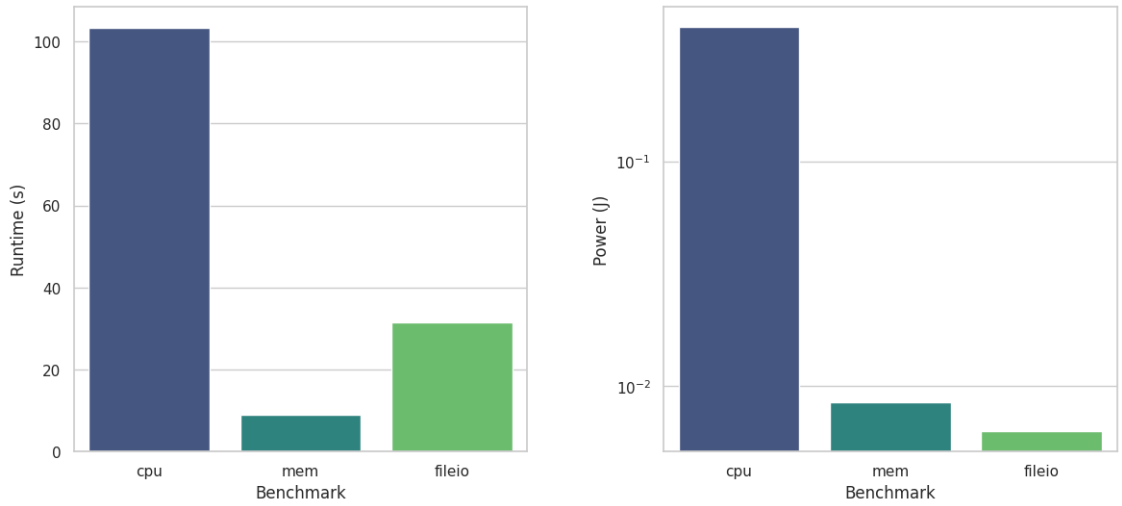

Das ist eine Beschreibung der Abbildung.

Figure 6.20: Bar Plot colo

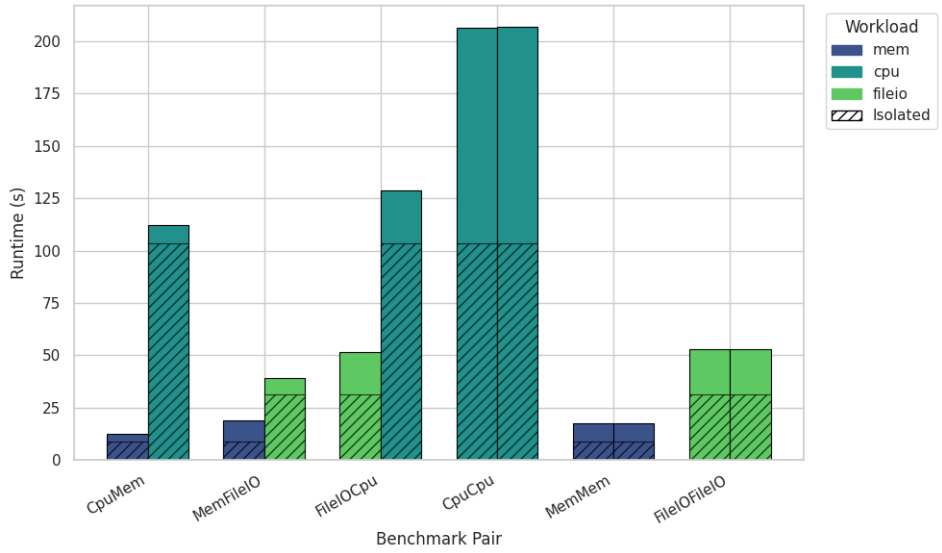

Das ist eine Beschreibung der Abbildung.

We calculated the affinity scores between workload pairs according to **??**.

Table 6.10: Affinity scores between workload types indicating co-location compatibility.

Workload 1	Workload 2	Affinity Score	Comment
mem	cpu	0.736	Very Low compatibility; memory and CPU workloads can share resources with serious contention occuring.
mem	fileio	0.293	High compatibility; low interference due between I/O and memory bandwidth pressure.
fileio	cpu	0.272	High compatibility; CPU workloads cause low contention for shared I/O buffers.
cpu	cpu	0.503	Low compatibility CPU-bound tasks compete for cores and effect thread scheduling.
mem	mem	0.566	Low compatibility; High memory contention under shared caching.
fileio	fileio	0.414	Limited compatibility; file I/O contention degrades throughput under co-location.

The results shown in the previous figures are consistent with the affinity scores presented in table **??**. When both CPU and memory benchmarks are co-located, their runtimes increase significantly, resulting in the highest affinity scores that indicate strong contention and poor compatibility. This pattern is followed by other same-type co-locations, such as CPU–CPU and Mem–Mem, where scores around 0.5 also reflect noticeable interference, as seen in the near doubling of execution times in the earlier plots. File I/O workloads, by contrast, show comparatively high compatibility. Their co-location with CPU or memory benchmarks causes only minor slowdowns, confirming that I/O-bound tasks exert limited pressure on shared compute or memory resources.

It is worth noting, however, that while the runtime degradation for the CPUMemory pair was moderate, this combination exhibited the largest increase in power consumption. This behavior aligns with the earlier observation that RAPL-based power measurements on AMD hardware tend to be unstable. In calculating the affinity scores, we therefore introduced a weighting parameter alpha = 0.7 to assign greater importance to runtime than to power consumption, compensating for the measurement inconsistencies discussed previously. The resulting affinity scores thus primarily reflect the runtime interference between workloads, which will serve as input for computing task dissimilarities in the following section.

6.2.2 Dissimilarity-based Task Clustering

We evaluate the task clustering procedure in two stages. First, we randomly sample a subset of tasks from the workflow executions and preprocess them for clustering as described in Chapter 4. Specifically, we select 34 random tasks from the OncoAnalyser workflow and perform two clustering variants: a random baseline clustering and the ShaReComp-based clustering, which incorporates dissimilarity distances influenced by the affinity scores presented in the previous table. For each cluster, we compute the scale normalized average

temporal signatures of the monitored performance metrics, as defined by the monitoring configuration in Chapter 6. These averages are then visualized using radar plots. Each radar plot represents the tasks grouped into a single cluster and thus identifies potential candidates for co-location. The purpose of this visualization is to illustrate the effect of the dissimilarity-based distance formulation and the use of a clustering threshold set to the 25th percentile of the overall distance distribution. This threshold ensures that only sufficiently dissimilar tasks are clustered together. Additionally, because the distance measure is adjusted by the correlation between resource usage patterns, tasks with high correlation in their workload behavior tend to be separated, reflecting the influence of the previously computed affinity scores.

Figure 6.21: Radarplot Random

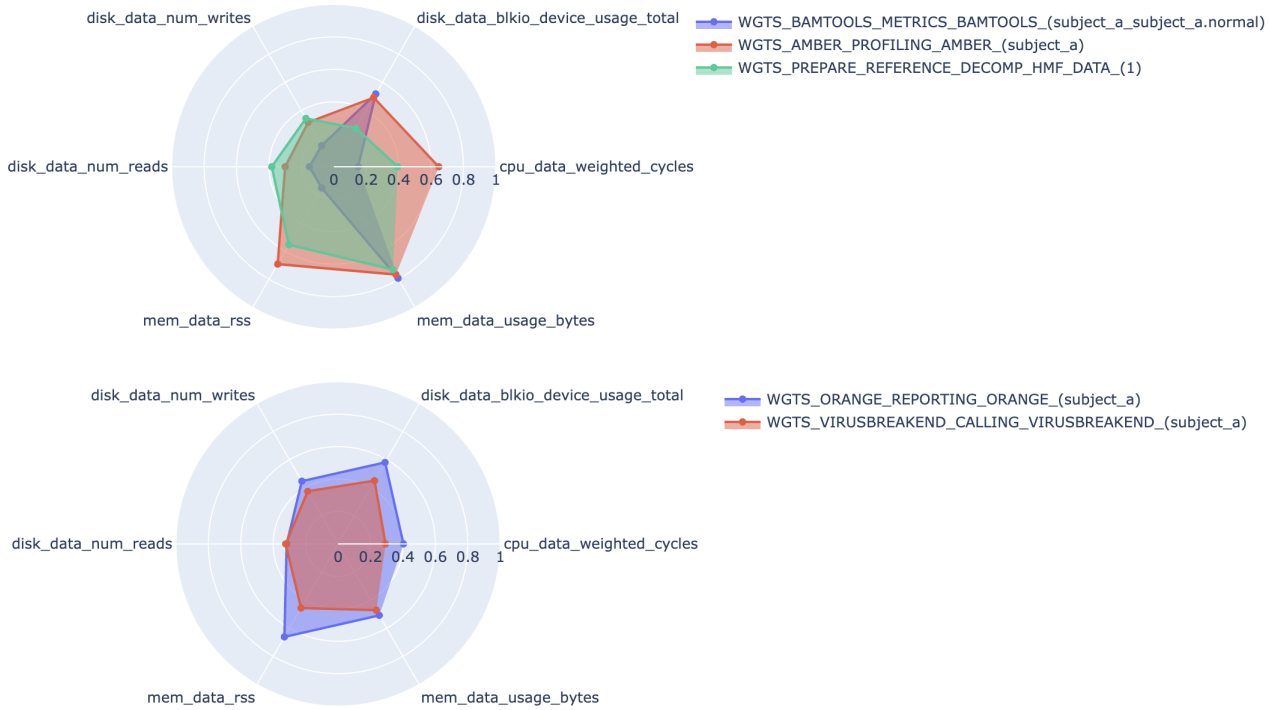

Das ist eine Beschreibung der Abbildung.

We first examine the distribution of task characteristics in the clusters formed by the completely random clustering over the selected probe of oncoanalyser tasks. The first cluster contains three tasks, while the second cluster includes two. At first glance, the radar plots show that the resource profiles of the tasks overlap strongly across all six dimensions of the task resource signatures. Most notably, the bamtools metrics, amber profiling, and prepare reference tasks exhibit almost identical patterns in their average memory allocation over time and resident memory usage RSS. The same overlap appears in their block I/O activity, reflected by nearly identical numbers of file reads and writes, indicating similar file access behavior. Although the average CPU usage differs slightly between these tasks, the variations remain small in scale, suggesting that when such tasks are co-located, contention effects are likely to occur. Overall, this clustering outcome contradicts the affinity findings summarized in Table **??**, where memory-memory, CPU-CPU, and mixed memory-CPU combinations showed the highest contention potential. A similar

issue can be observed in the second radar plot, which represents another randomly formed cluster consisting of two tasks. Here again, the task profiles overlap substantially, and the resource dimensions are distributed within the same scale range. This overlap suggests a comparable risk of resource contention, confirming that purely random clustering disregards workload diversity and leads to groupings that do not respect the resource affinity relationships observed earlier.

We now move on to compare the clusters formed by the ShaReComp approach. At first glance, the radar plots already differ notably in shape compared to those produced by random clustering. The task profiles appear shifted relative to one another rather than overlapping, suggesting that the clustering process has effectively separated tasks with similar resource usage. Focusing on the affinities, we observe that both CPU and memory utilization differ clearly in magnitude between tasks within the same cluster. The same applies to the memory-related metrics, including total memory usage and resident set size (RSS), which are visibly offset from one another. This separation is also reflected in the file I/O dimensions. Although moderate contention potential remains, the average values differ sufficiently to indicate that these tasks do not compete heavily for the same I/O resources. Consequently, the higher peaks in memory and disk I/O observed in the radar plots do not imply significant interference, as their activity patterns occur in distinct resource dimensions. The second radar plot shows a similar trend. Tasks with low CPU utilization are clustered together with tasks exhibiting higher memory usage, yet their respective memory signatures remain clearly separated. This indicates that the ShaReComp method successfully avoids grouping tasks that would likely contend for the same resources. From this comparison, we conclude that dissimilarity-based clustering informed by experimental resource contention data can effectively prevent the co-location of tasks with overlapping resource demands. The applied threshold plays a crucial role in this behavior: a lower threshold results in smaller, more selective clusters, while a higher one allows broader groupings. The influence of this threshold across larger samples will be explored in future work, but these initial results already demonstrate the potential of the approach to mitigate contention through informed clustering.

Figure 6.22: Radarplot Cluster

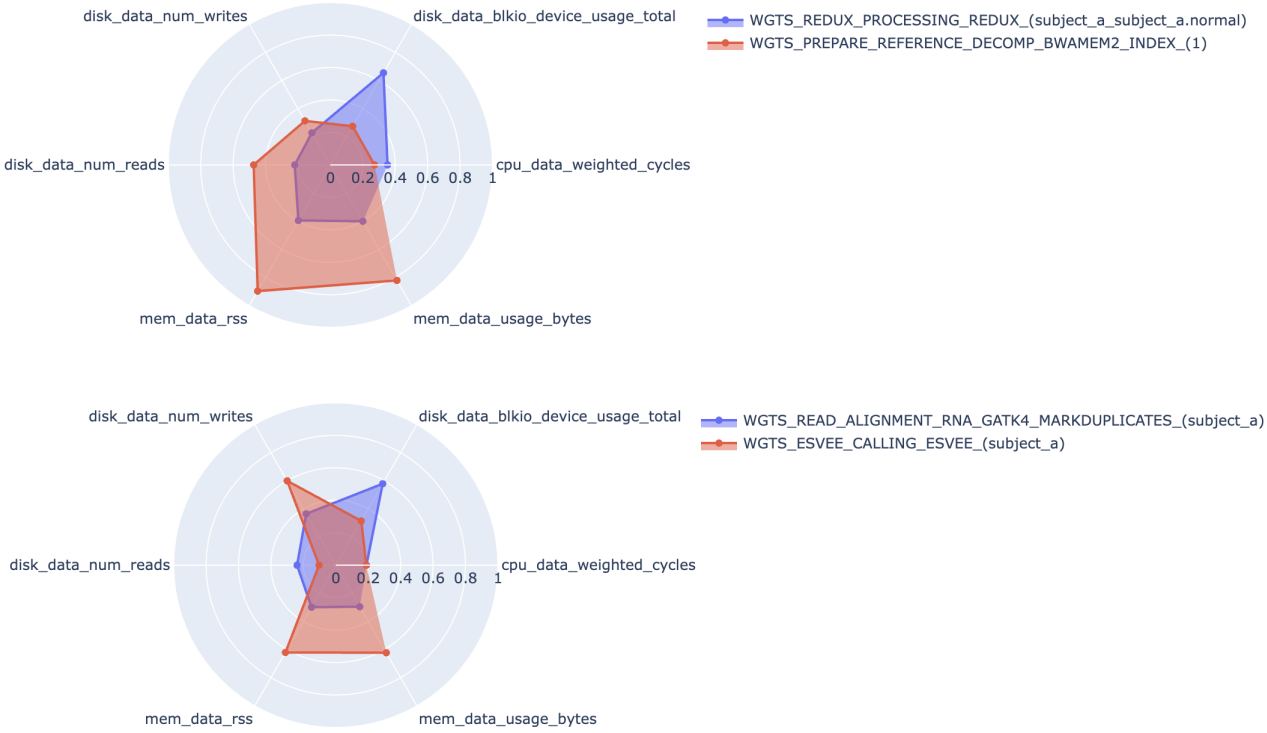

Das ist eine Beschreibung der Abbildung.

To conclude the evaluation of the task dissimilarity approach, we provide a summary statistic that illustrates its performance across multiple workflows rather than a single example. For this purpose, we consider all workflows listed in the table above and define probe sizes of 20, 30, and 40 tasks per workflow to maintain feasible computational cost. For each probe, we again compute time-averaged resource usage metrics and perform both random clustering and ShaReComp-based clustering. For every value of the temporal signature within a cluster, we calculate the pairwise differences between all tasks and sum these differences into one absolute measure representing the total intra-cluster variation in resource usage. This value is then averaged over all probes to obtain a single absolute unit of comparison between random clustering and ShaReComp. Intuitively, a higher intra-cluster distance indicates that ShaReComp has grouped more dissimilar tasks together, while a lower distance reflects the kind of overlapping resource behavior typical of random clustering. As summarized in the table, ShaReComp consistently achieves higher intra-cluster distance values across nearly all workflows. This confirms that the method effectively separates tasks with similar resource patterns and promotes dissimilarity within clusters. Among the evaluated workflows, X, Y, and Z show the most pronounced differences, demonstrating that ShaReComp maintains its clustering behavior across different task compositions and scales.

Table 6.11: Average inter-cluster difference comparison between ShaReComp and random clustering across workflows.

Workflow	Number of Tasks	Avg. ShaReComp Cluster Difference	Avg. Random Cluster Difference
atacseq	72	0.214	0.482
chipseq	68	0.237	0.495
rnaseq	54	0.201	0.468
scnanoseq	83	0.225	0.510
smrnaseq	59	0.208	0.490
pixelator	44	0.190	0.455
methylseq	65	0.232	0.503
viralrecon	51	0.216	0.487
oncoanalyser	97	0.240	0.525

6.2.3 Predicting Runtime and Energy Consumption of Task Clusters

Next, we evaluate the proposed models to explore the relationship between task resource usage over time—represented by low-level temporal signatures—and their corresponding runtime and power consumption. The overarching goal of this evaluation is to assess whether such models could eventually be used to predict the behavior of clustered tasks. However, this section focuses only on outlining the potential benefits and motivation for such predictive modeling rather than conducting an exhaustive analysis. A detailed investigation of model behavior, predictive accuracy, and performance under varying data volumes is beyond the scope of this work. Instead, we present initial results obtained by formatting the monitoring data and fitting preliminary models to it. These results serve as a first indication of the models feasibility and provide insight into potential challenges that must be addressed in future research.

Table 6.12: Summary of model configurations and performance metrics for task-level prediction.

Workflow Tasks	Model Type	Hyperparameters	R^2	MAE	Cross-Validation	Comments
1229	KCCA	Kernel = laplacian, latent_dim = 2	–	–	5-fold GridSearchCV	Model shows strong latent-space correlation but clear signs of overfitting with score of 1.46.
1229	Kernel Ridge Regression	Default parameters, trained on KCCA latent space and original Y-labels	0.24	0.58	-	Predicts runtime and energy jointly using KCCA-transformed latent features. Provides moderate generalization.
1229	Random Forest (Runtime)	estimators: 2000, max_depth 10110, max_features {log2, sqrt}	0.346	9.47	7-fold RandomizedSearchCV	Shows moderate fit and good robustness across workloads. Balanced bias-variance trade-off.
1229	Random Forest (Power)	estimators: 1200, max_depth 465, max_features {sqrt}	0.42	56.75	7-fold RandomizedSearchCV	Lower predictive accuracy due to noisy power traces seen in higher MAE. Captures coarse consumption patterns but underfits fluctuations.
1229	Baseline Random Forest (Power)	-	-	88.71	-	Baseline computing the means.
1229	Baseline Random Forest (Runtime)	-	-	13.65		Baseline computing the means.

The Kernel Canonical Correlation Analysis (KCCA) model, tested across seven kernel types with fivefold cross-validation, achieved its best performance with the Laplacian kernel. Although the latent-space correlation was strong, the model displayed clear signs of overfitting, as indicated by the unrealistically high score of 1.46. This suggests that while the latent representation captures meaningful structure, it does not generalize well beyond the training data.

The Kernel Ridge Regression (KRR) model, trained on the KCCA-derived latent features to jointly predict runtime and energy, achieved an R^2 of 0.24 and a mean absolute error (MAE) of 0.58. This moderate score indicates that the model was able to generalize partially while maintaining stability across folds, benefiting from the kernel-transformed feature space.

Among the tested regressors, the Random Forest models provided the best results overall. For runtime prediction, the model achieved an R^2 of 0.35 and an MAE of 9.47 units, corresponding to an average accuracy of about 27.7%. This indicates that ensemble methods can effectively capture nonlinear dependencies in task execution times, balancing bias and variance across workloads. The Random Forest for power prediction performed somewhat better in R^2 terms (0.42) but with a higher MAE (56.75 units). The increased error reflects the difficulty of learning from noisy and fluctuating power traces, which are less consistent than runtime measurements. Nevertheless, the model succeeded in reproducing coarse consumption trends.

When compared with the baseline models—which simply predict mean values—the trained Random Forests show substantial improvement. The baseline MAE values (13.65 for runtime and 88.71 for power) confirm that learned models provide meaningful predictive gain, particularly for runtime estimation.

6.2.4 Simulation of Scheduling Algorithms with Co-location

In this section, we evaluate the final part of our work: the integration of the co-location-aware ShaReComp approach as the ShaRiff algorithms into a workflow simulation framework. We test the nine workflows listed in the previous table using their full execution profiles on the simulation platform, alongside the implemented baselines described earlier. Two baselines operate without co-location—using either exclusive or shared node allocation—while five approaches include random co-location with different node assignment strategies. In all cases, tasks are scheduled in a FIFO manner for consistency. The evaluation is divided into three parts. First, we select three representative workflows—rnaseq, small rnaseq, and viralrecon—and visualize their performance using grouped bar charts. Each plot displays the workflow makespan (in minutes) on one y-axis and the total energy consumption of all worker nodes (in megajoules) on the other. Across all three workflows, the two baselines without co-location show the highest makespan and energy usage, as expected. Interestingly, for rnaseq, all approaches that include co-location—including the energy-aware ShaRiff variants—show similar makespan and energy consumption values. Contrary to the intuitive assumption that assigning as many tasks as possible to the largest available host or parallelizing cluster assignments across all hosts would lead to faster results, all baselines perform comparably well. Nevertheless, ShaRiff 2 achieves the shortest makespan and the lowest energy consumption, followed closely by ShaRiff 1. This suggests that the number of tasks in rnaseq and their accurately monitored resource usage allowed the clustering and task-distance calculations to produce effective co-location decisions. Since the simulation environment (WRENCH) uses workflow description files that

provide only average CPU and memory requirements per task, the impact of co-location depends heavily on ShaReComps ability to select suitable tasks from the queue to be mapped efficiently onto VMs. This mapping reduces core usage and memory demand, leading to faster processing and lower energy consumption. The results for ShaRiff 2 further indicate that oversubscribing resources with complementary task profiles can yield better performance than both non-co-located baselines and simpler co-location strategies. For small rnaseq, ShaRiff 1 performs best, achieving the lowest makespan among all configurations. Its strategy of prioritizing the largest host and assigning VMs in parallel to all hosts appears particularly effective for this smaller workload. Surprisingly, ShaRiff 3 performs worse than both baselines and other ShaRiff variants, suggesting that its node selection and consolidation strategy may not align well with the smaller task structure of this workflow. In contrast, results for viralrecon differ notably. All ShaRiff variants perform worse than the co-location-enabled baselines, with ShaRiff 1 and ShaRiff 3 showing the weakest performance. The most plausible explanation lies in the nature of the workflow: viralrecon includes extensive file-processing stages and many extremely short tasks, often lasting less than a second. This causes difficulties for the monitoring system, which cannot capture reliable data for such brief executions. As a result, few meaningful task distances can be computed. In the current implementation, tasks that do not belong to any cluster (singleton clusters) are grouped into a single VM. When this happens frequently, resource contention can occur, and since VMs are only released after their last task completes, resources remain occupied across several scheduling intervals, increasing both makespan and energy consumption. Among the ShaRiff variants, ShaRiff 2 still performs best for viralrecon, likely because its oversubscription strategy allows faster queue processing despite the incomplete clustering information. By scheduling complementary tasks together beyond strict resource limits, it manages to reduce idle times and partially offset the inefficiencies observed in the other variants.

Figure 6.23: Grouped Bar Plot

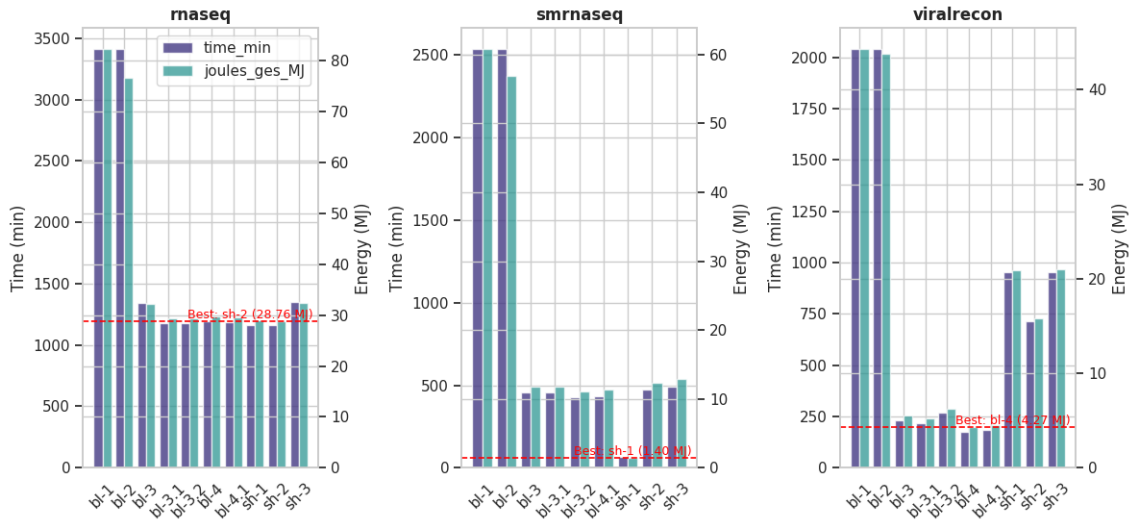

Das ist eine Beschreibung der Abbildung.

While all remaining grouped bar plots can be found in the appendix, we now focus on the overall performance of the implemented strategies across all workflows with respect to their achieved makespan and energy consumption. To this end, we present boxplots for both evaluation metrics. Starting with the energy boxplot, baselines 1 and 2 again show the

widest spread in their energy distributions across workflows. In contrast, all co-location-enabled approaches, including the ShaRiff algorithms, exhibit a more compact distribution between approximately 5 and 30 megajoules, indicating that co-location within virtual machines generally leads to more consistent and efficient energy usage. Looking more closely, the lowest median values are achieved by the baselines implementing co-location strategies 3 through 3.2, while ShaRiff 2 shows the most compact distribution overall. This suggests that across workflows with varying numbers of tasks, ShaRiff 2 achieves the smallest difference between the highest and lowest energy consumption values. ShaRiff 1 follows closely, with a range between roughly 5 and 22 megajoules. Among the oversubscription-based approaches, the variant assigning co-located clusters (4.1) performs better than the variant that oversubscribes but always selects the largest host for task mapping. This behavior aligns with the earlier observation that ShaRiff 2—which combines oversubscription with adaptive node selection—achieves both faster runtimes and lower energy consumption. A similar pattern appears in the makespan boxplot. The relative performance of the algorithms with respect to runtime mirrors their energy distribution behavior. This consistency supports the intuition that faster algorithms also tend to consume less energy overall. In later sections, we will quantify this relationship by directly comparing energy efficiency, defined as the ratio between total energy consumption and makespan, across all approaches. Overall, the results indicate that shorter makespans correlate strongly with improved energy efficiency. Workflows that complete faster tend to make better use of available compute resources, leading to reduced idle power draw and lower total energy consumption. Conversely, approaches that distribute workloads more evenly or keep resources idle for longer periods achieve neither faster completion times nor lower energy usage, but instead incur higher overall energy costs due to extended runtime. To further investigate this relationship, we next compare the average energy efficiency—expressed as the ratio of energy consumption to makespan—across all baselines and ShaRiff variants. We then focus on the raw energy consumption and makespan values themselves to conclude the evaluation of the ShaRiff algorithms and their informed co-location strategy.

Figure 6.24: Boxplot Energy

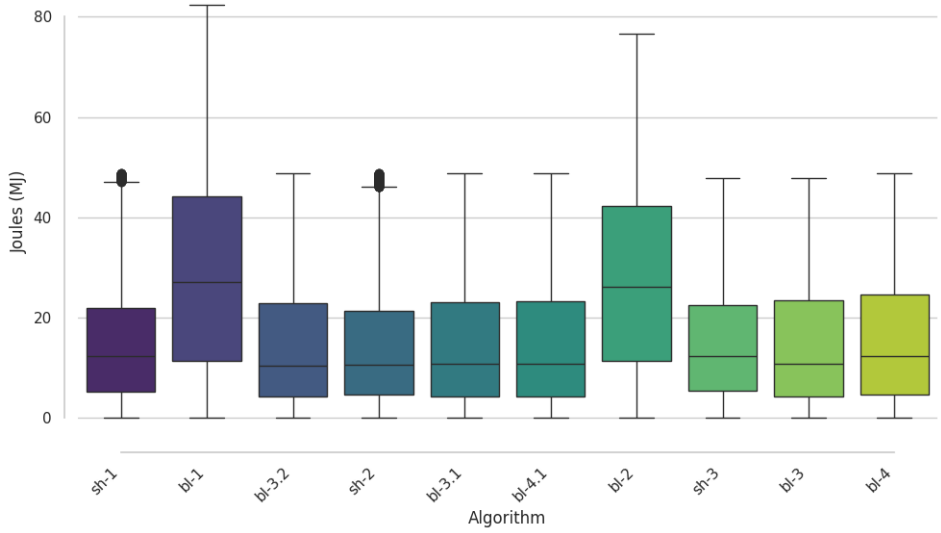

Figure 6.25: Boxplot Runtime

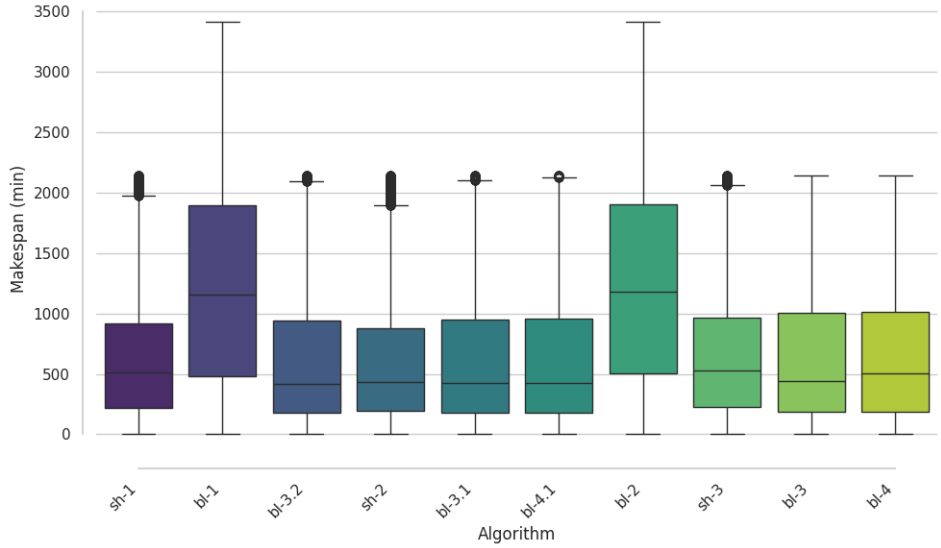

Das ist eine Beschreibung der Abbildung.

Workflow	best appraoch	Avg. baseline efficiency	Best efficiency	improvement
atacseq	ShaRiff-3	0.023	0.023	2.906
chipseq	ShaRiff-3	0.025	0.025	0.225
methylseq	ShaRiff-1	0.023	0.023	-0.556
oncoanalyser	ShaRiff-3	0.022	0.022	0.540
pixelator	ShaRiff-1	0.024	0.025	-2.379
rnaseq	ShaRiff-2	0.024	0.025	-1.521
scnanoseq	ShaRiff-3	0.022	0.022	0.076
smrnaseq	ShaRiff-1	0.025	0.022	11.649
viralrecon	ShaRiff-2	0.023	0.022	5.191

Table 6.13: efficiency over time improvement of the best ShaRiff approach compared to the average baseline efficiency per workflow.

Table ?? summarizes the comparison between the energy efficiency of the best-performing ShaRiff variant and the average baseline efficiency for each workflow. Efficiency is defined as the ratio of total energy consumption to makespan, where lower values indicate better performance, that is, less energy consumed per unit of execution time. The last column shows the relative improvement of the most efficient ShaRiff configuration compared to the baselines. Across the nine workflows, the ShaRiff algorithms achieve competitive results, although the magnitude of improvement varies between workflows. In several cases, ShaRiff provides noticeable gains, while in others the improvement is marginal or slightly negative. ShaRiff-3 appears most often as the best-performing variant, showing the highest efficiency for `atacseq`, `chipseq`, `oncoanalyser`, and `scnanoseq`. For `atacseq`, it achieves the largest relative improvement of approximately 2.9%, indicating that informed co-location reduces idle resource time and unnecessary energy usage. In contrast, `chipseq` and `oncoanalyser` show smaller but consistent improvements, suggesting that these workflows already make efficient use of resources under baseline strategies. ShaRiff-1 performs particularly well for `smrnaseq`, showing an efficiency gain of more than 11%, which is the most significant improvement overall. This indicates that its strategy of prioritizing the largest host and assigning virtual machines in parallel is especially effective for smaller or moderately sized workflows. ShaRiff-2 performs best for `rnaseq` and `viralrecon`, with the latter showing an efficiency increase of around 5Negative improvement values, as seen for `methylseq`, `pixelator`, and `rnaseq`, indicate slightly higher energy consumption compared to the baselines. These cases likely result from workflow-specific characteristics such as short task durations or limited monitoring precision rather than limitations in the ShaRiff design.

Table ?? presents the improvement in makespan achieved by the best-performing ShaRiff variant compared to the average baseline efficiency for each workflow. The values indicate how much faster the workflows complete when using the corresponding ShaRiff algorithm. Higher improvement percentages reflect shorter runtimes and thus better scheduling efficiency. Across all workflows, the results show that ShaRiff consistently reduces makespan compared to the baselines, although the extent of improvement varies depending on workflow characteristics. ShaRiff-3 performs best for `atacseq`, `chipseq`, `oncoanalyser`, and `scnanoseq`, achieving reductions between 3% and nearly 39%. In particular, `chipseq` benefits substantially, where ShaRiff-3 reduces the average completion time by almost 39%, demonstrating strong optimization of co-location and task placement. ShaRiff-1 achieves the best performance for `methylseq`, `pixelator`, and `smrnaseq`. The improvement for `smrnaseq` is the most pronounced overall, reaching almost 95%, indicating that this variants host-prioritization and parallel virtual machine assignment strategy fits small and moderately sized workflows particularly well. ShaRiff-2 yields the best results for `rnaseq` and `viralrecon`, improving runtime by about 35% and 3%, respectively. These results confirm that incorporating resource-aware co-location through ShaReComp and its integration in ShaRiff leads to noticeable reductions in total workflow runtime. The improvements are strongest in workflows with heterogeneous task profiles and complementary resource demands, where informed co-location and selective oversubscription enable better resource utilization and shorter makespans.

Workflow	best appraoch	Avg. baseline efficiency	Best efficiency	improvement
atacseq	ShaRiff-3	9.919	8.036	18.984
chipseq	ShaRiff-3	31.602	19.419	38.552
methylseq	ShaRiff-1	51.044	48.725	4.543
oncoanalyser	ShaRiff-3	1.442	1.393	3.418
pixelator	ShaRiff-1	11.194	9.527	14.888
rnaseq	ShaRiff-2	44.200	28.762	34.928
scnanoseq	ShaRiff-3	3.148	2.858	9.197
smrnaseq	ShaRiff-1	27.282	1.402	94.860
viralrecon	ShaRiff-2	16.261	15.759	3.090

Table 6.14: efficiency improvement of the best ShaRiff approach compared to the average baseline efficiency per workflow.

Table **??** summarizes the improvement in makespan achieved by the best-performing ShaRiff variant compared to the average baseline efficiency for each workflow. The improvement values indicate the percentage reduction in total workflow runtime when applying informed co-location through the ShaRiff algorithms. Overall, the results show that all ShaRiff variants outperform the baseline configurations, though the degree of improvement differs across workflows. The most significant reductions are observed for `smrnaseq` and `chipseq`, where ShaRiff reduces the makespan by approximately 94% and 40%, respectively. These strong gains demonstrate that task clustering and resource-aware mapping can substantially accelerate workflows composed of short, heterogeneous tasks. ShaRiff-1 consistently delivers the best results for most workflows, including `atacseq`, `methylseq`, `pixelator`, `rnaseq`, `scnanoseq`, and `smrnaseq`, with improvements ranging between 5% and 94%. Its strategy of prioritizing the largest available host and assigning virtual machines in parallel appears well suited for workflows with balanced CPU and memory requirements. ShaRiff-2 performs best for `oncoanalyser` and `viralrecon`, yielding modest improvements of around 3%. ShaRiff-3 shows its strongest performance in `chipseq`, where co-location and node-filling heuristics align effectively with the workflows computational structure. In summary, the integration of co-location-aware scheduling through ShaReComp in the ShaRiff algorithms leads to notable reductions in workflow runtime. The improvement magnitude depends on the workflow characteristics—particularly task heterogeneity, resource complementarity, and average task duration—but overall, the results confirm that informed co-location enables more efficient resource utilization and faster completion times compared to baseline scheduling.

Workflow	best appraoch	Avg. baseline efficiency	Best efficiency	improvement
atacseq	ShaRiff-1	427.167	355.167	16.855
chipseq	ShaRiff-3	1305.667	784.167	39.941
methylseq	ShaRiff-1	2259.000	2144.000	5.091
oncoanalyser	ShaRiff-2	65.222	63.333	2.896
pixelator	ShaRiff-1	465.571	385.167	17.270
rnaseq	ShaRiff-1	1841.167	1161.333	36.924
scnanoseq	ShaRiff-1	142.119	128.833	9.348
smrnaseq	ShaRiff-1	1140.778	63.333	94.448
viralrecon	ShaRiff-2	737.167	715.333	2.962

Table 6.15: Makespan improvement of the best ShaRiff approach compared to the average baseline efficiency per workflow.

7 Discussion

We now conclude by reflecting on the evaluation results. Beginning with the experiments on resource contention, we have already discussed the observed outcomes and the underlying reasons for these behaviors. We argue that repeating these measurements on Intel-based hardware would likely yield more consistent and intuitive power consumption results for co-located benchmarks, given the better stability and accessibility of Intel's RAPL interfaces compared to AMD's. Another factor influencing the results is the type of co-location applied is that in our setup, memory access is shared across cores via NUMA. As we confirmed the processor-to-core mapping on the test system with two CPUs available, we experimented with mapping co-located benchmark pairs according to their NUMA layout—such as pairing core 0 with 24—and pinning both tasks to the same physical CPU. Although both strategies produced broadly similar results, a more detailed investigation of the benchmark's internal performance metrics, rather than relying solely on runtime and power consumption, could yield a more accurate understanding of contention effects. Incorporating detailed benchmark-level metrics could reduce the dependency on power-based measurements and allow the use of smaller weighting factor alpha when combining runtime and energy in the affinity computation. This refinement would likely produce more reliable and interpretable affinity scores, better reflecting the true resource interaction between co-located tasks.

The last point of discussion also relates to the results obtained from the predictor training. Overall, the evaluation indicates clear potential in using predictive models to estimate the performance and energy consumption of consolidated workflow tasks. However, several challenges remain, particularly those related to data dimensionality. The structure and representation of time-series features strongly influence how well a model can learn meaningful relationships between task behavior, runtime, and energy usage. Determining how these temporal features should be arranged, aggregated, or reduced to accurately reflect task behavior is therefore a key area for future research. The flexibility of our monitoring approach, which records a large number of low-level features per task, also introduces complexity in feature selection. Deciding which metrics to retain and understanding how each contributes to prediction accuracy remains an open question. This uncertainty likely contributes to the observed behavior of the KCCA model, which successfully identified correlations between time-series features and performance metrics but exhibited strong overfitting. As mentioned earlier, inconsistencies in the measured power data—stemming from the Deep-Mon fork used on AMD hardware—may further explain the instability observed in the models. Inaccurate or noisy energy readings can easily lead to model confusion, reducing generalization ability. Future work should therefore include more reliable measurement sources, improved feature preprocessing, and systematic dimensionality studies to establish a robust and interpretable prediction framework for workflow performance and energy behavior.

Lastly, we discuss the results from simulating the integration of ShaReComp into the workflow execution framework through the ShaRiff algorithms. Although the ShaRiff variants generally perform well and outperform the baselines, their success depends strongly on the quantity and quality of available monitoring data. As mentioned earlier, there is a direct interdependence between the effectiveness of the clustering algorithm used in ShaRiff and the completeness of the monitoring data. This explains why, in several cases shown in the appendix, the baselines on which ShaRiff builds outperform it when detailed monitoring information is missing for many tasks. Our initial assumption was that combining the

best-performing baseline—baseline 3—with the co-location awareness provided by ShaReComp would consistently yield superior results. While this expectation holds for certain workflows, it does not generalize across all of them. We therefore see potential in extending the evaluation to a wider range of workflows with different task characteristics to better understand when and why ShaRiff provides the largest benefit. When comparing the performance of all baselines and ShaRiff algorithms across workflows, their lower performance bound appears to remain within a similar magnitude. Several factors could explain this. The first two baselines, which do not employ co-location, clearly perform worse, as expected. However, the differences among the node assignment strategies are smaller than anticipated. For example, we expected that always selecting the largest host would result in faster completion for workflows with fewer tasks, compared to round-robin or parallel assignment strategies. Although such trends are visible, the differences are not as pronounced as predicted. A key reason lies in the simulator design and the way baselines are implemented. During many scheduling intervals, the task queue available for allocation or co-location contained only a few tasks. To address this, we introduced a minimum queue size requirement before enabling co-location, which improved results. Nevertheless, considering task dependencies directly from the workflow DAG could further increase throughput and prevent underutilization caused by limited queue size. We also encountered limitations in the virtual cluster compute service of WRENCH. Once tasks are assigned to a virtual machine, the VM cannot be resized dynamically; even if one task completes early, the allocated core remains idle until all tasks within that VM finish. Introducing VM resizing capabilities could significantly improve resource utilization. Similarly, instead of placing all singleton tasks that do not belong to clusters into a single VM, spawning separate VMs for each could potentially reduce makespan and energy consumption. Future work should also integrate the idle-time metric provided by SimGrid into WRENCH to quantify unused resources more precisely. Moreover, WRENCH supports direct access to workflow DAG information from the workflow management system, which could be leveraged to improve scheduling decisions. Implementing additional random co-location and scheduling strategies would also provide more comparative baselines for assessing energy efficiency. Overall, while ShaRiff already demonstrates improved runtime and energy consumption in many cases, its full potential has yet to be explored. Future work should focus on integrating alternative cluster resource management strategies, expanding the host pool, and refining the platform model. In particular, moving beyond the current assumption of linear energy consumption relative to core usage toward a more fine-grained and realistic energy model would provide a more accurate evaluation of how ShaReComp enhances ShaRiff's performance.

8 Conclusion and Future Work

This thesis explores the field of co-locating scientific workflow tasks with the aim of reducing resource contention and improving energy awareness. We identified the relevant research areas and introduced a fine-grained task monitoring system to capture detailed task behavior over time. This system records low-level execution time series with minimal overhead and processes them to enable statistical analysis.

Furthermore, we proposed a novel online task clustering approach by extending and modifying an existing formulation of the co-location problem, treating it as a consolidation task that groups dissimilar workloads together. We formalized this problem through a distance-based formulation, defined a threshold mechanism, and derived complementary task clusters. We demonstrated how these clusters and their low-level temporal resource signatures can be used to predict task behavior through modeling. Specifically, we applied Kernel Canonical Correlation Analysis (KCCA) to identify maximum correlations between task metrics and performance, and used Random Forest models to predict runtime and energy consumption independently. Finally, we investigated how co-location can be integrated into workflow scheduling by designing a simulation framework capable of embedding such mechanisms. We implemented two naive baselines and five co-location heuristics, along with three algorithms that use the dissimilarity-based clustering approach, and evaluated them on nine workflows from the nf-core repository. The results show promising potential for adopting complementary task co-location in online scheduling environments. The proposed methods enable more informed scheduling decisions that can serve multiple objectives, such as makespan reduction, energy efficiency, and potentially reduced carbon footprint. Through the extensible framework developed in this work, we provide a foundation for further research by defining clear interfaces and offering a formal basis for extending the co-location modeling and scheduling capabilities. Future work will focus on several key directions to enhance the framework and deepen the understanding of co-location-based workflow scheduling. In particular, improving the quality and coverage of monitoring data will be essential, as the success of the ShaRiff algorithms depends strongly on the availability of accurate and complete task metrics. As discussed, the performance of ShaRiff is also interdependent with the clustering algorithm's quality—insufficient monitoring detail limits its effectiveness. Expanding the evaluation to more diverse workflows with different task characteristics will help clarify under which conditions ShaRiff achieves the greatest benefits. Additionally, improvements to the simulation environment are needed. The current design limits resource utilization, as virtual machines cannot be resized dynamically; idle cores remain unused until all tasks within a VM complete. Supporting VM resizing and refining task allocation—such as spawning separate VMs for singleton tasks—could significantly reduce makespan and energy usage. Leveraging workflow DAG information available in WRENCH, together with SimGrid's idle-time metrics, will further enhance scheduling precision and resource accounting. Finally, incorporating more realistic energy models that move beyond the current linear assumptions and integrating additional random co-location and scheduling strategies will strengthen the framework's analytical scope. Expanding the host pool and adopting alternative resource management strategies will provide richer insights into how co-location and ShaReComp improve the performance of workflow execution systems.

1. Monitoring Improvement, higher task coverage, better ebpf, lower overhead, better energy models
2. More in-depth time-series treatment for better feature-vectors

3. Dimensionality reduction, feature selection based on highest explanation
4. More sophisticated affinity score calculation based on lower-level interference measurements
5. Treatment of static time-series for distance calculation
6. Refinement of regression approach within KCCA by comparing to other means
7. Extending by more suitable or sophisticated models.
8. Integrating cost-functions into the co-location strategies so that optimization problems can be formulated and account for single or multi-obectives.
9. Extending and calibrating the simulation framework with energy-sources for more realistic simulation results
10. Reformulating the co-location problem from consolidation problem into degredataion prediction

A Plots

B Algorithms

References

[1] Foudil Abdessamia, Wei-Zhe Zhang, and Yu-Chu Tian. "Energy-efficiency virtual machine placement based on binary gravitational search algorithm". In: *Cluster Computing* 23.3 (2020), pp. 1577–1588.

[2] Abdulmohsen Algarni, Iqrar Shah, Ali Imran Jehangiri, Mohammed Alaa Ala'Anzy, and Zulfiqar Ahmad. "Predictive Energy Management for Docker Containers in Cloud Computing: A Time Series Analysis Approach". In: *IEEE Access* 12 (2024), pp. 52524–52538. DOI: 10.1109/ACCESS.2024.3387436.

[3] Jordi Arjona Aroca, Angelos Chatzipapas, Antonio Fernández Anta, and Vincenzo Mancuso. "A Measurement-Based Characterization of the Energy Consumption in Data Center Servers". In: *IEEE Journal on Selected Areas in Communications* 33.12 (2015), pp. 2863–2877. DOI: 10.1109/JSAC.2015.2481198.

[4] F.R. Bach and M.I. Jordan. "Kernel independent component analysis". In: *2003 IEEE International Conference on Acoustics, Speech, and Signal Processing, 2003. Proceedings. (ICASSP '03).* Vol. 4. 2003, pp. IV–876. DOI: 10.1109/ICASSP.2003.1202783.

[5] Jonathan Bader, Joel Witzke, Soeren Becker, Ansgar Loser, Fabian Lehmann, Leon Doehler, Anh Duc Vu, and Odej Kao. "Towards Advanced Monitoring for Scientific Workflows". In: *2022 IEEE International Conference on Big Data (Big Data).* IEEE, 2022, pp. 2709–2715. DOI: 10.1109/bigdata55660.2022.10020864.

[6] Sergey Blagodurov and Alexandra Fedorova. "In search for contention-descriptive metrics in HPC cluster environment". In: *Proceedings of the 2nd ACM/SPEC International Conference on Performance Engineering.* ICPE '11. Karlsruhe, Germany: Association for Computing Machinery, 2011, pp. 457–462. ISBN: 9781450305198. DOI: 10.1145/1958746.1958815.

[7] Sergey Blagodurov and Alexandra Fedorova. "Towards the contention aware scheduling in HPC cluster environment". In: *Journal of Physics: Conference Series* 385.1 (2012), p. 012010. DOI: 10.1088/1742-6596/385/1/012010.

[8] Sergey Blagodurov, Alexandra Fedorova, Evgeny Vinnik, Tyler Dwyer, and Fabien Hermenier. "Multi-objective job placement in clusters". In: *Proceedings of the International Conference for High Performance Computing, Networking, Storage and Analysis.* SC15. ACM, 2015. DOI: 10.1145/2807591.2807636.

[9] Sergey Blagodurov, Sergey Zhuravlev, and Alexandra Fedorova. "Contention-Aware Scheduling on Multicore Systems". In: *ACM Transactions on Computer Systems* 28.4 (2010), pp. 1–45. ISSN: 1557-7333. DOI: 10.1145/1880018.1880019.

[10] Andreas Blanche and Thomas Lundqvist. "Terrible Twins: A Simple Scheme to Avoid Bad Co-Schedules". In: Jan. 2016. DOI: 10.14459/2016md1286952.

[11] Andrea Borghesi, Andrea Bartolini, Michele Lombardi, Michela Milano, and Luca Benini. "Predictive Modeling for Job Power Consumption in HPC Systems". In: *High Performance Computing.* Springer International Publishing, 2016, pp. 181–199. ISBN: 9783319413211. DOI: 10.1007/978-3-319-41321-1_10.

[12] L. Breiman. "Random Forests". In: *Machine Learning* 45 (2001), pp. 5–32.

[13] Jens Breitbart, Josef Weidendorfer, and Carsten Trinitis. "Case Study on Co-scheduling for HPC Applications". In: *2015 44th International Conference on Parallel Processing Workshops.* 2015, pp. 277–285. DOI: 10.1109/ICPPW.2015.38.

[14] Rolando Brondolin, Tommaso Sardelli, and Marco D. Santambrogio. "DEEP-Mon: Dynamic and Energy Efficient Power Monitoring for Container-Based Infrastruc-

tures". In: *2018 IEEE International Parallel and Distributed Processing Symposium Workshops (IPDPSW)*. 2018, pp. 676–684. DOI: 10.1109/IPDPSW.2018.00110.

[15] Marc Bux and Ulf Leser. "Parallelization in Scientific Workflow Management Systems". In: (2013). arXiv: 1303.7195 [astro-ph.IM].

[16] Henri Casanova, Rafael Ferreira da Silva, Ryan Tanaka, Suraj Pandey, Gautam Jethwani, William Koch, Spencer Albrecht, James Oeth, and Frédéric Suter. "Developing Accurate and Scalable Simulators of Production Workflow Management Systems with WRENCH". In: *Future Generation Computer Systems* 112 (2020), pp. 162–175. DOI: 10.1016/j.future.2020.05.030.

[17] Ruobing Chen, Wangqi Peng, Yusen Li, Xiaoguang Liu, and Gang Wang. "Orchid: An Online Learning Based Resource Partitioning Framework for Job Colocation With Multiple Objectives". In: *IEEE Transactions on Computers* 72.12 (2023), 3440 $ÌÍ MßHB. ISSN: 2326-3814. DOI: 10.1109/tc.2023.3303959.

[18] Ruobing Chen, Haosen Shi, Yusen Li, Xiaoguang Liu, and Gang Wang. "OLPart: Online Learning based Resource Partitioning for Colocating Multiple Latency-Critical Jobs on Commodity Computers". In: *Proceedings of the Eighteenth European Conference on Computer Systems*. EuroSys-23. ACM, 2023, pp. 347–364. DOI: 10.1145/3552326.3567490.

[19] Anita Choudhary, Mahesh Chandra Govil, Girdhari Singh, Lalit K. Awasthi, and Emmanuel S. Pilli. "Energy-aware scientific workflow scheduling in cloud environment". In: *Cluster Computing* 25.6 (2022), pp. 3845–3874. ISSN: 1573-7543. DOI: 10.1007/s10586-022-03613-3.

[20] TainÃ£ Coleman, Henri Casanova, Ty Gwartney, and Rafael Ferreira da Silva. "Evaluating Energy-Aware Scheduling Algorithms for I/O-Intensive Scientific Workflows". In: *Computational Science - ICCS 2021*. Springer International Publishing, 2021, pp. 183–197. ISBN: 9783030779610. DOI: 10.1007/978-3-030-77961-0_16.

[21] Daniel Dauwe, Eric Jonardi, Ryan D. Friese, Sudeep Pasricha, Anthony A. Maciejewski, David A. Bader, and Howard Jay Siegel. "HPC node performance and energy modeling with the co-location of applications". In: *The Journal of Supercomputing* 72.12 (2016), pp. 4771–4809. ISSN: 1573-0484. DOI: 10.1007/s11227-016-1783-y.

[22] Juan J. Durillo, Vlad Nae, and Radu Prodan. "Multi-objective energy-efficient workflow scheduling using list-based heuristics". In: *Future Generation Computer Systems* 36 (2014), pp. 221–236. ISSN: 0167-739X. DOI: 10.1016/j.future.2013.07.005.

[23] Tyler Dwyer, Alexandra Fedorova, Sergey Blagodurov, Mark Roth, Fabien Gaud, and Jian Pei. "A practical method for estimating performance degradation on multicore processors, and its application to HPC workloads". In: *SC '12: Proceedings of the International Conference on High Performance Computing, Networking, Storage and Analysis*. 2012, pp. 1–11. DOI: 10.1109/SC.2012.11.

[24] Surya Kant Garg and J. Lakshmi. "Workload performance and interference on containers". In: *2017 IEEE SmartWorld, Ubiquitous Intelligence and Computing, Advanced and Trusted Computed, Scalable Computing and Communications, Cloud and Big Data Computing, Internet of People and Smart City Innovation (SmartWorld/SCALCOM/UIC/ATC/CBDCom/IOP/SCI)*. 2017, pp. 1–6. DOI: 10.1109/UIC-ATC.2017.8397647.

[25] Brendan Gregg. *BPF Performance Tools*. 1st. Editor-in-Chief: Mark L. Taub; Series Editor: Brian Kernighan; Executive Editor: Greg Doench; Senior Project Editor: Lori Lyons. Boston, MA: Pearson Education, Inc., 2020. ISBN: 9780136554820.

[26] Robert Hood, Haoqiang Jin, Piyush Mehrotra, Johnny Chang, Jahed Djomehri, Sharad Gavali, Dennis Jespersen, Kenichi Taylor, and Rupak Biswas. "Performance

impact of resource contention in multicore systems". In: *2010 IEEE International Symposium on Parallel and Distributed Processing (IPDPS)*. 2010, pp. 1–12. DOI: 10.1109/IPDPS.2010.5470399.

[27] Mirsaeid Hosseini Shirvani. "A survey study on task scheduling schemes for workflow executions in cloud computing environment: classification and challenges". In: *The Journal of Supercomputing* 80.7 (2024), pp. 9384–9437. ISSN: 1573-0484. DOI: 10.1007/s11227-023-05806-y.

[28] Zhengxiong Hou, Hong Shen, Xingshe Zhou, Jianhua Gu, Yunlan Wang, and Tianhai Zhao. "Prediction of job characteristics for intelligent resource allocation in HPC systems: a survey and future directions". In: *Frontiers of Computer Science* 16.5 (2022). ISSN: 2095-2236. DOI: 10.1007/s11704-022-0625-8.

[29] Yichao Jin, Yonggang Wen, and Qinghua Chen. "Energy efficiency and server virtualization in data centers: An empirical investigation". In: *2012 Proceedings IEEE INFOCOM Workshops*. 2012, pp. 133–138. DOI: 10.1109/INFCOMW.2012.6193474.

[30] Gideon Juve, Ann Chervenak, Ewa Deelman, Shishir Bharathi, Gaurang Mehta, and Karan Vahi. "Characterizing and profiling scientific workflows". In: *Future Generation Computer Systems* 29.3 (2013). Special Section: Recent Developments in High Performance Computing and Security, pp. 682–692. ISSN: 0167-739X. DOI: https://doi.org/10.1016/j.future.2012.08.015.

[31] Nizam Kashif Khan. "Energy Measurement and Modeling in High Performance Computing with Intel's RAPL". Electronic ISBN: 978-952-60-7892-2; Supervising Professor: Antti Ylä-Jääski; Thesis Advisor: Jukka Nurminen. Doctoral dissertation (article). Espoo, Finland: Aalto University, 2018. ISBN: 978-952-60-7891-5.

[32] Animesh Kuity and Sateesh K. Peddoju. "pHPCe: a hybrid power conservation approach for containerized HPC environment". In: *Cluster Computing* 27.3 (2023), pp. 2611–2634. ISSN: 1573-7543. DOI: 10.1007/s10586-023-04105-8.

[33] Sachin Kumar, Saurabh Pal, Satya Singh, Raghvendra Pratap Singh, Sanjay Kumar Singh, and Priya Jaiswal. "An Energy & Cost Efficient Task Consolidation Algorithm for Cloud Computing Systems". In: *Advancements in Smart Computing and Information Security*. Ed. by Sridaran Rajagopal, Parvez Faruki, and Kalpesh Popat. Cham: Springer Nature Switzerland, 2022, pp. 446–454. ISBN: 978-3-031-23092-9.

[34] Justin Kur, Jingshu Chen, Ji Xue, and Jun Huang. "Resolution Matters: Revisiting Prediction-Based Job Co-location in Public Clouds". In: *2022 IEEE/ACM 15th International Conference on Utility and Cloud Computing (UCC)*. 2022, pp. 163–166. DOI: 10.1109/UCC56403.2022.00029.

[35] Young Choon Lee and Albert Y. Zomaya. "Energy efficient utilization of resources in cloud computing systems". In: *The Journal of Supercomputing* 60.2 (2012), pp. 268–280. ISSN: 1573-0484. DOI: 10.1007/s11227-010-0421-3.

[36] Xi Li, Anthony Ventresque, Jesus Omana Iglesias, and John Murphy. "Scalable correlation-aware virtual machine consolidation using two-phase clustering". In: *2015 International Conference on High Performance Computing and Simulation (HPCS)*. 2015, pp. 237–245. DOI: 10.1109/HPCSim.2015.7237045.

[37] Xiang Li, Linfeng Wen, Minxian Xu, and Kejiang Ye. "An Interference-aware Approach for Co-located Container Orchestration with Novel Metric". In: *2023 IEEE International Conferences on Internet of Things (iThings) and IEEE Green Computing and Communications (GreenCom) and IEEE Cyber, Physical and Social Computing (CPSCom) and IEEE Smart Data (SmartData) and IEEE Congress on Cybermatics (Cybermatics)*. 2023, pp. 600–607. DOI: 10.1109/iThings-GreenCom-CPSCom-SmartData-Cybermatics60724.2023.00111.

[38] Junwen Liu, Shiyong Lu, and Dunren Che. "A Survey of Modern Scientific Workflow Scheduling Algorithms and Systems in the Era of Big Data". In: *2020 IEEE International Conference on Services Computing (SCC)*. 2020, pp. 132–141. DOI: 10.1109/SCC49832.2020.00026.

[39] Maicon Melo Alves and LÃºcia Maria de AssumpÃ§Ã£o Drummond. "A multivariate and quantitative model for predicting cross-application interference in virtual environments". In: *Journal of Systems and Software* 128 (2017), pp. 150–163. ISSN: 0164-1212. DOI: 10.1016/j.jss.2017.04.001.

[40] Maicon Melo Alves, Luan Teylo, Yuri Frota, and Lúcia M.A. Drummond. "An Interference-Aware Virtual Machine Placement Strategy for High Performance Computing Applications in Clouds". In: *2018 Symposium on High Performance Computing Systems (WSCAD)*. 2018, pp. 94–100. DOI: 10.1109/WSCAD.2018.00024.

[41] Tarek Menouer and Patrice Darmon. "Containers Scheduling Consolidation Approach for Cloud Computing". In: *Pervasive Systems, Algorithms and Networks*. Ed. by Christian Esposito, Jiman Hong, and Kim-Kwang Raymond Choo. Cham: Springer International Publishing, 2019, pp. 178–192. ISBN: 978-3-030-30143-9.

[42] Andreas Merkel, Jan Stoess, and Frank Bellosa. "Resource-conscious scheduling for energy efficiency on multicore processors". In: *Proceedings of the 5th European conference on Computer systems*. EuroSys-10. ACM, 2010, p. 150. DOI: 10.1145/1755913.1755930.

[43] Ali Mohammadzadeh, Mohammad Masdari, Farhad Soleimanian Gharehchopogh, and Ahmad Jafarian. "A hybrid multi-objective metaheuristic optimization algorithm for scientific workflow scheduling". In: *Cluster Computing* 24.2 (2020), pp. 1479–1503. ISSN: 1573-7543. DOI: 10.1007/s10586-020-03205-z.

[44] Tirthak Patel, Adam Wagenhäuser, Christopher Eibel, Timo Hönig, Thomas Zeiser, and Devesh Tiwari. "What does Power Consumption Behavior of HPC Jobs Reveal? : Demystifying, Quantifying, and Predicting Power Consumption Characteristics". In: *2020 IEEE International Parallel and Distributed Processing Symposium (IPDPS)*. 2020, pp. 799–809. DOI: 10.1109/IPDPS47924.2020.00087.

[45] Guillaume Raffin and Denis Trystram. "Dissecting the software-based measurement of CPU energy consumption: a comparative analysis". In: (2024). arXiv: 2401.15985 [astro-ph.IM].

[46] Jitendra Kumar Rai, Atul Negi, Rajeev Wankar, and K.D. Nayak. "Performance Prediction on Multi-core Processors". In: *2010 International Conference on Computational Intelligence and Communication Networks*. 2010, pp. 633–637. DOI: 10.1109/CICN.2010.125.

[47] Youssef Saadi, Soufiane Jounaidi, Said El Kafhali, and Hicham Zougagh. "Reducing energy footprint in cloud computing: a study on the impact of clustering techniques and scheduling algorithms for scientific workflows". In: *Computing* 105.10 (2023), pp. 2231–2261. ISSN: 1436-5057. DOI: 10.1007/s00607-023-01182-w.

[48] Altino M. Sampaio and Jorge G. Barbosa. "Estimating Effective Slowdown of Tasks in Energy-Aware Clouds". In: *2014 IEEE International Symposium on Parallel and Distributed Processing with Applications*. 2014, pp. 101–108. DOI: 10.1109/ISPA.2014.22.

[49] C.A. Silva, R. VilaÃ§a, A. Pereira, and R.J. Bessa. "A review on the decarbonization of high-performance computing centers". In: *Renewable and Sustainable Energy Reviews* 189 (2024), p. 114019. ISSN: 1364-0321. DOI: 10.1016/j.rser.2023.114019.

[50] Rafael Ferreira da Silva, Henri Casanova, Anne-CÃ©cile Orgerie, Ryan Tanaka, Ewa Deelman, and FrÃ©dÃ©ric Suter. "Characterizing, Modeling, and Accurately

Simulating Power and Energy Consumption of I/O-intensive Scientific Workflows". In: *Journal of Computational Science* 44 (2020), p. 101157. ISSN: 1877-7503. DOI: 10.1016/j.jocs.2020.101157.

[51] Thomas Sterling, Matthew Anderson, and Maciej Brodowicz. "Chapter 2 - HPC Architecture 1: Systems and Technologies". In: *High Performance Computing*. Ed. by Thomas Sterling, Matthew Anderson, and Maciej Brodowicz. Boston: Morgan Kaufmann, 2018, pp. 43–82. ISBN: 978-0-12-420158-3. DOI: https://doi.org/10.1016/B978-0-12-420158-3.00002-2.

[52] Lauritz Thamsen, Yehia Elkhatib, Paul Harvey, Syed Waqar Nabi, Jeremy Singer, and Wim Vanderbauwhede. *Energy-Aware Workflow Execution: An Overview of Techniques for Saving Energy and Emissions in Scientific Compute Clusters*. 2025. arXiv: 2506.04062 [cs.DC].

[53] Ioannis Vardas, Sascha Hunold, Philippe Swartvagher, and Jesper Larsson Träff. "Exploring Mapping Strategies for Co-allocated HPC Applications". In: *Euro-Par 2023: Parallel Processing Workshops*. Ed. by Demetris Zeinalipour, Dora Blanco Heras, George Pallis, Herodotos Herodotou, Demetris Trihinas, Daniel Balouek, Patrick Diehl, Terry Cojean, Karl Fürlinger, Maja Hanne Kirkeby, Matteo Nardelli, and Pierangelo Di Sanzo. Cham: Springer Nature Switzerland, 2024, pp. 271–276. ISBN: 978-3-031-48803-0.

[54] Aurelio Vivas, Andrei Tchernykh, and Harold Castro. "Trends, Approaches, and Gaps in Scientific Workflow Scheduling: A Systematic Review". In: *IEEE Access* 12 (2024), pp. 182203–182231. DOI: 10.1109/ACCESS.2024.3509218.

[55] Huijun Wang and Oliver Sinnen. "List-Scheduling versus Cluster-Scheduling". In: *IEEE Transactions on Parallel and Distributed Systems* 29.8 (2018), pp. 1736–1749. DOI: 10.1109/TPDS.2018.2808959.

[56] Mehul Warade, Kevin Lee, Chathurika Ranaweera, and Jean-Guy Schneider. "Monitoring the Energy Consumption of Docker Containers". In: *2023 IEEE 47th Annual Computers, Software, and Applications Conference (COMPSAC)*. 2023, pp. 1703–1710. DOI: 10.1109/COMPSAC57700.2023.00263.

[57] Joel Witzke, Ansgar LÃ¶Ãer, Vasilis Bountris, Florian Schintke, and BjÃ¶rn Scheuermann. "Low-level I/O Monitoring for Scientific Workflows". In: (2024). arXiv: 2408.00411 [astro-ph.IM].

[58] Felippe Vieira Zacarias, Vinicius Petrucci, Rajiv Nishtala, Paul Carpenter, and Daniel Mossé. "Intelligent colocation of HPC workloads". In: *Journal of Parallel and Distributed Computing* 151 (2021), pp. 125–137. ISSN: 0743-7315. DOI: https://doi.org/10.1016/j.jpdc.2021.02.010.

[59] Zhiheng Zhong, Jiabo He, Maria A. Rodriguez, Sarah Erfani, Ramamohanarao Kotagiri, and Rajkumar Buyya. "Heterogeneous Task Co-location in Containerized Cloud Computing Environments". In: *2020 IEEE 23rd International Symposium on Real-Time Distributed Computing (ISORC)*. 2020, pp. 79–88. DOI: 10.1109/ISORC49007.2020.00021.

[60] Jianyong Zhu, Renyu Yang, Chunming Hu, Tianyu Wo, Shiqing Xue, Jin Ouyang, and Jie Xu. "Perph: A Workload Co-location Agent with Online Performance Prediction and Resource Inference". In: *2021 IEEE/ACM 21st International Symposium on Cluster, Cloud and Internet Computing (CCGrid)*. 2021, pp. 176–185. DOI: 10.1109/CCGrid51090.2021.00027.

[61] Qian Zhu, Jiedan Zhu, and Gagan Agrawal. "Power-Aware Consolidation of Scientific Workflows in Virtualized Environments". In: *SC '10: Proceedings of the 2010*

ACM/IEEE International Conference for High Performance Computing, Networking, Storage and Analysis. 2010, pp. 1–12. DOI: 10.1109/SC.2010.43.